# Membrane evaluation and thermal modelling of the vanadium redox flow battery

by

Anders Kronander


A THESIS

submitted to

Lund University of Technology

In partial fulfillment of the requirements for the degree of

Master of Science in Chemical Engineering

Presented 20160902

Lund University

# Sammanfattning

Användningen av förnyelsebara energikällor ökar runt om i världen. För att fullständigt övergå till dessa intermittenta energikällor sätts stora krav på möjligheterna att lagra energin. En potentiell teknik för storskalig energilagring är ett så kallat Vanadium Redox Flow battery, ett flödesbatteri baserat på grundmetallen Vanadium. Denna lagringsteknik kan ytterligare bana väg för förnyelsebara källor på våra elnät och därmed göra oss mindre beroende av fossila bränslen såsom kol och naturgas.

Som med all typ av ny teknik finns det förbättringsmöjligheter, inte minst ur ett ekonomiskt perspektiv. Detta gäller även för VRB teknologin som i dagsläget är mycket dyr, mestadels på grund av ett selektivt membran som används för att separera elektrolyterna från varandra. Forskning på funktionella och billigare membran pågår runt omkring världen och potentiella kandidater för denna typ av teknik har producerats av flertalet aktiva bolag runt om i världen. I synnerhet behöve följande egenskaper vara uppfyllda för att membranet skall fungera i flödesbatterier: det behöver vara billigt, ha låg resistens, låg permeabilitet för vanadium joner samt vara mycket kemiskt stabilt i den ofta korrosiva miljön.

I detta examensarbete har nya membran testats både med hjälp av olika experimentella förfaranden samt genom datorbaserade simulationer. Membranet FAP450 och F930 från Fumatech™ testades tillsammans med GN-115, GN-212C, GN-212 från General energy and New Materials™ samt VB-1 och VB-2 från V-Fuel Pty Ltd. Energieffektiviteten (EE) visade sig vara högst för F930 från Fumatech™ på 89% vilket är liknande energieffektivitet på dagens Nafion-membran. Däremot visade sig samma membran tappa 90% av kapaciteten efter 60 cykler vid simuleringar i MATLAB på grund av storleksskillnader i diffusionshastigheter. FAP-450 visade sig inte tappa någon nämnvärd kapacitet över 60 cykler på grund av sina låga permeabilitetskonstanter för alla olika vanadium joner. Termodynamiska modelleringar påvisade att det föreligger risk för överhettning vid användning av bland annat GN-115 och GN-212. Detta beror på att permeabilitetskonstanterna är så pass höga att exoterma sidoreaktioner ökar temperaturen hos elektrolyterna vilket kan leda till flertalet problem. Detta var inte fallet med FAP-450 som bedömdes som det bästa alternativa membranet för användning i VRB-teknologin.

# Abstract

In this study, different membranes were tested for their use in a vanadium redox flow battery (VRB). The membranes were first tested under charge-discharge operation of the VRB over four charge-discharge cycles at different current densities (20 $mAcm^{-2}$, 40 mA $cm^{-2}$ and 60 $mAcm^{-2}$) and the corresponding cell performance was evaluated in terms of total energy efficiency (EE), coulombic efficiency (CE) and voltage efficiency (VE).

The anion exchange Fumasep® series FAP-450 as well as the cation exchange series, Fumapem®, F-930 by Fumatech™ (located in Baden-Württemberg, Germany) and the GN-115, GN-212, GN-212C (all from General Energy and New Materials Co Ltd,. Nanjing, China) and the VB1 (supplied by V-Fuel Pty Ltd) were all evaluated during charge-discharge operation. It was found that the F930 membrane outperformed all other membranes at all current densities tested in this study with a peak average EE of 89,6% at 500 mA (20 $mAcm^{-2}$) and CE of 98,8% at 1500 mA (60 $mAcm^{-2}$). The second best at charge-discharge evaluation was the FAP450 with an overall EE of 81,0%.

In order to further quantify any differences between the membranes, these membranes were tested for permeability rates at constant temperature for all vanadium ions present in a VRB without influence of any current. The diffusion coefficients through the FAP-450 and the F930, VB2 (same as VB1 but thicker) and the GN-115 membrane were determined for the following ions V(II), V(III), V(IV) and V(V). It was found that the VB2 had the lowest measured permeability rates for the V(II), V(III) and V(IV) ions. Furthermore, the FAP450 membrane was the membrane with the second best diffusion coefficients which was consistent with the high coulombic efficiencies observed in the laboratory scale VRB cell.

To predict the overall capacity loss during long term operation, the battery was simulated in MATLAB™ using mathematical models developed at UNSW Australia for 60 cycles (without electrolyte remixing). It was found that the FAP450 performed better than the F930 and the GN-115 membrane based on experimentally determined diffusion coefficients. The self-discharge reactions led to almost 0% capacity loss after about 60 cycles for the FAP450 membrane. For the F930, which had about 10 times higher diffusion coefficients compared to the FAP450, about 90% capacity was lost over the same number of cycles. The GN-115 membrane, which had higher diffusion coefficients than the F930

gave better results at simulations and had lost about 50% of the capacity after 60 cycles. This is believed to be due to the F930 having a factor of 20 difference between the diffusion coefficients which leads to a buildup of vanadium ions on one side of the cell and a deficit of the other. As the F930 had overall smaller diffusion coefficients compared to the GN-115, it was unexpected that the latter would prove better than the F930 at extended use. It can thus be concluded that not only do the diffusion coefficients have to be low, they also have to be the same order of magnitude for all the different ions to prevent severe capacity drop.

As the vanadium electrolytes may irreversibly precipitate at low respectively high temperatures it is imperative to understand how non-electrochemical, exothermic side reactions as well as surrounding temperatures interact with the electrolytes. Therefore, thermal modelling was also undertaken using the MATLAB model developed at UNSW. It was found that higher permeability rates gave much higher temperatures in the cell stacks and the electrolyte tanks. After 5 days, the electrolyte temperature in the tanks of the VRB using the F930 was about 30°C and increasing while the stacks reached temperatures of as high as 38°C and increasing. The FAP450, which had lower permeability rates than the F930, reached a stack temperature of only a few more degrees than the tank temperature due to the low influence of exothermic self-discharge reactions inside the cell stack. By comparison, previous thermodynamic simulation studies using Nafion showed that the temperature of the stack increased to about 40°C which indicates that external cooling should be considered when the pumps are turned off and the battery is at standby.

The GN-115 membrane from General Energy © gave good results in the VRB cycling tests as well as for permeability rates and was therefore further evaluated by immersion in 1 M V(5), 2,5 M H2SO4 for 7 weeks in order to test its chemical resistance to the oxidizing V(5) solution. It displayed a 26% increase in thickness and about 6% increase in length and width. The weight increased by about 10%. This indicates that the pore size of the membrane might have changed during immersion which could influence the performance of the membrane in VRBs.

# Acknowledgements

First and foremost I would like to thank Maria Skyllas-Kazacos at the University of New South Wales for all the help and support throughout the exchange period. I also thank the University of New South Wales for allowing me write my master thesis at such an amazing place.

It would have been impossible for me to carry out my master thesis without the financial support by Göteborgs Energi Miljöfond, the scholarship from the Swedish Royal Academy of Science and from Carl Levin's Stiftelse.

I'd like to thank my family in Sweden for all the support and the same goes for the Ferry family for all the help during our stay in Sydney. Especially, I'd like to thank my beloved girlfriend Viktoria for all encouragement and love throughout this study and for always being there when I need a hand or two.

TABLE OF CONTENTS

**CONTENTS**

TABLE OF CONTENTS

TABLE OF CONTENTS

TABLE OF CONTENTS

TABLE OF CONTENTS

TABLE OF CONTENTS

# Nomenclature

| Short | Meaning |
|---|---|
| **A** | surface area ($m^2$) |
| **$C_i$** | concentration of *I* (mol $L^{-1}$) |
| **d** | membrane thickness (m) |
| **I** | current (A) |
| **$D_s$** | diffusion coefficient ($m^2$ $s^{-1}$) |
| **R** | universal gas constant (J $mol^{-1}K^{-1}$) |
| **$A_S$** | electrode area |
| **Q** | flowrate ($m^3$ $s^{-1}$) |
| **T** | temperature (°C) |
| **V** | volume ($m^3$) |
| **W** | thermal power (J $s^{-1}$) |
| **V** | vanadium |
| **ρ** | density (kg $m^{-3}$) |
| **$E^0$** | standard electrode potential (V) |
| **i** | molar ionoc strength (moles $L^{-1}$) |
| **ΔG** | Gibbs free energy (J) |
| **S** | Entropy (J $K^{-1}$) |
| **U** | Voltage (V) |

# Constants

| Symbol | Description | Value (unit) |
|---|---|---|
| **F** | Faraday's constant | 96485 (C/mol) |
| **$N_A$** | Avogadro's constant | $6.022 \cdot 10^{23}$ ($mol^{-1}$) |
| **h** | Planck's constant | $6.626 \cdot 10^{-34}$ (Js) |
| **e** | Elementary charge | $1.6022 \cdot 10^{-19}$ (C) |
| **R** | Ideal gas constant | 8.3145 (J $K^{-1}mol^{-1}$) |

# List of Abbreviations

| Abbreviation | Meaning |
|---|---|
| **AC** | Alternating current |
| **AEM** | Anion exchange membrane |
| **CC Charge** | Energy input during charge (mJ) |
| **CC Discharge** | Energy output during discharge (mJ) |
| **CE** | Coulombic Efficiency |
| **CEM** | Cation exchange membrane |
| **Chg** | Charge (cycle) |
| **DC** | Direct Current |
| **Dischg** | Discharge (cycle) |
| **EE** | Energy Efficiency (EE = CE x VE) |
| **EMF** | Electromotive Force |
| **ESS** | Energy storage solutions |
| **VE** | Voltage Efficiency |
| **FB** | Flow Battery |
| **GHG** | Greenhouse gases |
| **ICP-AES** | Inductively coupled plasma atomic emission spectrometry |
| **IEA** | International Energy Agency |
| **IEC** | Ion Exchange Capacity |
| **J.** | Journal |
| **LTH** | Lunds Tekniska Högskola |
| **OCV** | Open circuit voltage |
| **PEM** | Proton exchange membrane |
| **PV** | Photovoltaic (cells) |
| **RAPSS** | Remote Area Power Supply System |
| **SOC** | State of charge |
| **UNSW** | University of New South Wales |
| **VRB** | Vandium Redox Battery |

# CHAPTER 1

## 1.1 Introduction

The all-vanadium redox flow battery (VRB), initially pioneered by Skyllas-Kazacos and coworkers at UNSW in the mid 1980's [1], is considered one of the most promising large-scale energy storage solutions (ESS) to be combined with intermittent renewable resources such as wind and solar energy and for load levelling in smart grid applications [1-3]. As the share of renewables continuously increases around the world it is imperative to implement large scale energy storage which will be discussed in chapter 2. Some of the key characteristics of the VRB is low cost for large storage capacities, long cycle life and easy maintenance and flexibility [4].

The VRB has already been installed around the world for wind energy storage, UPS, emergency backup, large PV-systems energy storage as well as remote area power supply system (RAPSS) applications. Another aspect of the VRB is the growing market of electric vehicles where the spent solutions could be recharged either through electrical recharge or instant mechanical refueling.

As with all types of batteries, the VRB may suffer capacity losses due to self-discharge reactions which take place as a result of the differential rate of diffusion of vanadium species across the membrane. Although this capacity loss can be restored by simply remixing the electrolyte periodically, it is desirable to minimize the frequency of remixing by using highly selective membranes with good long-term stability in the highly corrosive V(V) electrolyte.

The self-discharge reactions can also generate heat within the battery stack, so the permeability of the membrane will also impact on the thermal behavior of the battery, especially during standby periods when the pumps are turned off. The properties of the membrane are therefore critical in determining the cost, efficiency, capacity loss and thermal characteristics of the VRB. Although a number of commercial membranes is currently available for VRB applications, these are relatively expensive, so new materials are still being developed and tested as lower cost alternatives.

In order to understand the battery and its tradeoffs as well as to develop controllers for automation and to be able to optimize and test the technology in different harsh environments, very sophisticated models have been developed which describe the phenomena occurring inside the battery during charge-discharge cycling [1, 5-7]. These models can be used to automate and control the battery in order to maximize the energy efficiencies and to decide when to optimally rebalance the electrolytes to restore the initial capacity. However, these models are relying on experimentally determined diffusion coefficients which do not exist for many of the commercial VRB membranes in use today. Different experiments performed by different research groups may give severe fluctuations in the measured diffusion coefficients which will lead to large errors in computer based simulations. Depending on the choice of chemical analysis and experimental procedure, different results are obtained which leads us to the motivation for this study.

## 1.2 Motivation for this study

The membrane is one of the critical components of the VRB since it will affect not only the performance of the cell and its cycle life, but as one of the most expensive components of the system, the membrane will also affect the overall cost. Although several commercial membranes have been used in commercial VRB systems to date, most of these are relatively expensive, so significant effort is currently underway to develop and identify new lost cost membranes for the VRB. The focal point of this study therefore is to assess a number of new membranes that could be potential candidates for the VRB. These membranes are expected to be considerably cheaper than Nafion membrane currently used by several VRB producers. The aim is to determine and evaluate different properties of these membranes that are imperative for their application in the VRB battery.

Although experimental studies are useful in assessing the performance of membranes during short-term operation, mathematical modelling is also being used to predict the behavior of the battery during long term operation under different conditions and climatic environments. In order to run computer based simulations in different harsh environments and to optimize the battery operation however, reliable experimental data is needed which do not exist for many commercially available membranes today. As will be discussed in chapter 3, the experimental methods reported in literature vary considerably and give

different results. Therefore, this study goes through different phenomenon which may influence the diffusion coefficients experimentally. Based on this assessment, an improved experimental procedure is suggested and this was used to determine the permeability rates of vanadium ions across the FAP450, F930, GN-115 and VB2 membrane.

Also, several ion exchange membranes were further evaluated for their use in the VRB. These membranes were tested in an actual laboratory scale flow cell and their performance was determined in terms of energy efficiency (EE), coulombic efficiency (CE) as well as voltage efficiency (VE).

The experimentally determined vanadium permeability of each vanadium ion was then used in computer based simulations to determine capacity loss during extended use as well as in thermal models in order to evaluate the thermal behavior of a VRB system during charge-discharge operation and standby. The need for external heating or cooling under different climatic conditions can thereby be established. The results are also discussed and compared to the laboratory scale VRB results.

As the highly oxidizing V(V) electrolyte may severely oxidize membranes and materials used in the VRB, the suitability of the membranes for use in the VRB was also tested by evaluating their chemical stability in this electrolyte.

## 1.3 Aim and scope

In this study, the FAP-450, F-930, GN-115, GN-212, GN-212C and the VB1 membranes were evaluated for their use in the laboratory scale VRB. The F930, FAP-450, GN-115 and VB2 membranes were chosen to also be evaluated in a diffusion cell where the permeability rates for each of the vanadium ions were determined.

The diffusion rates for the F930, FAP450 and GN-115 were used in computer based simulations at extended charge-discharge operation of 60 cycles to predict capacity loss caused by differential diffusion of the vanadium ions across the membrane that leads to a build-up on one side of the cell and dilution on the other. These data were also used as parameters for thermal models which estimated the cell stack temperature and the tank electrolyte temperature after 5 days of operation.

## 1.4 Method of approach

Initially, a literature review was conducted to compile previous work and developments and also to get basic understanding of the battery itself. The major source of information and knowledge was mainly from different energy and membrane journals (Electrochem. Adv. Energy. Mater, J. Power Sources, J. Membr. Sci among other). As the aim of this project was to evaluate different membranes, different membrane technologies were studied and discussed initially. Most of the work was carried out in a laboratory at UNSW with inductively coupled plasma atomic emission spectrometry (ICP-AES) analysis as the main source of chemical analysis. Meetings with the rest of the research group at UNSW under Maria Skyllas-Kazacos was also a major source of inspiration and knowledge throughout this work.

## 1.5 Disposition

In order to place the VRB in a broader perspective, chapter 2 contains a brief introduction to energy politics, the history of energy and its use and government legislation regarding energy production and storage. Pros and cons regarding renewable energy sources are discussed and different large scale energy storage solutions are presented. The VRB is introduced as a possible contribution to energy management in a world where the growing share of renewables introduces new challenges to the energy sector where it is imperative to maintain harmony between the supply and demand.

Chapter 3 is the literature review and background section where the VRB technology is thoroughly presented. The battery is discussed in detail in different aspects such as its working electrochemistry, EE, CE, membrane permeability, membrane technology and cell stack configuration and maintenance. The purpose of this chapter is to give a broader knowledge of different problems and solutions for the VRB and its technology.

Chapter 4 is the experimental section which consists of detailed information regarding electrolyte preparation, cell stack and battery assembly and how the chemical analysis was conducted. The results of this study, which includes membrane evaluation at charge-discharge cycling and permeability rate measurements of different membranes, is compiled in chapter 5. Energy-, coulombic and voltage efficiencies are compiled for all membranes as well as the overall cell resistance. As different membrane thicknesses and characteristics

gives different results at different current densities and temperatures, the best membrane was discussed based on this relation.

Chapter 6 briefly discuss the mathematical models used for charge-discharge simulations. The parameters used for these computer based simulations were obtained for different membranes in this study and tested for extended charge-discharge operation for as much as 60 cycles in order to obtain the capacity loss after extended use. Chapter 6 also includes the thermodynamic simulations of the battery where the stack temperature as well as the tank temperature is discussed and evaluated based on the permeability of different vanadium ions and the surrounding temperature.

Chapter 7 consists of the conclusions of this study and a summary of the results (the best membrane for different current densities) as well as general trends in regard of CE, EE and VE. Furthermore, in the same chapter is also a discussion both regarding experimental results as well as simulations. Finally, ideas for future work is presented. All raw data from experiments are attached as appendices. With this disposition at hand, let us begin with an introduction to energy and electricity in order to understand where the VRB comes into play.

# CHAPTER 2

## 2.1 Introduction to energy reserves and electricity use and production

A safe and reliable energy delivery is imperative for modern societies in order to maintain high living standards as well as economic growth [8]. Needless to say, the use and supply of energy has powerful social and economic effects. Table 1 consists of a comparison between different countries and their respective energy use in kg oil per capita [9]. In poor countries, such as Sudan, the energy usage per capita is as low as 59 which is about 100 times lower compared to Sweden or Norway. Of course, the temperature in Sweden and Norway is lower compared to Sudan and a considerable energy usage is needed in colder countries for heating of houses which is not needed in Sudan. However, if Sudan was a rich country, it would have a quite severe energy usage for refrigeration units and air conditioning as is the case in Qatar where energy is cheap and readily available. Qatar uses 4 times more energy per capita compared to very cold and developed countries such as Norway and Sweden, and about 320 times more energy per capita when compared to Sudan.

*Table 1. Energy usage in kg oil per capita for different countries around the world. Data from Worldbank.org [9]*

| ***Country*** | ***Kg oil per capita*** |
|---|---|
| *Sudan* | 59 |
| *Nepal* | 370 |
| *Cambodia* | 396 |
| *Sweden* | 5132 |
| *Norway* | 6439 |
| *Qatar* | 19120 |

About 80% [8] of the total energy usage of the world in 2015 came from non-renewable resources but today, problems related to non-renewables have been recognized as they may face an array of severe challenges in the near future. Higher prices, global warming, military conflicts and depletion of reserves are just some of many issues related to these sources. However, with a growing concern about carbon emissions and greenhouse gases (GHG), government legislation has started to increase the use of renewable resources around the world.

The use of renewable resources increases the total domestic energy production which divides the country from being subject to severe price fluctuations which is the case with oil based electricity production. The price of oil has fluctuated heavily since 2004, as seen in Figure 1, and prices are believed to increase as the supply is diminishing [8]. Countries which rely heavily on imported oil are, inevitably, very vulnerable and exposed to serious economical threats if the prices would skyrocket as they did in 2008. In order to avoid these severe economic consequences, countries have to be prepared in a way that allows them to produce a certain amount of energy, a base-load, without being dependent on a functioning world economy and trade routes for fossil fuels [10, 11].

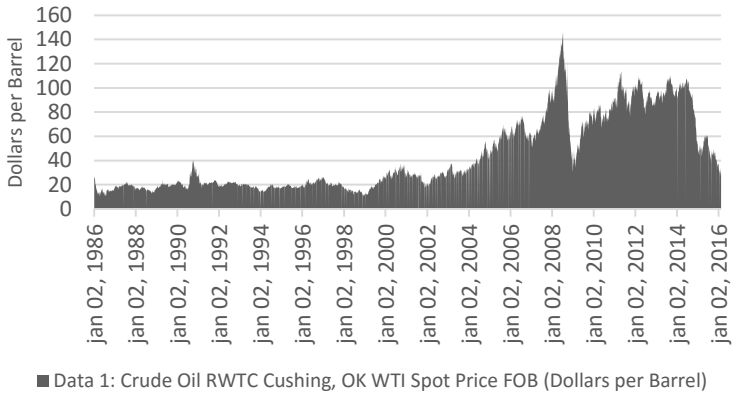


*Figure 1. Historical crude oil given in dollars per barrel since 1986 to 2016. [Source U.S. Energy Information Administration [10]]*

Even though the share of renewables continues to increase around the world, oil and coal maintain the major energy source for electricity production [12]. However, according to BP's Statistical Review of World Energy [12], this may not be the case in the future. According to that study, the overall consumption of renewables in the US and Europe has increased steadily since 2004 as seen in Figure 2.

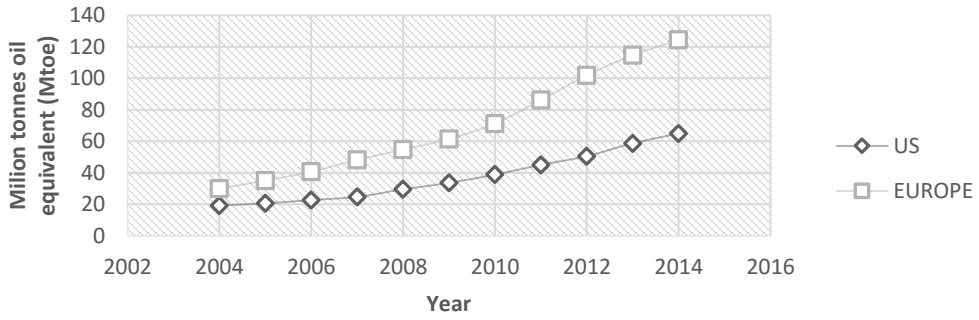


*Figure 2. Total usage of renewable energy in the US and Europe since 2004. Units given in Million tons oil equivalents (Mtoe)*

The aforementioned problems with non-renewables and greenhouse gases (GHG) have spread awareness among people which have further boosted the interest of renewable resources throughout the world. However, with an increased share of renewable resources, other problems start to appear. Such as how to cope with the intermittency of these sources in order to find the necessary harmony between supply and demand as discussed in [8, 11, 13]. In order to understand the importance of reliable electricity storage solutions, one has to be briefed regarding the nature of electricity.

## 2.2 Introduction to Electricity

The grid cannot store electricity, which is why electricity must be generated and consumed at the same time. Moreover, as the demand and use of electricity changes throughout the day, unbalances between supply and demand may occur which is highly undesirable. These unbalances can lead to a lower energy quality, temporary shut-downs and can damage electrical equipment connected to the grid. Lower power quality means voltage- and frequency variations, interruptions in service and low power factor.

According to the International Energy Agency (IEA) [14], about 100 MW wind power has to be backed up with 100 MW power from non-renewable resources in order to maintain grid quality and reliability. People of developed countries around the world are used to a functioning grid which offers a stable supply of energy when needed and if we want to maintain this standard and still use a larger share of renewables, large-scale energy-storage solutions must be implemented. The VRB, which is discussed in this study, is such an energy-storage system which can help mitigate the use of thermal spinning reserves and unlock the full potential of renewable resources by providing necessary storage capacity

[1-3]. Figure 3 visualizes how the electricity demand in Ireland follows a certain pattern during the day. However, the total wind farm energy production on all islands provides a severe intermittency and cannot cope with the actual demand at any point during the period from 24th Jan to 24th Feb 2016. Noteworthy is also the large peak on the 11th Feb when the wind-generated electricity produced was almost zero, which resulted in a large peak in carbon dioxide emission from the gas turbines from around the country. This behavior highlights the importance of increased renewable energy production in order to decrease our greenhouse gas (GHG) emissions. Furthermore, also from Figure 3, at February the 16th wind production increased to above 2000 MW which cut carbon dioxide intensity from production of energy to about 300 g/kWh from 550 g/kWh.

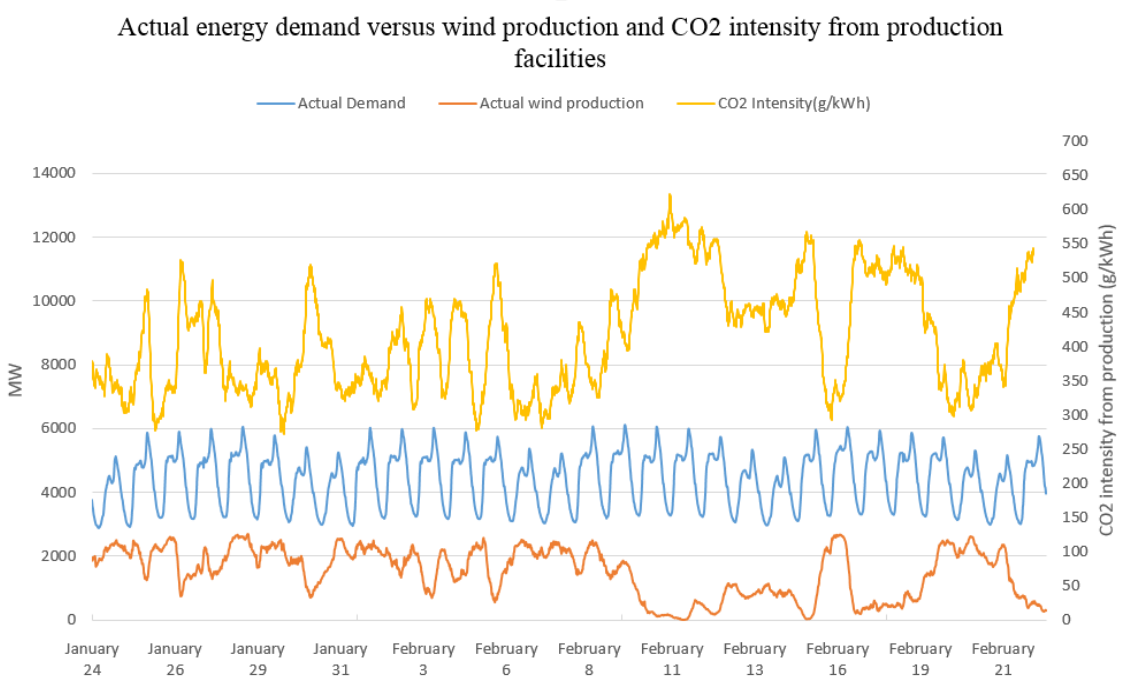


*Figure 3. Actual energy demand versus wind production in Ireland for 24 jan – 24 feb 2015 from actual measurements from Eirgrid. To visualize the relation between the carbon footprints from Ireland's energy facilities the CO2 intensity is plotted using the seconday Y-axes given in g/kWh. The average demand of electricity follow a pattern but the production from wind does not. Furthermore, if the wind production decreases, gas production facilities have to start produce electricity which gives a massive peak in carbon dioxide intensity. Data from Irish Grid company, Eirgrid.com [15].*

The demand for electricity changes due to a number of variables such as time of day, outdoor temperature and whether it is sunny or windy, to mention a few reasons. The same fluctuating behavior is noticed concerning the energy production from renewables as wind speeds may change and that could may interfere with photovoltaic (PV)- cell electricity

production. With these aforementioned problems, it is concluded that the fluctuating nature of renewables must be controlled in order to maintain high energy quality on the grid. Otherwise, it is impossible to maintain the necessary harmony between supply and demand when utilizing the power of wind- and PV cells. Needless to say, the world demands reliable and robust ESS units and the market has been estimated to 60 billion dollars [16].

### 2.2.1 Supply/demand mismatch

Today, these instantaneous variations in demand require backup generators to rapidly increase electricity production in order to cope with the vastly shifting load. A quick response time of the generation unit is therefore important as the supply may quickly change. Rapid changes usually causes the oil- or gas based electricity generation to run at low efficiency (some gas turbines run at energy efficiencies as low as 30% [17]) and high emission of pollutants [14]. The power from these generators is very expensive, but flexible; therefore, these generators are quickly shut off when the peak period is over. Once again, as the VRBs offer quick response times and high round-trip efficiencies it can very well be integrated in smart grids to cope with these peak-hours at the grid [14]. The VRBs can also act as a buffer, which could be used to store cheap electricity harvested at off-peak periods. The stored energy can later be resold during peak-hours in order to profit from price differentials. This would also decrease the stress on the base-load applications as usage would be averaged out through the day and night. Therefore, the peaks would not be as severe as indicated in Figure 4. This is only one of many uses of the VRB. However (as seen in Table 2), most VRBs are installed to help maintain energy quality output from PV-farms or windfarms and based on recently government legislations, the amount of energy from these renewable resources will definitely increase.

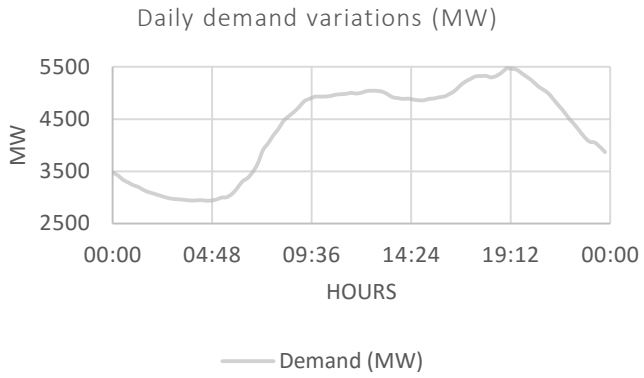


*Figure 4. Daily electricity demand versus time of day. Low-peak is observed during night time with a slight rise from 05.00 hours to decay during midday with a highest top at about 20:00 hours. Electricity prices vary with demand and peak hours is covered with inefficient gas turbines in general. The graph was made from data from the 23th of Mars 2016 from Eirgrid.com [15].*

## 2.3 The future of renewable resources and the necessity of reliable energy storage solutions

The European Union voted through a directive in 2009 in which regulations promotes the use of renewable resources [18]. Under the Climate Change Act from 2008, the UK government sets out to cut 34% of carbon dioxide emissions compared to the levels of the 1990s to the year 2020. Furthermore, the government of Scotland have been discussing to aim for 100% of electricity from renewable energy by 2020 [17]. With today's growing trend and beneficial government supports, the installed wind power capacity is believed to reach a level of 230 GW in 2020 which will represent about 25% of the total energy production capacity in EU according to the annual report of the European Wind energy Association [19]. In the same report, it is assumed that this amount will account for about 16% of the total electricity demand in the EU by 2020.

Energy production from renewable sources has increased enormously throughout the world [12]. Today, large amounts of energy can be produced during fruitful weather. In a recent study by Muneer et al. [8], a total solar photovoltaic farm of 61km$^2$ (accounting to 0.005% of the total areal of Gobi desert) would be sufficient to cover China's expected total energy demand in 2020. According to the same study, China is also one of the frontier countries in the change to renewable resources, increasing its total generated amount of energy from renewables by approximately 25% annually [8]. Nevertheless, renewable energy production is not fully reliable due to its intermittency. The hard task to control and predict

the output from wind farms and PV cells, for example, brings concern about its reliable operation, which is why integrated ESS units should be standardized at wind farms. Otherwise, a total energy input share of 10-25% of renewables to the grid could lead to power system instability and as mentioned before, 100 MW of wind energy will have to be backed up with 100 MW of fossil fuel to maintain stability. If the share of wind power is to increase even further, there is no other way than to increase the storage capacity [8, 20]. Figure 5 visualizes the problems which have to be dealt with in order to increase the use of renewable resources.

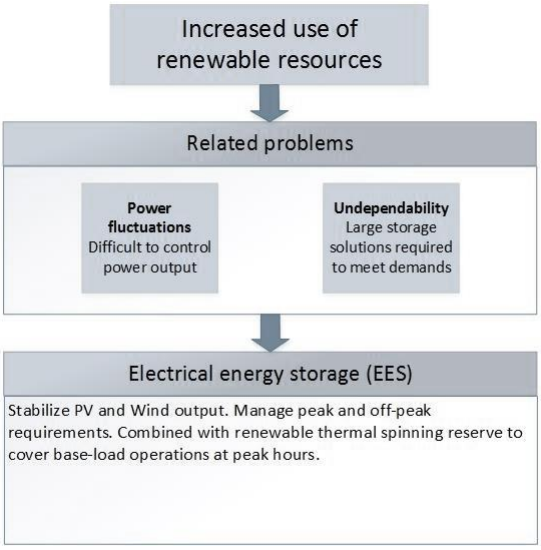


*Figure 5. Problems related to an increased amount of renewable resources such as fluctuations and undependability which can be controlled by using electrical energy storage solutions.*

Needless to say, to mitigate the use of a thermal-based spinning reserve and to realize and release the full potential of renewable resources, the intermittency has to be controlled by means of consistent and reliable ESS solutions so that the supply can better meet the demand. In other words, energy must be stored and used when it is needed. With such solutions (which do exist, as we will see in the next section), renewables could be considered as base-load electricity [3, 8, 20].

## 2.4 Energy Storage Solutions

There are several different energy storage solutions on the market. Depending on capacity, efficiency, response time and power output, these sources have different uses and different markets. There are three major classifications that are at the forefront in the search for

useful energy storage solutions. These include; electrical (super capacitators and Superconducting magnetic energy storage (SMES)), mechanical (flywheels, compressed air, pumped hydro) and electrochemical (hydrogen production, flow batteries and batteries) storage systems. The pumped hydro facilities correspond to about 98% of the total energy storage solutions in the world and summarizes to 75 GW [14], which is about 3% of the global generation capacity. Hydro facilities have provided reliable and large scale energy storage for a long time but appropriate locations for these large installations are seldom found today [12, 16].

### 2.4.1 Introduction to flow batteries in general and the VRB in particular

Flow batteries (FB) use two soluble redox couples to convert electricity into chemical energy during charge and to convert chemical energy to electricity during discharge. During discharge, the redox reactions taking place at the inert electrodes exchange electrons with each other which generates a flow of electrons through the external circuit – a current. The battery typically consists of two external electrolyte storage-reservoirs from which the electrolytes are pumped to a cell stack using pumps. Figure 6 represents a simplified FB setup. Inside the cell stack (which comprises an anode, cathode and a membrane) the redox reactions occur which generate electricity. The reactions occur at the surface of the inert electrodes and the membrane keeps the active electrolytes from mixing but allows charge-balancing ions to pass through to complete the circuit. FBs have lower current densities compared to solid-state batteries such as the lithium ion battery. However, as there are severe safety issues associated with most solid state batteries, they are not suitable for large scale applications. This is one of many reasons to why a lot of interest has been directed towards the inherently safe FB technology [21].

In order to provide the reactions in the FB's with a surplus of mobile protons, the supporting electrolyte is usually a strong acid such as sulfuric acid. There are several different FBs which are based on different active components such as all-vanadium, iron/chromium, iron/titanium and polysulfide/bromine. FB's are interesting as they can be easily modified in contrast to usual batteries such as the Lithium-ion battery. Capacity, for example, is easily adjusted in FB's to meet the demand by simply increasing the electrolyte volume in the external reservoirs. The power is controlled by the amount of cells inside the

cell stack. These batteries can therefore be freely designed to meet capacity (kWh) and power (kW) requirements which makes them suitable for large scale energy storage solutions [20, 2].

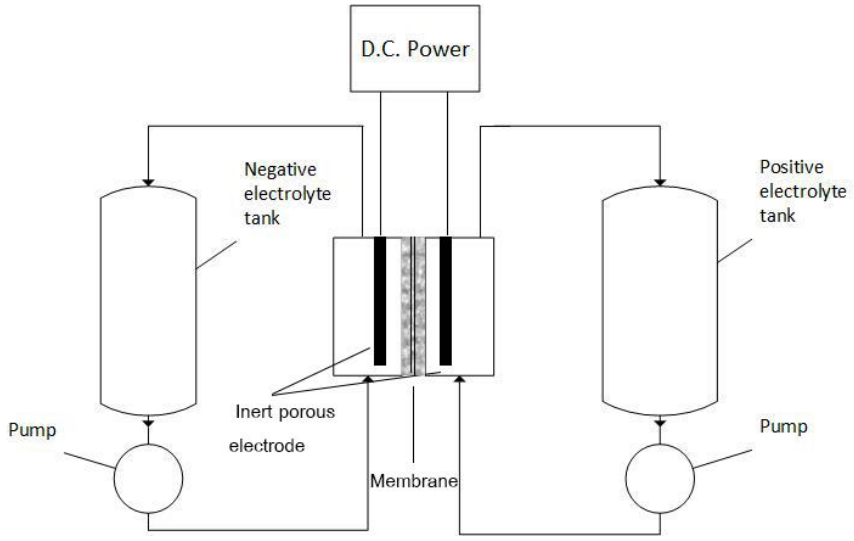


*Figure 6. Typical FB set-up with two external electrolyte storage tanks, two pumps, two porous electrodes and a membrane*

The cell stacks can be freely designed to meet the necessary voltage requirements by placing a number of cells in parallel and/or in series. Figure 7 shows a simplified cell stack configuration, which consists of two endplates, two flow frames with two carbon felts, one membrane and two current collectors. The endplates provide the necessary pressure to squeeze the rubber gaskets together in order to prevent leakage. Rubber gaskets are not visualized in Figure 7 but are nevertheless present in between each and every compartment.

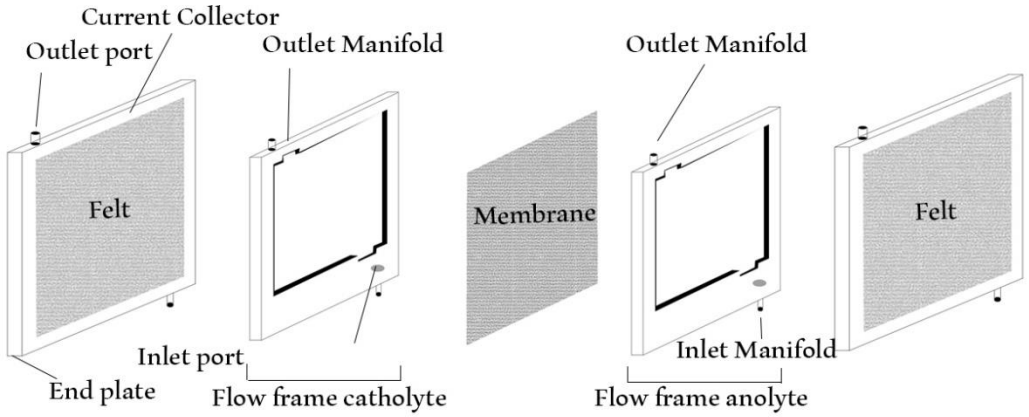


*Figure 7. Components of a VRB cell stack. Not visualized in the figure are the rubber gaskets which are placed between each compartment in order to decrease the risk of leakage.*

The VRB is believed by many to be a possible grid-scale storage solution as these batteries offer quick response time, long cycle life, pollution-free energy, high round trip efficiency and easy load-shifting abilities [2, 20, 22]. An ideal solution, visualized in Figure 8, for wind farms is to be combined with VRB in order to control the output and maintain harmony between supply and demand. Although batteries cannot store enough energy in order to fully cover the energy demands of a country, it will play an important role in stabilizing grid fluctuations, meet peak demands and act as a buffer for the increasing amount of wind- and solar power around the world. The VRB will be discussed in detail in the following chapter.

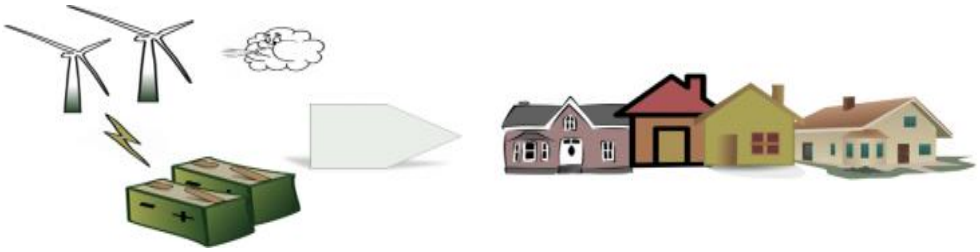

*Figure 8. Wind Park complemented with a VRB battery is a useful way to realize the full potential of renewable energy solutions which could help to mitigate the use of a thermal spinning reserve.*

# CHAPTER 3

# LITERATURE REVIEW

# AND THEORETICAL BACKGROUND

## 3.1 The working principles of the Vanadium Redox Flow battery

The all-vanadium redox flow battery (VRB), initially pioneered by Skyllas-Kazacos in the mid 1980's, is considered one of the most promising large-scale energy storage solutions (ESS) to be combined with intermittent renewable resources such as wind and solar energy due to its simplicity, high energy efficiencies (above 80% in large installations) and long cycle life [1-3].

The major difference between the VRB and other FBs discussed in section 2.4.1, is that the VRB uses the same active component in both half-cells, which diminishes the often severe and irreversible chemical reactions that can occur as cross contamination take place in other types of flow batteries [1, 23]. In order to reestablish the capacity which has been lost due to vanadium movement through the membrane, the electrolytes of the VRB can be remixed and then recharged. The ability to restore the capacity provides the VRB with almost unlimited cycle life and also a competitive price [1, 23]. This feature among others make the VRB a lot more interesting than the other FBs on the market.

The membrane inside the cell stack is an important component in the VRB and is subject to much research around the world. For a membrane to be suitable in VRB applications, it has to meet the following characteristics: (1) low permeability of vanadium ions (2) excellent chemical stability and structure (3) low electrical resistance (4) high permeability for charge-carrying ions such as $H^+$ and/or $HSO_4^-$ and (5) low cost. Usually, ion exchange membranes (IEM) are used in VRB applications, in particular, the cation exchange membrane called Nafion® by DuPont™. The membrane will be discussed in detail in the membrane section.

The Generation 1 VRB technology, which uses a solution of vanadium in sulfuric acid with V(II)/V(III) and V(V)/V(IV) redox couples operating in two separate half-cells, has been

developed and proven since 1984 and offers quick response time, long cycle life, pollution-free energy, high round-trip efficiency and easy load-shifting abilities [2, 20, 22]. The battery has been installed and proven at a grid scale with capacities on MW/MWh scale as compiled in Table 2 [13, 24].

| Company | Year | Country | Use | Power/ capacity | Ref |
|---|---|---|---|---|---|
| Sumito Electric Industries (SEI) | 2005 | Japan | Wind energy storage and wind power stabilization (Subaru Wind Farm) | 4MW/6MWh | [1] |
| VRB power, Eskom | 2001 | USA | | 250kW/500kWh | [14] |
| Pinnacle VRB | 2003 | King Island | Wind energy storage and diesel fuel replacement | 250kW/1MWh | [1] |
| SEI | 2003 | Japan | UPS/peak shaving | 500kW/2MWh | [1] |
| Redtenergy | | Isle of Gigha, Scotland | Balance variable generation from renewable sources and time shifting, peak shaving and load leveling, backup power supply & replacement of diesel generators, Electricity arbitrage (trading) | n.a/1.68MWh | |
| VRB power, Hydro Tasmania | 2003 | King island | Wind energy storage and diesel fuel replacement | 200kW/800kWh | [14] |
| SEI | 2001 | Japan | Totori Sanyo Electric load leveling and peak shaving | 3MW/1.25kWh | [14] |

*Table 2. Installations of the VRB battery with different power- and capacity requirements around the world. n.a.: not available*

Enormous progress has been made in recent years, which has made the VRB systems fully prepared for market establishment and commercialization in areas ranging from large-scale ESS to load-levelling applications. In some aspects (such as the use in electric vehicles) the G1 VRB does not have sufficient energy density. Flow batteries are potentially excellent candidates for electric vehicle applications due to the possibility of instant recharge in situ by replacing the used liquid electrolytes with fully charged ones [25]. Nonetheless, for this to become reality, the energy density of the VRB must be increased.

The Generation 2 (G2) VRB, or the vanadium bromine redox flow battery (V/Br) utilizes bromine/chloride combined with vanadium in both half-cells which increases the solubility of vanadium from about 1.6M to about 3-4 M which, could double the energy density of the battery [26]. The G2 V/Br requires the use of special bromine complexing agents to prevent formation of hazardous bromine vapors however and although these are very

effective, their current high cost makes their use impractical. New low cost bromine complexing agents are therefore needed and this is the focus of current research.

## 3.2 The electrochemistry and working principles of the VRB

The VRB stores energy by utilizing the four different oxidation states of the vanadium ion in two separate electrolyte tanks. The VRB employs a V(II)/V(III) sulfate solution at the anode side and a V(V)/V(IV) sulfate solution at the cathode side. Just as with the other FBs, the cell stack consists of a membrane that keeps the electrolytes from mixing but allows cations or anions (depending on the type of membrane) to pass through to complete the cycle and to balance the charge. Furthermore, each half-cell also consists of one porous conducting electrode, which is in contact with the membrane inside the flow frame as seen in Figure 7. The porous electrode provides a large surface area for the redox reactions to occur and also forces the electrolyte to disperse homogeneously across the full area of the flow frame, which ensures uniform current distribution for efficient operation. A more in depth illustration of the working principles of the VRB battery is visualized in Figure 9. The green arrow indicates the charge carrying ions which move through the membrane in order to complete the circuit. Furthermore, the pumps provide the cell stack with electrolytes and reactants in order to maintain the load. The V(x) diffusion arrow, indicated by the pink color in Figure 9 indicates the cross-diffusion of vanadium ions which will lead to capacity drop. This will be explained in detail in the following sections.

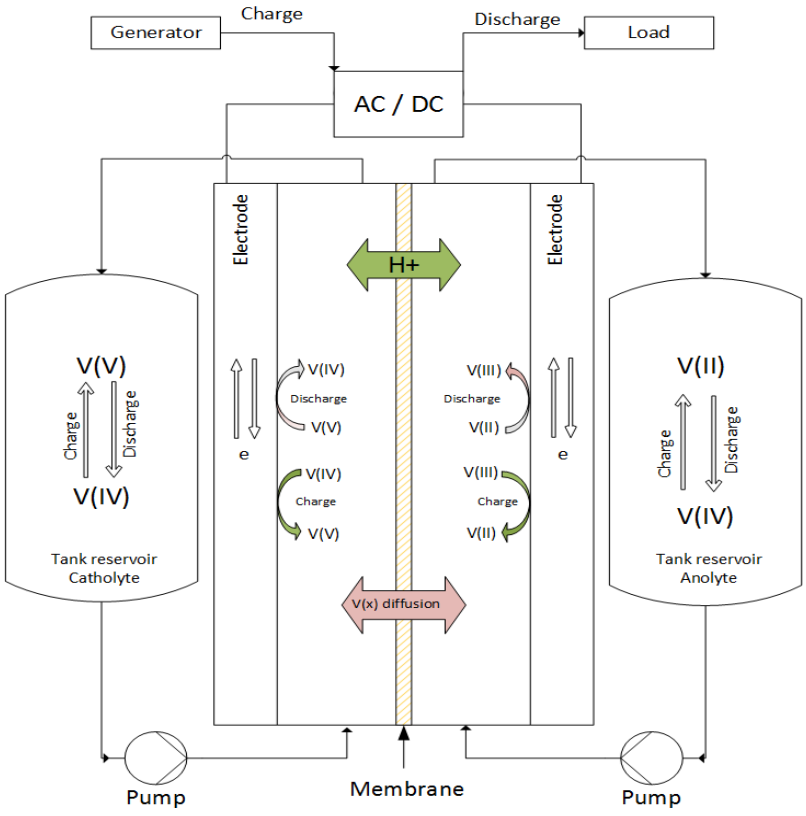


*Figure 9. Operating principles and configuration of a VRB battery. The V(x) diffusion double arrow illustrates the cross-diffusion of different vanadium ions through the membrane during charge- and discharge. The H+ double arrow indicates cross diffusion of protons in order to maintain charge balance between the electrolytes.*

In contact with the porous graphite felt electrode is often an inert graphite sheet which conducts electricity but keeps the copper current collector protected from the corroding effect of the electrolytes. If the current collector is subject to severe oxidation, the resistance will increase, which will lower the overall efficiency. The current collector conducts electrons generated from the redox reactions, which occur at the surface of the porous electrode.

The electroactive species are fully dissolved in sulfuric acid (which acts as supporting electrolyte) to provide a large source of mobile hydrogen ions needed as charge carriers to complete the cycle. The electrolytes are pumped to the cell stack where the redox reactions occur which generate electricity. The vanadium oxides have different colors so when the battery is charged or discharged, it changes color according to the colors in Figure 10.

*Figure 10. 1-2M of V(V) (yellow), V(III) (green), V(IV) (blue) and V(II) (purple) in 2.5-5M sulfuric acid.*

During charge and discharge, the electrolytes are pumped to the cell stack where the redox reactions (1) and (2) occur which generate electricity [14]. To complete the electrical circuit and stoichiometry between the electrolytes, charge-balancing ions (such as $H^+$, $HSO_4^-$ and $SO_4^{2-}$ depending on the membrane used) have to move through the membrane and water ($H_2O$) has to be present in the cathodic reaction. Reaction (1) and reaction (2) occur in the left direction during charge and in the reverse direction during discharge and the concentrations change as compiled in Table 3.

$$VO_2^+ + 2H^+ + e^- \rightleftharpoons VO^{2+} + H_2O \quad E^0_{cathode} = 1.0 \qquad (1)$$

$$V^{2+} \rightleftharpoons V^{3+} + e \qquad E^0_{anode} = -0.255\ V \qquad (2)$$

Equation (3) represents the overall electrochemical cell reaction retrieved by combining (1) and (2) which results in a total electromotive force (EMF) of about 1.26 V.

$$VO_2^+ + 2H^+ + V^{2+} \rightleftharpoons VO^{2+} + H_2O + V^{3+}\ E^0 = 1.255\ V \qquad (3)$$

State of charge (SOC) indicates the amount of energy stored in the battery and it is calculated using equation (4), according to [14].

$$SOC = \left(\frac{C_{V^{2+}}}{C_{V^{2+}} + C_{V^{3+}}}\right) = \left(\frac{C_{VO_2^+}}{C_{VO^{2+}} + C_{VO_2^+}}\right) \quad (4)$$

where $C_V^{2+}$ is the concentration of divalent vanadium and $C_V^{3+}$ is the concentration of the trivalent vanadium species. At 100% State of Charge (SOC) the negative and positive half-cell electrolytes consists only of pentavalent, V(V), and divalent vanadium, V(II), ions respectively. Moreover, at 0% SOC, the negative electrolyte consists of only trivalent vanadium, V(III), ions and the positive electrolyte consists of only tetravalent vanadium ions, V(IV). The concentration change is as indicated in Table 3.

The SOC can be monitored by measuring the open circuit voltage (OCV) between the half-cells through electrodes at the inlets and outlets respectively by using an open-circuit voltmeter [27]. As with all batteries, the VRB can suffer capacity loss due to many different phenomena such as gassing side reactions, air oxidation of $V^{2+}$ ions and the differential transfer of vanadium ions across the membrane. This is why many researchers now focus on developing mathematical models that can predict these phenomena during charge and discharge of the battery in order to develop reliable and refined VRB controllers [5, 20, 28].

*Table 3. Visualization of how the concentration of the different Vanadium ions change during charge and discharge cycling.*

| | | **Concentration change during** | |
|---|---|---|---|
| **Ion (salt)** | Electrolyte | Charge | Discharge |
| **$V^{2+}$ ($VSO_4$)** | Anolyte | ↑ | ↓ |
| **$V^{3+}$ ($V_2(SO_4)_3$** | Anolyte | ↓ | ↑ |
| **$V^{4+}$ ($VO^{2+}$)** | Catholyte | ↓ | ↑ |
| **$V^{5+}$ ($VO_2^+$)** | Catholyte | ↑ | ↓ |

The performance of the VRB is usually correlated to the EE of the battery, which is a combination of the CE and the VE. The CE is the ratio of the withdrawn charge during discharge and the supplied charge during charge, according to (5) [14].

$$CE = \frac{Q_{discharge}}{Q_{charge}} \cdot 100\% = \frac{\int_0^{t_d} I_{discharge}\, dt}{\int_0^{t_{ch}} I_{charge}\, dt} \cdot 100\% \quad (5)$$

where $Q_{discharge}$ is the withdrawn charge at discharge, $Q_{charge}$ is the supplied charge during charge, $t_d$ is the discharge time and $t_{ch}$ is the charge time. If vanadium ions travel through

the membrane and thus avoiding electrochemical reactions which produces electricity they decrease the capacity of the battery. Therefore, these non-electrochemical self-discharge reactions also decrease the CE and these reactions are explained in detail in the self-discharge in section 3.4.1.

A value of the CE of 100% indicates zero permeability of vanadium ions through the membrane and no side reactions. The permeability rate is mainly correlated to the membrane selectivity as the membrane should be able to isolate the active vanadium ions while still allowing charge-balancing ions to move [26].

Furthermore, the VE is calculated by the ratio of the mean discharge voltage $\bar{U}_{dis}$ and its mean charge voltage $\bar{U}_{charge}$ over the whole discharge/charge cycle respectively. $U_{discharge}$ can be represented as $U_{discharge} = E - \Delta U_{activation} - \Delta U_{ohmic} - \Delta U_{masstransport}$ where E is the theroretical OCV, $\Delta U_{ohmic}$ is ohmic losses associated with membrane, electrode and electrolyte resistances, $\Delta U_{masstransport}$ is voltage loss due to mass transfer and $\Delta activation$ is due to activation energy losses associated with the kinetics of the electron transfer reactions. The VE is given by equation 6.

$$VE = \frac{\int_0^{t_d} U_{discharge} dt}{\int_0^{t_c} U_{charge} dt} \cdot 100\% = \frac{\bar{U}_{dis}}{\bar{U}_{charge}} \cdot 100\% \quad (6)$$

the EE is governed by the product of CE and VE according to equation 7.

$$EE = CE \cdot VE \quad (7)$$

The EE is thus affected by both the CE and the VE and as the CE and VE tends to change with relation to current, an optimal current can be determined experimentally but can also be obtained through mathematical models as will be seen in chapter 5.

## 3.3 The ion exchange membrane

It is hard to emphasize enough, the purpose and impact of the membrane selectivity and function in a VRB. According to Tang et al [5] (among others [23, 29, 30]) it is named the most critical component in the VRB. The main purpose of the membrane, as visualized in Figure 6, is to separate the positive and the negative electrolytes and to complete the electric circuit by allowing charge-carrying ions to pass through. The most important characteristics of the IEMs [31] in VRB are listed below and will be discussed in detail in the following paragraphs:

(1) Low permeability rates of vanadium species in order to maintain high CE as self-discharge reactions will occur if any cross-over takes place.

(2) Very high ion conductivity for easy movement of charge-balancing ions to reduce losses in VE.

(3) Excellent chemical stability in acidic environments and in the presence of the strong oxidizing $VO_2^+$ electrolyte.

(4) Low cost as the membrane can contribute to a large extent of the overall costs of the battery

(5) Prevent the preferential transfer of water as this would lead to dilution of one electrolyte and higher concentrations in the other which may lead to precipitation of vanadium and flooding of one of the electrolyte reservoirs.

(6) Low area resistance to prevent voltage losses and maintain high energy efficiency.

Needless to say, the membrane is the key material in the VRB as it heavily influences the performance- and economic viability of these ESS systems and a good membrane will provide the battery with long periods in between maintenance [21, 26, 32].

Even though some membranes such as the Selemion AMV [5] offer low vanadium transfer rates, the diffusion of vanadium ions cannot be completely controlled. This is due to the concentration gradient across the membrane which, unavoidably, will lead to diffusion of vanadium ions and water across the membrane and, consequently, also a capacity loss after a certain number of charge-discharge cycles [6]. This capacity loss is easily controlled by remixing of the electrolytes after a number of cycles.

New membranes that are cheap and still meet the aforementioned requirements with high proton conductivity and low permeability rates for vanadium ions are subject to intensive research around the world. Some already determined and available diffusion coefficients from literature for a number of membranes have been compiled in Table 4. Different membranes have been studied very extensively both in regard of chemical stability and structural integrity but also with regard to vanadium crossover by the group of Skyllas-Kazacos at UNSW, Australia, since early versions of the Generation 1 VRB [23, 27, 29].

### 3.3.1 Different types of membranes

There are different types of IEMs on the market and many different membranes have been evaluated for the use in G1 VRB systems since 1984 [23, 30, 33-35]. IEM membranes are usually tubes or sheets which separate two liquids but allow anions or cations to pass through. If anions are allowed to pass through, the IEM is referred to as anion exchange membrane (abbrev. AEM) and if cations are allowed through it is referred to as cation exchange membrane (abbrev. CEM).

These membranes differ depending on its functional groups, which influence the movement of different ions. The CEM membranes (N115®, N117® by DuPont™), allow passage of cations such as protons and consists of negatively charged functional groups such as $-SO_3^-$ or $-COO^-$ among other. Proton-exchange membranes (PEMs) are used in VRB applications where protons are used to carry the charge and complete the circuit. PEMs offer low ohmic losses as the sulfuric acid electrolytes are highly proton conductive. AEM (Selmion AMV®, *Asahi Glass, Japan*) allow anions such as the charge-balancing $HSO_4^-$ present in the VRB to move through the membrane while repelling the vanadium ions and the protons due to a membrane phenomenon known as the Donnan exclusion effect. Previous anion-exchange membranes, such as the Asahi Glass' Selmion Series (AMV, DMV, ASS, CMV), have not proven ideal with regard to long-term stability and have to be improved considerably before they can become interesting in VRB applications [26, 36]. AEMs consists of positively charged functional groups such as $-NH_3^+$ or $-SR_2^+$ which can repulse vanadium cations.

AEMs have superior ion selectivity and will suffer only little from vanadium crossover when compared to CEMs. However, as the AEMs also have poor proton conductivity,

higher current densities give low VE when using this type of membrane. Further, as mentioned before, the earlier AEMs could not withstand the corrosive environment present in the VRB batteries which is why perfluorsulfonic acid based CEMs have been the dominating membrane for use in VRB applications today [37].

### 3.3.2 Membrane materials

IEM membranes are very different in how they are constructed and developed. So called *Pore filled* IEMS receive their mechanical stability through a cheap but chemically resistant porous support material such as polypropylene (PP) or Daramic (W.R. Grace). The ion exchange of the membrane is controlled by the ion exchange resins (any polymer with ion exchange functional groups) coated on top of the support material.

According to a recent study by Li et al in [29], most of the commercial VRB's employ sulfonated fluorocarbon copolymers such as the cation exchange membranes called Nafion® series by DuPont™ with a thickness of about 100-150μm. These membranes have superior chemical and structural integrity in the strong acid solutions which are present in the VRBs as well as a high proton conductivity making it a suitable membrane for the use in VRBs. The structure consists of a hydrophobic, tetrafluoroethylene (Teflon), backbone which provides excellent structural integrity and chemical strength to the membrane. Hydrophilic sulfonated groups are attached to the Teflon backbone and ensures high ion exchange capacity (IEC) [37]. However, according to a recent study by Dongyang *et al*., the water uptake and swelling ratio increased with increasing IEC due to the high hydrophilicity of these membranes [21]. Therefore, there is a trade-off in IEC and EE which has to be considered.

However, the Nafion membranes are expensive and is, according to Schwenzer et al., in [31] accountable for 11% (Priffi et Al state costs up to 20% [26]) of the total cost of a 1MW/8MWh system and about 41% of the total cost of the cell stack [38]. These membranes also suffer from drawbacks such as relatively high vanadium permeability as compiled in Table 4. The vanadium permeation can be decreased by hybridization with other components and is subject to much research [21, 37].

### 3.3.3 Chemical stability and structural integrity

The low pH of the VRB (often 0.1-0.5) combined with the strong oxidation potential of the $V^{5+}$ ions puts serious pressure on the materials used inside the battery due to the harsh conditions present [31]. The batteries often have 1-2 M vanadium species dissolved in 2-5 M sulfuric acid which makes many membranes which are used in fuel cell applications and alike, unsuitable for use in the VRB [31].

It is important for the membrane to have a high structural integrity as any swelling may increase the pore size and therefore also the cross-mixing of vanadium ions. Furthermore, to develop batteries with long cycle-life it is imperative to have membranes with lifetimes of several years as a minimum threshold. Of course, other materials used in the VRB other than the membrane must also be very stable to cope with the electrolytes. This will be discussed in section 3.4.2.

### 3.3.4 Vanadium permeability

As the diffusion of protons through the membrane is imperative to complete the circuit in order to receive high voltage efficiencies, mostly CEM are used in the VRB. However, these membranes are not very selective and will therefore also allow vanadium ions to diffuse through, which is highly undesirable as this will decrease the coulombic efficiency of the battery as well as increase the temperature of the electrolytes due to the exothermic self-discharge reactions [31]. These reactions are explained in detail in the self-discharge section 3.4.1.

### 3.3.5 Preferred water transfer

In order to maintain high overall operation of the cells, the membrane should also impede the preferential transfer of water from one electrolyte to another as this would lead to flooding and dilution of one electrolyte and higher concentrations of the other and hence increasing the risk of irreversible precipitation of vanadium ions. As the water changes the concentrations of the electrolytes, it also changes the complex thermodynamics of the liquids, which may influence the solubility of the different vanadium species. Therefore, preferred water transfer may present a risk for vanadium precipitation. However, any imbalance between the electrolytes will also lead to capacity losses.

The cause of water transfer through the membrane itself is manifold with different phenomena such as transport of water molecules to alleviate concentration gradients (osmosis) between the two electrolytes as well as water molecules being dragged through the membrane with ions that are allowed to pass through. The direction of the water transfer is dependent on the type of membrane used and may change during different SOC [31]. In general, however, a difference in net transfer of water can be seen when comparing anionic- and cationic membranes. For anionic membranes (such as the Selmion AMV), the preferred water transfer is toward the $V^{2+}/V^{3+}$ side while cationic membranes tend to have water transfer toward the $V^{5+/}V^{4+}$.

### 3.3.6 Permeability of charge-carrying ions

While trying to impede vanadium crossover it is important to maintain high conductivity of the charge-carrying ions as this will increase the voltage efficiency of the VRB and thus also the EE. Zero vanadium crossover would maximize the CE of the battery and the highest possible proton conductivity would maximize the voltage efficiency [31].

## 3.4 Technical challenges with the VRB

### 3.4.1 Self Discharge

Self-discharge reactions occur as a consequence of the transport of vanadium ions through the membrane and leads to a subsequent decreased CE) and to an increased electrolyte temperature due to the self-discharge reactions being exothermic [39]. In the positive half-cell the diffusing divalent and trivalent vanadium ions participate in reactions (8) – (10) below

$$V^{2+} + 2V^{5+} \rightarrow 3V^{4+} \quad (8)$$

$$V^{3+} + V^{5+} \rightarrow 2V^{4+} \quad (9)$$

$$V^{2+} + V^{4+} \rightarrow 2V^{3+} \quad (10)$$

while in the negative half-cell reactions (11) – (13) occur as pentavalent and tetravalent vanadium species diffuse through the membrane.

$$V^{5+} + 2V^{2+} \rightarrow 3V^{3+} \quad (11)$$

$$V^{4+} + V^{2+} \rightarrow 2V^{3+} \quad (12)$$

$$V^{5+} + V^{3+} \rightarrow 2V^{4+} \quad (13)$$

Skyllaz-Kazacos research group at UNSW identified the problem of self-discharge reactions and cross-mixing of vanadium ions at an early stage of the development of the VRB and have proposed different anion and cation membranes and treatments in order to control the amount of vanadium cross-contamination [28, 30, 33, 40].

### 3.4.2 Material degradation

The cycle life of the VRB is limited by the stability of the positive electrode as well as the membrane employed in the cell stack. Except from a very acidic environment due to the high content sulfuric acid in the electrolytes, the battery also consists of highly oxidizing V(V), which may cause severe deterioration of materials inside the battery. Therefore, one of the biggest challenges with the IEMs is the balance between oxidation stability and ion conductivity [41]. Previous studies by Sukkar et al. [42] have discussed how membranes may suffer physical degradation, loss of ionic exchange capacity (IEC), poisoning and/or replacement of functional groups and fouling from precipitating vanadium ions and the importance of good chemical stability for the long-term stability of the VRB. The deteriorating effect of the V(V) is apparent and could be very challenging unless the membranes show excellent chemical- and structural integrity [42]. As a general procedure of Skyllas-Kazacos and co-workers at UNSW, membranes which provide low permeability for vanadium ions are immersed into V(V) solution and kept there for a number of months (or years) in order to measure any weight loss and changes in length, width and thickness.

### 3.4.3 Energy density of the VRB and vanadium solubility

In order to give the VRB a broader use, such as the use in electrical vehicles, the specific energy density (Wh/kg) has to be increased. This would also decrease the material cost of the battery. One way is to increase the solubility and thermal stability of the active species in the supporting electrolyte. A characteristic G1 VRB (up to 2M) have a specific energy of about 20-25Wh/kg (about 67.5% of the energy density of a typical lead-acid battery [14]) and operate in a temperature interval between 10-40°C [27, 43-44]. Higher concentrations than 2M of vanadium ions in the solution may cause irreversible precipitation, which leads to a decreased capacity and fouling of the membranes [2, 13, 22, 45].

In order to understand why the vanadium precipitates due to temperature changes and/or concentration, it is necessary to understand which ions are being dealt with. In the case of the VRB, the task to understand the thermodynamics of the electrolytes is even harder as the different vanadium ions can form many different complexes when dissolved in sulfuric acid. These ions depend on the pH, temperature and concentration and have different stability as reported in [46]. The $V^{5+}$ for example, has been reported by Kausar et al. [47] to exist as $VO_2^+$, $VO_2SO_4^-$, $VO_2(SO_4)_2^{3-}$, $VO_3^-$, $VO_2HSO_4$, $VO_2(HSO_4)_2^-$, $V_2O_3^+$ and $V_2O_4^{2+}$ in sulfuric acid. Preferential water transfer leads to changes in concentration and may cause precipitation. Therefore, it has to be controlled by selective membranes.

In order to achieve the highest solubility of *all* vanadium ions, present in the solution, one has to be considerate to the different effects of higher and lower acidic strength between the vanadium ions. For example, the risk of thermal precipitation of V(V) was found by Skyllas-Kazacos et al. [46] to decrease with higher acidic concentrations. On the other hand, the stability of V(III) did instead decrease with higher acidic concentrations in the electrolytes creating a trade-off situation in relation to acidic strength.

Different approaches have been investigated to reach higher energy density such as the use of precipitation inhibitors in the electrolytes [48, 49]. For example, the bromine-based Generation 2 VRB (Bromine Redox Flow Cell, Br/V) which utilizes bromine in both half-cell have been reported in [27] to operate at electrolyte concentrations of 4M without precipitation. This would, in theory, double the energy density of the previous G1 VRB [27]. The use of the bromide/bromine couple in the positive electrolyte eliminates problems of thermal precipitation of the V(V) ions, but introduces another problem: toxic gases at gassing. Gassing will be discussed in section 3.4.4. A recent study of the possibility to replace the positive electrolyte with air has been investigated by Menicas et al [25] which could possibly double the energy density of the battery and also eliminates the positive half-cell electrolyte and associated problems of thermal precipitation at elevated temperatures.

In the G1 VRB, the temperature of the battery has to be kept between 10-40°C to prevent precipitation of vanadium ions. So additional active cooling (or heating) may be necessary in order to decrease the risk of precipitation as the electrolyte may be heated, or cooled,

due external temperature gradients, exothermic self-discharge reactions and internal resistance or by overheated pumps inside the system. However, these temperature increases are usually not a problem during normal operation as any heat buildup is dispersed in the large electrolyte tanks or cooled through the piping in the system. On the other hand, during stand-by, when the electrolytes are stationary inside the cell stack, the heat released from self-discharge reactions may accumulate and potentially cause irreversible precipitation.

### 3.4.4 Oxygen and hydrogen evolution

At high and low SOC, hydrogen and oxygen evolution may occur during charging which is referred to as gassing. These water-splitting reactions are highly undesired as they cause irreversible capacity losses and a potential hazard. At high SOC the risk for gassing increases because there are not enough vanadium species to react in redox reactions at the electrode surface. Usually, the risk of gassing is minimized inside systems by determining a threshold voltage (upper and lower) which corresponds to a certain upper- and lower SOC limit.

## 3.5 Cell configuration and optimization

As the battery suffers from many different tradeoffs in almost every aspect including flowrate, concentration, charge/discharge currents, SOC, temperature, pressure drop, proton conductivity and diffusivity of vanadium ions and preferential water transfer there is certainly an optimal solution which could increase the overall efficiency of the battery. Except from cross-mixing inside the battery, different side reactions such as hydrogen- and oxygen evolution at the negative and the positive electrodes, respectively, may occur during charge. As these side reactions may cause imbalance among the different vanadium species between the electrolytes it may cause severe capacity losses. Even in the best membranes, these aforementioned problems may occur, which is why sophisticated control systems must be developed for the automation process.

## 3.6 Literature review of membrane studies in the VRB

Automated controller systems for the VRB is dependent on reliable experimental data. However, as can be seen in Table 4, there are significant differences between different experiments for the same membranes. This could be due to membrane handling and influence of different experimental procedures among other. Some diffusion coefficients values from different literature reports have been compiled in Table 4. These differences may be attributed to various phenomena. For example, $V^{2+}$ is very hard to measure accurately due to its extreme sensitivity to oxygen which will convert it to $V^{3+}$; temperature variations may, in some cases, lead to membrane swelling which causes the pores to expand and get bigger, which will influence the diffusion coefficients with as much as 3% per °C [50]. In addition, the size of the membrane pores may also change as the membrane ages. Depending on the extent of fouling and swelling, the diffusion coefficients may increase or decrease with time and between experiments. Differences in the ionic strength of the test solution and blank solution used in the diffusion tests can also lead to water transfer across the membrane that will give erroneous vanadium ion concentrations and calculated diffusion coefficient values. These unreliable data will heavily influence the use and applicability of the sophisticated models that have been developed.

In order to get reliable results from dynamic simulations, the diffusion coefficients have to be trustworthy and the experimental procedure has to be discussed and planned in detail in order to decrease the error margin of different variables. Today, there is a strong need of reliable data for many new membranes in order to simulate the extended behavior of these membranes.

Sun et Al. in [50], investigated the diffusivity through a Nafion 115 membrane using a static cell (as visualized in Figure 11). The concentration was determined using a titration unit for all the different vanadium species and the values from their research are compiled in Table 4. Magnetic stirrers were used to avoid concentration polarization at the membrane surfaces.

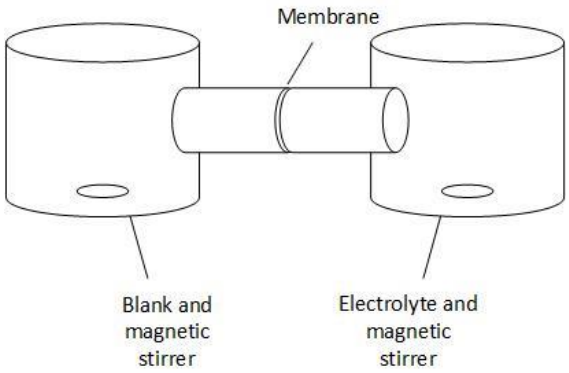


Figure 11. Experimental static-cell setup using magnetic stirrers for vanadium permeability test used by Sun et Al. in [50].

Furthermore, when comparing Wang et Al's work (where UV-visible was used to determine the concentration) in [34] (where the diffusion coefficients were determined using UV-visible) with Sun et Al. in [50] – large differences are noticed. That the temperature may change the diffusion coefficients gives a large error margin from experiments where active temperature control units have not been used. For example, from experiments at UNSW using a flow cell arrangement, pump heat was shown to increase the electrolyte temperature from 20°C to well above 40°C during a 24 h runtime and operation of a laboratory scale VRB. Therefore, any permeability rates may have been accelerated from start to finish.

Table 4. Summary of different diffusion coefficients for different membranes found in literature. All diffusion coefficients are given in terms of 10-7 cm2s-1. If not stated otherwise, these values were obtained at room temperature by Fick's first law of diffusion. Different pre-treatment procedures of the membranes might influence the overall diffusion coefficient.

| **Membrane** | **Diffusion Coefficient, P ($10^{-7}$ $cm^2s^{-1}$)** | | | |
|---|---|---|---|---|
| | **V(II)** | **V(III)** | **V(IV)** | **V(V)** |
| **Nafion (n.a) [34]** | n.a | 2,16 | 1,96 | 0,50 |
| **SPPEK* [34]** | n.a | 0.0525 | 0,046 | 0,012 |
| **SPPEK-TPA-8** [34]** | n.a | 0.118 | 0,060 | 0,019 |
| **Nafion 117 [23]** | n.a | n.a | 0,42 | n.a |
| **Nafion 117 [36]** | | 0,59 | 0,5 | 0,117 |
| **Nafion 117 [4]** | n.a | n.a | 0,61 | n.a |
| **SPFEK*** [23]** | n.a | n.a | 0,16 | n.a |
| **Nafion 115 [51]** | 0,10 | 0,019 | 0,043 | 0,024 |
| **Nafion 115 [35]** | 0,88 | 0,32 | 0,68 | 0,59 |
| **Nafion 115 [50]** | 0,53 | 0,19 | 0,41 | 0,35 |

* SPPEK: Sulfonated poly(phthalazinone ether ketone)

** SPPEK-TPA-8: Sulfonated poly(phthalazinone ether ketone) with tungstophosphoric acid (TPA) 8 wt-%

*** SPFEK: Sulfonated poly(fluorenyl ether ketone)

n.a : not available

In most studies, UV-visible is used to determine the concentration of vanadium ions as in [34]. However, as the V(2) may be easily oxidized to V(3), UV-visible would not be a suitable approach to determine the concentration of vanadium ions, specially not the V(II) electrolyte. Figure 12 represents a photo taken by the author while testing V(2) permeability through a F930 membrane. The photo was taken after an experimental uptime of 22 hours with an experimental setup which decreased air ingress to the electrolyte and the blank using Parafilm™. The photo visualizes the color change of the blank during diffusion test. Instead of light purple it was completely green which means the V(2) had been oxidized to V(3) during testing. As the V(2) was severely oxidized when entering the blank, it would (if determined by UV-visible spectroscopy analysis) absorb light at another wavelength and maybe go undetected. Therefore, any approach to determine the diffusion coefficients using UV-visible for V(2) could contain a considerable error, so an alternative analytical technique such as inductively coupled plasma analysis (ICP) that measures total vanadium, should be used to determine the concentration in these samples.

Figure 12. To the left is V(2) solution which, during diffusion test, ended up looking green in the blank solution after 22h of testing in the F930 membrane. This is why UV-visible cannot be used to determine the diffusion coefficients for these membranes – the V(2) has been oxidized and will not give an absorption peak where the purple color was initially absorbed at. Therefore, the peak has shifted to another wavelength and cannot be detected.

# CHAPTER 4
# Materials and Methods

## 4.1 Methodology; experimental setup and procedures

This section contains experimental setup, preparation of electrolytes, cell stack configuration, VRB setup and battery testing configurations. Each section is described individually.

The FAP450, F930, VB1, GN-115, GN-212, GN-212C membranes were evaluated in a laboratory scale VRB. These membranes were evaluated at three different current densities which were 20, 40 and 60 $mAcm^{-2}$. From these experiments, the EE, CE and VE were determined and evaluated.

Furthermore, to understand any difference between these membranes at charge-discharge operation, some membranes were evaluated in a diffusion cell for permeability rate measurements. In this study, the FAP450, F930, VB2, GN-115 membranes were evaluated in terms of vanadium permeability rates at constant temperature for all vanadium ions present in the VRB which are V(II), V(III), V(IV) and V(V). The structural integrity of the GN-115 membrane was tested through immersion in 1M V(5) solution for 7 weeks to determine weight difference, swelling ratio and oxidation of the membrane. All different experiments are discussed and presented in detail in the following sections and all experimental data have been compiled in *Appendix A* (charge discharge evaluation), *Appendix B* (permeability data) and *Appendix C* (chemical stability data).

### 4.1.1 Cell design and battery configuration

The cell stack for charge-discharge operation was assembled as presented in Figure 7 with a configuration of: 2 endplates of PVC plastic, 2 polished copper current collectors, 2 flow frames, 2 carbon paper sheets (to protect the copper surface from oxidation), 4 rubber/neoprene gaskets, 2 carbon felts (SGL Carbon, Germany) and one membrane. Both half-cells comprised of a 3.5 mm PVC flow-frame with inlet and outlet channels for the negative and positive electrolytes. The flow-frame was sandwiched between 1 mm rubber gaskets to prevent leakage and the 5 mm thick carbon felt was inserted into the flow frame and squeezed together by the endplates in the final

construction. As a rule of thumb the carbon felt was squeezed to about 25-30% in order to keep the pressure drop minimal but still provide good electrical contact with the carbon plate current collector. A battery test system unit from RePower™ including software was used to carry out the experiments.

An overview of the experimental electrolyte preparation setup can be seen in its entirety in Figure 13. The setup consists of two of the aforementioned cell stacks, 2 glass beakers for electrolyte storage covered with Parafilm™ in order to decrease any air ingress, two pumps (Iwaki Magnet Pump *MD-10-230GS01*) and plastic piping to connect the different sections together. The cell was sealed in order to prevent any air ingress that could oxidize the divalent vanadium ions further.

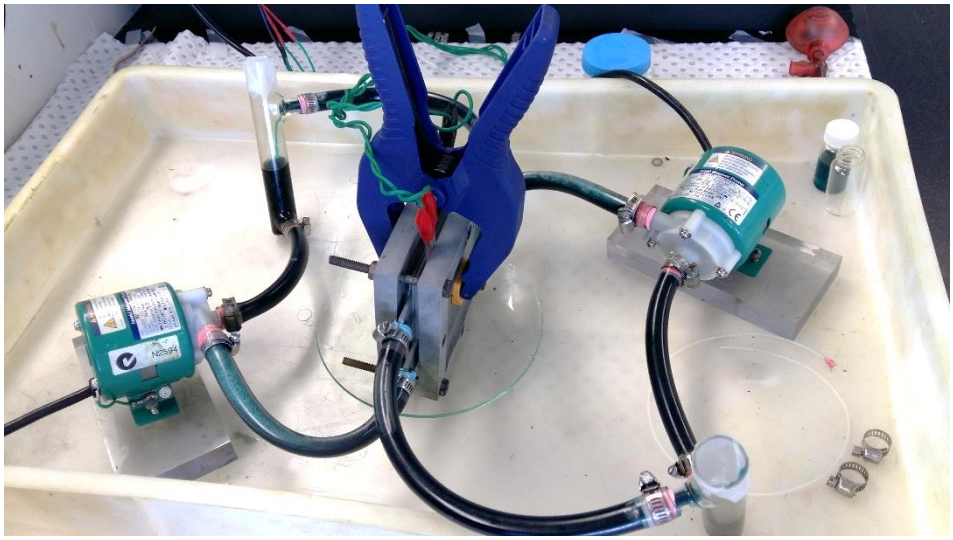

*Figure 13. Experimental setup for the VRB electrolyte preparation [Photograph by author]*

The battery was tested for any leakage prior to charging by having a constant flow of electrolytes through the unit for several hours and for the membranes and carbon felt electrodes to become fully wetted. The cell and the battery were assembled inside a tray with sufficient volume to cope with any accidental spill from the VRB. Pumps and electrical wires were elevated from the tray bottom to keep them safe from any acidic leakage. A full experimental material list is compiled in Table 5.

.

*Table 5. Compiled experimental material list for the electrolyte preparation*

| Full experimental material list | |
|---|---|
| **Magnetic pumps** | 2 |
| **Endplate** | 2 |
| **Membrane** | 1 |
| **Carbon felt** | 2 |
| **Rubber gaskets** | 4 |
| **Flow frame** | 2 |
| **Carbon paper** | 2 |
| **Metallic clippers** | 16 |
| **Plastic piping** | 8 |
| **Charging station** | 1 |

### 4.1.2 Electrolyte preparation

The vanadium solution electrolyte was prepared by slowly adding $V_2O_3$ and $V_2O_5$ powders to a 5M $H_2SO_4$ solution. The solution was covered by Parafilm™ and continuously stirred using a magnetic stirrer and heated to about 70°C using an electric heat plate. Heating was applied until the powder was dissolved to a large extent. Some of the powder was not dissolved fully which is why the concentration after heating was determined using ICP-analysis.

Unless otherwise stated, the electrolytes used in the laboratory scale VRB were measured to a total volume of 100 ml each and inserted to the glass beaker storages. The solutions were electrolyzed at 40 $mAcm^{-2}$ (1000 mA divided by the total membrane area of 25 $cm^2$) with an upper voltage limit of 1.8 V which corresponds to about 90% SOC in an electrolytic cell as illustrated in Figure 6. The electrolytes were balanced by removing a certain volume of V(V) from the positive electrolyte and replacing it with a V(3.5) buffer until the V(III) in the negative half-cell was fully converted to V(II) which was noticed by the purple color change. The reason for the V(V) to reduce quicker is because of the V(II) being constantly oxidized to V(III) due to the presence of oxygen inside the system. It could also be due to the initial oxidation state of the solution being closer to $V^{3.7+}$ instead of the desired 50:50 mixture of V(III):V(IV) - denoted $V^{3.5+}$.

The electrolyte balancing procedure was carried out until both sides were fully charged to V(5) and V(2) which was noticed by the OCV as well as the color of the electrolytes. A typical charge curve from the electrolyte preparation is seen in Figure 14. All

experimental measurements were conducted using an automated battery testing system from RePower™.

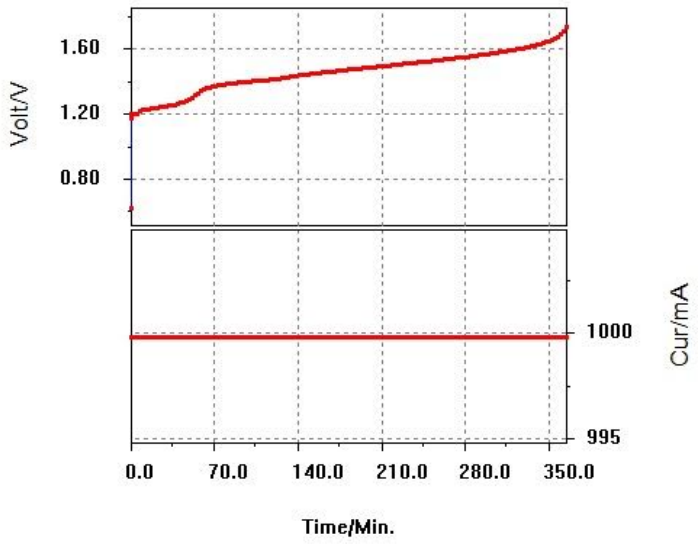


*Figure 14. Charge curve for the laboratory scale VRB battery. The shorter time from start at 15:00h to 18:00h indicates that the oxidation state is closer to V4+ than to V3+.*

The $V^{3+}$ and $V^{4+}$ electrolytes could be created by mixing different volume ratios of $V^{5+}$ and $V^{2+}$ according to the equation (14) and equation (15). Table 6 contains the mixing ratios of V(II) and V(V) in order to create V(III) and V(IV) respectively.

$$xV^{2+} + (1-x)V^{5+} = V^{3+} \quad (14)$$

$$xV^{2+} + (1-x)V^{5+} = V^{4+} \quad (15)$$

*Table 6. Measure ratio to produce V3+ and V4+ from V2+ and V5+.*

| | Volume ratio $V^{5+}$:$V^{2+}$ |
|---|---|
| $V^{3+}$ | 1:2 |
| $V^{4+}$ | 2:1 |

## 4.2 Determination of diffusion coefficients for different vanadium ions

### 4.2.1 Preparation of Blank

As any difference in ionic strength between the electrolytes would lead to a severe volume transfer across the membrane the ionic strength of the blank solution was partially balanced with appropriate non-vanadium salts dissolved in the $H_2SO_4$ supporting electrolyte. However, due to lack of vanadium speciation in the electrolyte it is impossible to fully balance the ionic strength of the solutions [47]. To minimize osmotic effects (and therefore also any water transfer) $MgSO_4$ was used to balance and equalize the ionic strength for the $V^{2+}$-, $V^{3+}$-, $V^{4+}$ ions, respectively, and $K_2SO4$ was used for the $V^{5+}$. The ionic strength was calculated using Equation (16).

$$I = \frac{1}{2}\sum_{i=1}^{n} c_i z_i^2 \quad (16)$$

Where $c_i$ is the molar concentration of ion $i$, $z_i$ is the charge number of that ion and the sum is to consider all the ions in the solution. The blank solution was prepared by adding $MgSO_4$ powder to the corresponding concentration of $H_2SO_4$ in order to obtain a 1M $MgSO_4$ and 2.5M $SO_4^{2-}$ solution. To balance the ionic strength of the V(5) electrolyte, $K_2SO_4$ was dissolved in the corresponding concentration of $H_2SO_4$ in order to obtain 1M K+ and 2.5M $SO_4^{2-}$.

### 4.2.2 Experimental setup and configuration

The permeability rate of the different vanadium ions through the different membranes were determined by an experimental setup explained in Figure 16. Cooling was applied using a coil of plastic tubing wrapped around a metal rod, which was immersed in a water bath (PolyScience™ Digital Temperature Controller) to control the temperature. By using this approach, the temperature of the electrolytes could be controlled and the heat of the pumps was efficiently cooled down during testing. Also, any temperature difference in the laboratory during day and night was controlled with this approach.

*Figure 15. The cooling coil which was used to cool the electrolytes during operation.*

The membrane to be tested was inserted between two flow-frames with rubber gaskets on either side to prevent solution contamination and leakage in the workspace. The stack was squeezed together using two PVC endplates and sealed to decrease the risk of oxidation of the sensitive vanadium ions. The experimental setup was similar to the one used for electrolyte preparation except that the latter did not have copper current collectors and graphite felts.

A solution of the specific vanadium ion of 1 M and 100 ml was inserted into one half-cell and the prepared blank was inserted to the other and samples of 1 mL were periodically drawn from the blank and sent for concentration determination using ICP-AEM analysis.

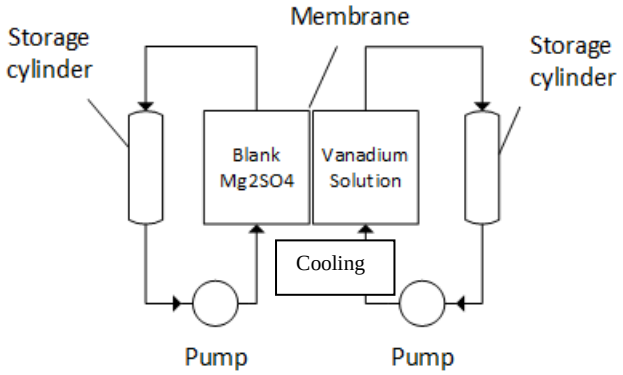


*Figure 16. Experimental set-up for determination of diffusion coefficients*

The total membrane area for each of the different membranes was 25cm$^2$ (5x5 cm). The actual experimental setup can be seen in Figure 17 in which the V(IV) permeability rate through the F930 membrane is experimentally determined.

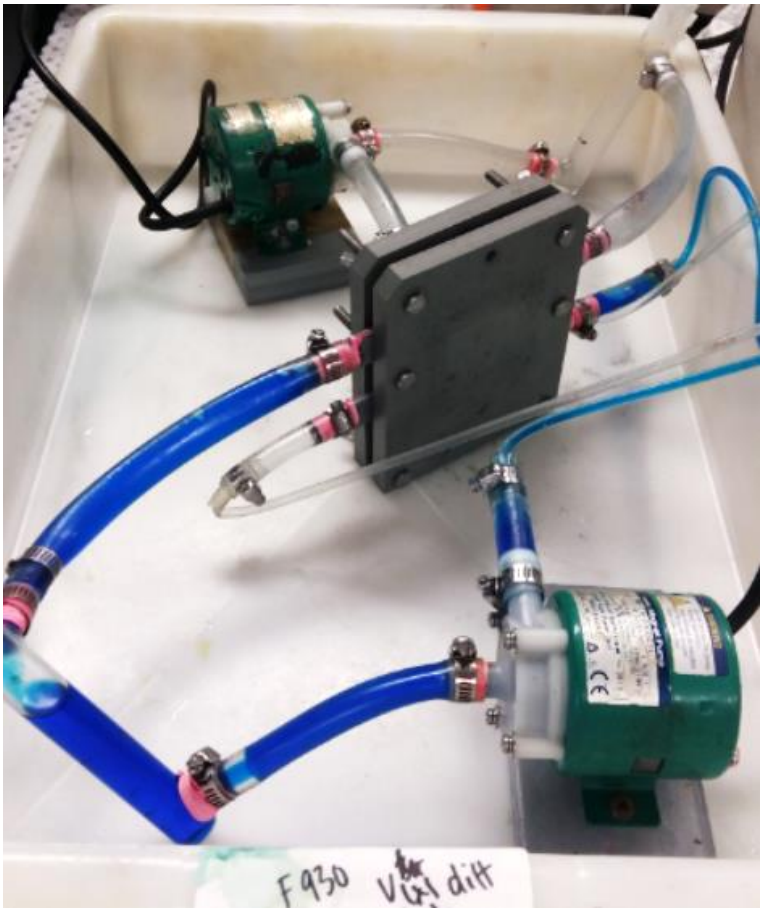


*Figure 17. Experimental setup for permeability measurement of V(IV) (Blue) and Mg2+ blank (white) through F930 membrane.*

### 4.2.3 Determination of concentration of V in Blank

In order to determine the concentration of the different samples the absorbance for each sample can be measured using a UV-Visible spectrophotometer. The sample must then be returned to the system in order to maintain the initial volume. However, as mentioned in the introduction, the $V^{2+}$ can be easily oxidized to $V^{3+}$ which makes the UV-Visible measurements a source of error. Therefore, ICP analysis was used to determine the concentrations of the different samples which were obtained from the blank at different time intervals depending on the color difference of the blank and in order to decrease the risk of oxygen ingress, only 3 samples were withdrawn through the Parafilm.

ICP (Inductively Coupled Plasma mass spectrometry) analysis, or ICP testing, can detect one part of $10^{15}$ by ionizing either liquid or solid samples with plasma and separating the ions using mass spectrometry. It is, however, a destructive test and therefore the samples were not returned to the electrolyte reservoirs. Nevertheless, to decrease the influence of the actual volume change, the withdrawn samples were diluted

and only sampled 3 times in total for each membrane and each ion, which corresponds to a total volume of 3 ml, accounting for a decrease in volume of 3% which could be neglected from the correlation of Fick's diffusion.

The molecular diffusion of vanadium ions is governed by Fick's first law of diffusion in absence of potential [52]. According to Fick's law, the diffusion is driven by the concentration gradient in equation 17.

$$J_A = -D_s \cdot \left(c_{V,A} - c_{V,B}\right) \quad (17)$$

where $J_A$ is the flux of species A (moles $L^{-1}$ $s^{-2}$), Ds is the diffusion coefficient (m $s^{-1}$), $c_{VA}$ is the concentration of vanadium in solution A and $c_{VB}$ is the concentration of the vanadium ion in solution B. At the start of the experiment, t=0, the concentration of vanadium ion in solution B is $C_B^0$ and for the other solution $C_A^0$ which combined gives equation (18).

$$J_A = D_s A(c_B - c_A) = V_A \frac{dC_A}{dt} \quad (18)$$

where A is the area ($m^2$). But we also have equation (19), stating that

$$V_B C_B = V_B C_B^0 - V_A(C_A - C_A^0) \quad (19)$$

where $V_B$ is the volume in reservoir B and $V_A$ is the volume of reservoir A. Combining reaction 18 and equation (19) we get equation (20)

$$\left\{C_B^0 + \frac{V_A}{V_B} C_A^0 - \left(1 + \frac{V_A}{V_B}\right) C_A\right\} = \frac{V_A}{D_s A} \frac{dC_A}{dt} \quad (20)$$

separating and integrating for VB and with $V_A = V_B = V$ and $C_A^0 = 0$ we get;

$$\ln[C_B^0 - 2C_A] = \ln[C_B^0] - \frac{2D_s A}{V_A} t \quad (21)$$

According to equation (21), the plot of ln $[C_B^0 - 2C_A]$ will give a straight line with slope $-\frac{2D_S A}{V_A}$ from which the diffusion coefficient $D_s$ can be obtained. These calculations, including raw data from ICP analysis and dilution procedure are compiled in *Appendix B.*

## 4.3 Calculation of permeability rates for the specific membranes

The permeability rates for all of the different vanadium species were tested for FAP450, F930, VB2 and the GN-115 membrane. According to the correlation in 4.2.3, using the tabulated values from ICP analysis in *Appendix B*, the slopes of the lines were multiplied with the blank volume and divided with the area of the membrane.

## 4.4 Membrane evaluation through 4 charge-discharge cycling

To evaluate the performance of all the membranes to be tested, they were tested in a small flow cell through a series of four charge-discharge cycles at different current densities (500 mA, 1000 mA, 1500 mA). The cell was assembled as explained in section 4.1.1 and the electrolytes were diluted to 1.6 M in 4 M $H_2SO_4$.

The electrolytes were prepared as explained in the previous paragraph and the following procedure was used:

(1) The cell stack was assembled as explained in section 4.1.1.
(2) The electrolytes were allowed to circulate through the system over night to ensure the membrane to be wet and to activate the carbon felt.
(3) The electrolytes were charged and balanced at 1000 mA (40mAcm$^{-2}$)
(4) Four charge-discharge cycles were tested. First at a current density of 1000 mA then 1500 mA and finally and with an upper voltage limit of 1.65 V and a lower voltage limit of 1.0 V. These voltage limits were set to decrease risk of side-reactions and gassing.

Before evaluating and reusing the electrolytes at another current density, the electrolytes were remixed and rebalanced. The initial volume of all experiments was 100mL.

## 4.5 Experimental setup for chemical stability test in V(5) electrolyte

In order for a membrane to be suitable in the VRB, it has to maintain its structural integrity over extended contact in time with the highly oxidizing environment supplied by the V(5) electrolyte. To test swelling ratio and membrane degradation, the

membrane to be tested was first measured (thickness, width and length) and then immersed into a 1-2 M V(5), 2.5 M $H_2SO_4$ solution for extended time. After about 7 weeks, the membrane was dried in air, measured again and the ratio of swelling was determined from the difference in length, thickness and width.

# CHAPTER 5
# RESULTS AND DISCUSSION

This chapter contains the experimental results and is divided into three parts. Section 5.1 contains results from membrane evaluation through charge-discharge operation, section 5.2 contains results from experimental determination of diffusion coefficients and membrane chemical stability in V(5) solution is summarized in section 5.3. Furthermore, in chapter 6, the results from this section are used as parameters in efficiency and thermal modelling and simulations of the VRB in order to further evaluate any differences between the behaviors of the membranes in the VRB.

All experimental raw data are compiled in *Appendix A* for charge-discharge evaluation at 500 mA, 1000 mA and 1500 mA and consists of charge-discharge capacities, charge-discharge graphs as well as energy input during both charge and discharge. These data were used to calculate the EE, CE and VE. Furthermore, *Appendix B* contains raw data for permeability which includes linear regression of the measured concentrations versus time and *Appendix C* contains information from the membrane stability test in V(V) solution. *Appendix D* contains a rough estimate of the cell resistance based on 50% SOC.

## 5.1 Cell performance and membrane evaluation during charge-discharge cycling at different current densities

The results in this study were obtained from four charge-discharge cycles for each membrane at three different currents (1500 mA, 1000mA and 500 mA) using a battery test system unit from RePower™ explained in section 4.4 with a cell assembled as explained in section 4.1.1. In each case, the electrode comprised a 6 mm thick graphite felt compressed against a 5 mm thick graphite plate current collector, while the electrolyte was 1.6 M V in 2.5 M $H_2SO_4$. The different currents represent current densities of 60 $mAcm^{-2}$, 40 $mAcm^{-2}$ and 20 $mAcm^{-2}$ over the 25 $cm^2$ membranes. The membranes are listed in the following order: VB-1, GN-115, GN-212, GN-212C, F930, FAP-450. Each membrane section consists of an average EE, CE, VE and a charge-discharge graph at 1000 mA.

The equations for calculation of CE, EE and VE are compiled in section 3.2. To evaluate the CE for the VB1 membrane at 1000 mA, the total discharge capacity (total dischg cap.) (mAh) was divided with the total charge capacity (total chg cap) (mAh) which are found in Table 31. Furthermore, the EE was calculated by dividing the total energy input during charge (abbrev. *CC Charge* in tables of *Appendix A*) (mJ) with the total energy output during discharge (abbrev. *CC Discharge* in tables of *Appendix A*) *(*mJ), also found in Table 31. Finally, the VE was calculated by dividing the EE with the CE. This procedure was carried out for all cycles, for all membranes at all current densities.

### 5.1.2 VB-1 Membrane

The charge-discharge curve of the laboratory scale VRB assembled with the VB-1 30µm membrane at 1000mA (40mA $cm^{-2}$) is shown in Figure 18. The total cycling time was 30 h and the CE, EE and VE from the experiment are compiled in Table 7. The highest EE of the VB-1 membrane was 77,5% at 500 mA, the highest CE was obtained at 1500 mA with 93.9% and the highest VE was 85.7 at 1000 mA.

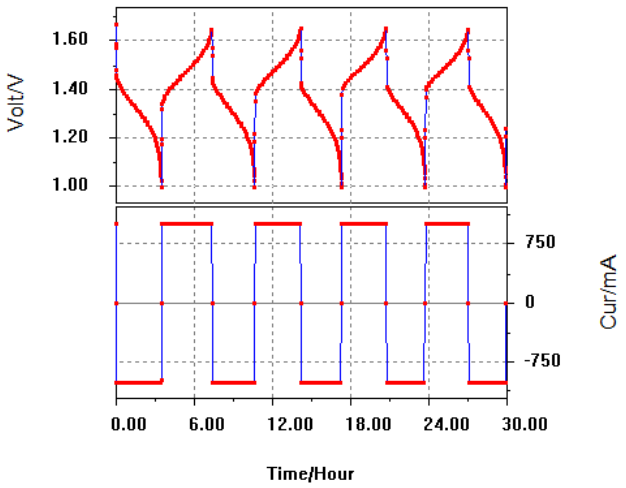


*Figure 18. Experimental charge-discharge curve for membrane evaluation of the VB1 30 at 1000 mA (40 mA cm-2) with a total cycle time of 30 hours.*

*Table 7. Average cycle energy efficiencies for the VB-1 30um membrane. Highest EE was obtained at 500 mA at 77,5%.*

| VB-1 | EE (%) | CE (%) | VE (%) |
|---|---|---|---|
| 500 mA | **77,5** | 83,6 | 80,2 |
| 1000 mA | 73,9 | 86,3 | **85,7** |
| 1500 mA | 75,3 | **93,9** | 80,2 |

As expected, the coulombic efficiency decreases with decreasing current density due to the increased effect of the self-discharge processes over the longer cycling times. Voltage efficiency is expected to decrease with increasing current density due to higher iR losses, but the observed trends are inconsistent. This could be due to variations in electrolyte flow and temperature during the cycling that will affect concentration polarization and cell resistance.

### 5.1.3 GN-115 Membrane

The GN-115 membrane reached a highest EE of 80,3% at 500mA as compiled in Table 8. However, at higher current densities (1500 mA) the discharge current decreased from 1500 mA to about 1000 mA as seen in compiled experimental results in *Appendix A*, Figure 64. Therefore, the discharge at 1500 mA was *not* carried out at constant current. The highest CE was 95,1 at 1000 mA and the highest VE was 83,8% at 1500 mA.

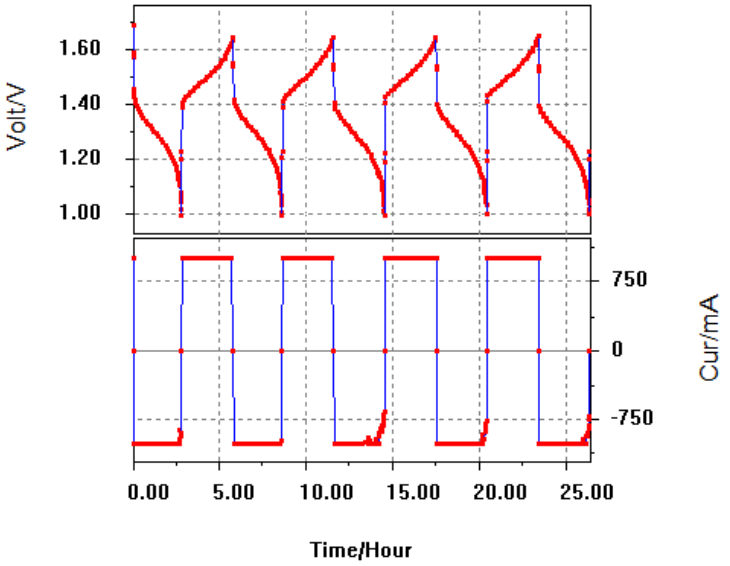


*Figure 19. Charge-discharge curve for the GN-115 membrane. A slight drop in discharge current was noticed at end of cycle 3,4 and 5 respectively.*

*Table 8. Average cycle energy efficiencies for the GN-115 membrane. Highest EE was obtained at 500 mA at 80,3%.*

| GN-115 | EE (%) | CE (%) | VE (%) |
|---|---|---|---|
| 500 mA | **80,3** | 92,0 | 83,4 |
| 1000 mA | 79,8 | **95,1** | **83,8** |
| 1500 mA | 69,1 | 90,6 | 76,1 |

The VE decreased with higher currents and the CE did not seem to follow any pattern. The EE peaked at around 80% at 500 mA.

### 5.1.4 GN-212 Membrane

The GN-212 membrane reached a maximum EE of 78,2% at 500 mA, a maximum CE of 93,3% at 1000 mA and maximum VE of 89,1% at 500 mA. At higher current densities, the discharge current dropped of quite severe as seen in Figure 21 as compared to Figure 20, which was conducted at 1000 mA. This phenomenon cannot be explained by is associated with the stability of the battery cycling equipment. Despite the instability in current during cycling at the higher currents, the trends in CE and VE can still be compared as shown in Table 9 that contains all CE, VE and EE for the different experiments. These values are average values out of 4 charge-discharge cycles from Appendix A, Table 45 and Table 46.

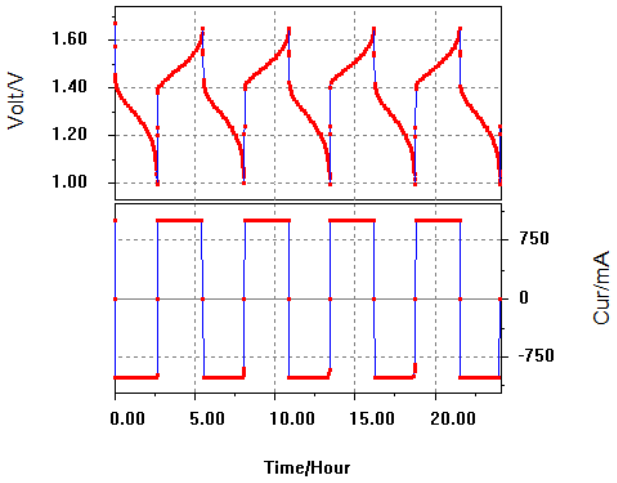


*Figure 20. Charge-discharge curve for GN-212 membrane. The discharge current was maintained at 1000 mA.*

*Table 9. Average cycle energy efficiencies for the GN-212 membrane. Highest EE was obtained at 500 mA at 78,2%.*

| GN-212 | EE (%) | CE (%) | VE (%) |
|---|---|---|---|
| 500 mA | **78,2** | 87,8 | **89,1** |
| 1000 mA | 77,2 | 91,5 | 84,1 |
| 1500 mA | 73,9 | **93,3** | 79,3 |

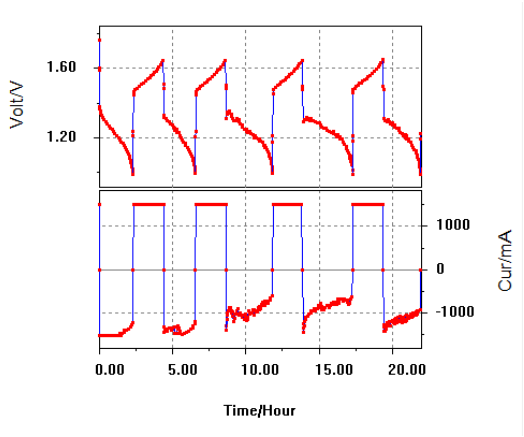


*Figure 21. Charge-discharge curve for the GN-212 membrane. The discharge current drops severely during the third, fourth and last cycle.*

### 5.1.5 GN-212C Membrane

The difference between the GN-212 and the GN-212C is that the latter has embedded graphene particles which, in theory, should decrease resistance and increase the voltage efficiency during charge-discharge cycling. Figure 22 is the charge-discharge curve from 1000 mA operation.

Table 10 consists of the experimental results. The highest EE was achieved at 500 mA with a maximum value of 78,8%, the highest CE was 91,5 at 1000 mA and the highest VE was 91,7% at 1500 mA.

*Table 10. Average cycle energy efficiencies for the GN-212C membrane. Highest EE was noticed at 500 mA with 78,8%*

| GN-212C | EE (%) | CE (%) | VE (%) |
|---|---|---|---|
| 500 mA | **78,8** | 86,0 | **91,7** |
| 1000 mA | 77,7 | 89,6 | 86,8 |
| 1500 mA | 71,6 | **91,5** | 78,2 |

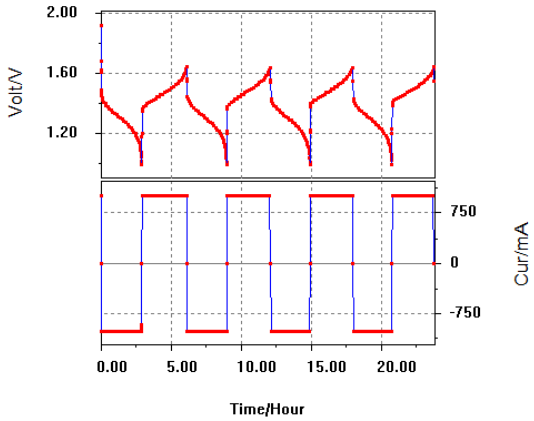


*Figure 22. Charge-discharge operation of the GN-212C membrane at 1000 mA.*

Figure 23 contains the charge-discharge cycle of the GN-212C. The discharge current was maintained at 1500 mA through most of the cycle except for a slight decline at the end. When compared to the GN-212 in which case the discharge current dropped of severely after 2 cycles, the GN-212C could maintain the discharge current of 1500 mA. This irregularity in the stability of the charge-discharge current between different cells and membranes is unlikely to be due to the difference between the two membranes – the graphite layer inside the GN-212C- and is more likely to reflect the instability of the battery tester output that could not unfortunately be controlled.

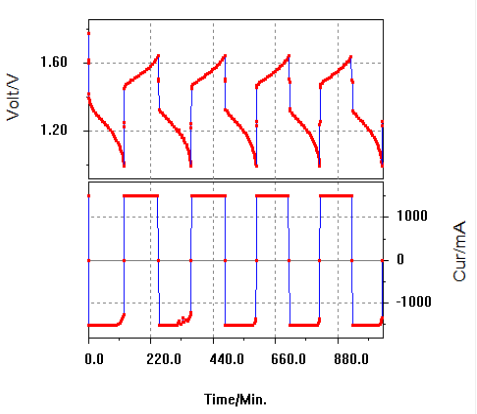


*Figure 23. Charge-discharge curve for GN-212C at 1500mA for comparison with the GN-212 membrane which could not maintain a stable discharge current.*

The results suggest however that the graphite layer provides a higher conductivity which should provide higher voltage efficiencies which was also observed when comparing the GN-212 with the GN-212C, as compiled in Table 11.

*Table 11. Comparison of VE between the GN-212 and the GN-212C at different current densities*

| | **500 mA** | **1000 mA** | **1500 mA** |
|---|---|---|---|
| **GN-212C** | 91,7 | 86,8 | 78,2 |

| | | | |
|---|---|---|---|
| **GN-212** | 89,1 | 84,1 | 79,3 |

### 5.1.6 F930 Membrane

The F930 membrane outperformed the other membranes at all current densities and provided a peak EE at 89,6% at 500mA and a maximum CE at 98,8% at 1500 mA and voltage efficiency of 92,7% at 1500 mA as compiled in Table 12. Figure 24 is the charge-discharge curve for the F930 at 1000 mA.

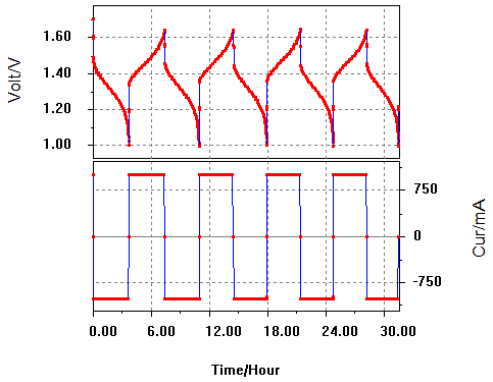


*Figure 24. Charge-discharge curve at 1000mA for F930*

*Table 12. Experimental data from F930 at 500 mA, 1000 mA, 1500 mA. The highest EE was 89,5% at 500 mA, CE was maximized with 98,8% at 1500 mA and VE at 92,7% at 500 mA.*

| F930 | EE (%) | CE (%) | VE (%) |
|---|---|---|---|
| 500 mA | **89,6** | 96,7 | **92,7** |
| 1000 mA | 84,4 | 96,8 | 87,1 |
| 1500 mA | 80,8 | **98,8** | 81,8 |

The VE decreased at higher currents while the CE increased. A maximum EE was obtained at the highest CE and VE which was at 500 mA giving a total EE of about 89%.

### 5.1.7 FAP450 Membrane

The highest EE was 81,0% at 500 mA the highest CE was recorded at 96,2% both 1000mA and 1500mA. The highest VE was obtained at 500 mA at 89,9% as compiled in Table 13. The discharge current was maintained at 1000 mA during discharge as seen in Figure 25.

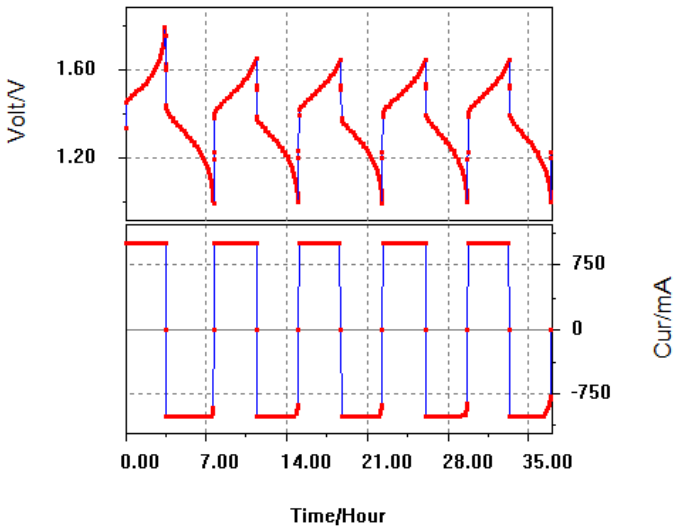


*Figure 25. Charge discharge graph of the FAP450 membrane at 1000 mA (40 mAcm-2)*

*Table 13. Experimental data from FAP450 at 500mA (20mA cm-2), 1000 mA (40mAcm-2) and 1500 mA (60 mA cm-2).*

| FAP450 | EE (%) | CE (%) | VE (%) |
|---|---|---|---|
| 500 mA | **81,0** | 90,1 | **89,9** |
| 1000 mA | 79,8 | 96,2 | 87,1 |
| 1500 mA | 74,1 | 96,2 | 77,1 |

As with most experiments, there was a clear trend in regard of CE and VE. The VE decreased at higher currents while the CE increased. A maximum EE was obtained at around 81%.

### 5.1.8 Influence of air ingress through the Parafilm®

To make sure that the Parafilm™ provided enough protection of the V(II) electrolyte, an experiment was setup in order to quantify the protection of the film. Two different experiments were conducted where one was designed to decrease the surface area of V(II) using a pipe and one was kept as explained in the experimental section. The pipe was inserted into the electrolyte storage container as seen in Figure 26 to decrease surface area which was exposed to air.

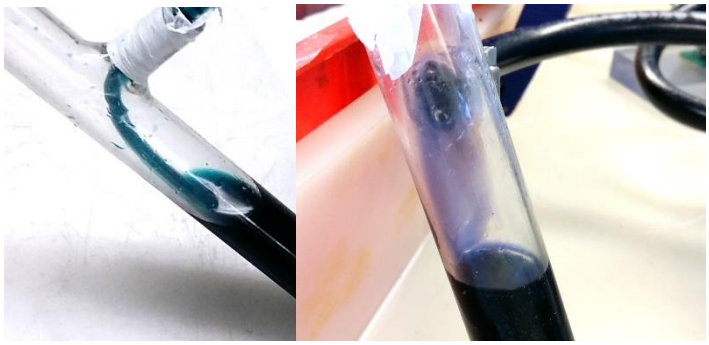

*Figure 26. Left: Inserted pipe to decrease surface area of electrolyte. Right: normal experimental setup with large surface area of electrolyte which is exposed to air inside the electrolyte storage container.*

The results was compiled in Table 14 below and about 1% higher CE was achieved during the exact same conditions which lead to a higher EE of about 2%. This is not a significant change and can therefore be neglected.

*Table 14. Determination of oxidation effects of large surface area in electrolyte storage at charge-discharge operation of the VRB battery. Low- or no changes in oxidation was observed between the two laboratory setups.*

| I = 1350 mA [54 mA $cm^{-2}$] | | | | | | |
|---|---|---|---|---|---|---|
| | **Without pipe (low surface area)** | | | **With pipe (large surface area)** | | |
| Cycle | **EE (%)** | **CE (%)** | **VE (%)** | **EE (%)** | **CE (%)** | **VE (%)** |
| **1** | 74,4 | 93,0 | 80,0 | 80,1 | 94,1 | 85,1 |
| **2** | 74,1 | 93,0 | 79,7 | 76,0 | 94,5 | 80,4 |
| **3** | 74,0 | 93,1 | 79,5 | 76,3 | 94,6 | 80,7 |
| **4** | 74,4 | 93,0 | 80,0 | 75,3 | 93,8 | 80,3 |

The total discharge capacity of the two experiments cannot be compared as any difference in initial SOC after balancing the electrolytes will affect the capacity of the battery. However, any *change* of capacity during operation might be attributed to oxidation of the vanadium ions. Almost no difference was noticed during testing and it was concluded that the oxygen ingress from the large surface area of the electrolyte tanks was low and could be neglected. The 1-2% difference could be due to measurement errors and it was therefore concluded that the negative half-cell electrolyte did not need any extra protection from air inside the reservoir. Moreover, as the average discharge capacity in Table 15 was kept fairly constant throughout the experiments the problem with air ingress, was indeed very low.

*Table 15. Charge- and discharge capacity between Parafilm protected electrolyte storage and Parafilm plus extra piping to decrease surface area storage solution. No considerable difference was noticed.*

| I = 1340 mA [54 mA $cm^{-2}$] | | | | |
|---|---|---|---|---|
| | **Without pipe** | | **With pipe** | |
| Cycle | **Total charge capacity (mAH)** | **Total discharge capacity (mAH)** | **Total charge capacity (mAH)** | **Total discharge capacity (mAH)** |
| **1** | 2615 | 2430 | 2700 | 2542 |
| **2** | 2596 | 2414 | 2743 | 2591 |
| **3** | 2576 | 2399 | 2780 | 2629 |
| **4** | 2583 | 2401 | 2855 | 2680 |

### 5.1.9 Summary charge-discharge membrane testing & experimental trends

Table 16 summarizes all measured the experimentally determined EE of all the different membranes which were evaluated in the laboratory scale VRB. Furthermore, Table 17 contains all CE and Table 18 all VE. It was found that the Fumapem®, F-930 by Fumatech™ outperformed the other membranes and peaked with an EE of 89,6%, at 20mA$cm^{-2}$, CE of 98,8% at 60mA$cm^{-2}$ and VE at 92,7% at 20mA$cm^{-2}$. The second best membrane was the FAP450, also by Fumatech™.

*Table 16. Summary EE from charge-discharge evaluation*

| *Summary Energy Efficiency (EE)* | | | |
|---|---|---|---|
| **Membrane** | ***500 mA*** | ***1000 mA*** | ***1500 mA*** |
| **VB1** | 75,5 | 73,9 | 75,3 |
| **FAP450** | *81,0* | 79,8 | 74,1 |
| **F930** | **89,6** | **84,4** | **80,8** |
| ***GN-115*** | 80,3 | 79,8 | 69,1 |
| **GN-212-C** | 78,8 | 77,7 | 71,6 |
| **GN-212** | 78,2 | 77,2 | 73,9 |

*Table 17. Summary CE from charge-discharge evaluation*

| *Summary Coulombic Efficiency (CE)* | | | |
|---|---|---|---|
| **Membrane** | ***500 mA*** | ***1000 mA*** | ***1500 mA*** |
| **VB1** | 83,6 | 86,3 | 93,9 |
| **FAP450** | 90,1 | 96,2 | 96,2 |
| **F930** | **96,7** | **96,8** | **98,8** |
| ***GN-115*** | 92,0 | 95,1 | 90,6 |
| **GN-212-C** | 86,0 | 89,6 | 91,5 |
| **GN-212** | 87,8 | 91,5 | 93,3 |

*Table 18. Summary VE from charge-discharge evaluation*

| *Summary Voltage Efficiency (VE)* | | | |
|---|---|---|---|
| **Membrane** | ***500 mA*** | ***1000 mA*** | ***1500 mA*** |
| **VB1** | 80,2 | 85,7 | 80,2 |
| **FAP450** | 89,9 | 82,9 | 77,1 |
| **F930** | **92,7** | **87,1** | **81,8** |
| ***GN-115*** | 83,4 | 83,8 | 76,1 |
| **GN-212-C** | **91,7** | 86,8 | 78,2 |
| **GN-212** | 89,1 | 84,1 | 79,3 |

Previous studies by Qingtao et al in [4] have shown EE of around 85% using a Nafion117 membrane. Although the cells used in each study may be quite different, the highest EE obtained in our study was 89,6% for the F930 membrane at 500mA ($20mAcm^{-2}$). As can be seen in Figure 27, the EE is fairly constant throughout different current densities, which is explained by the behavior of CE and VE.

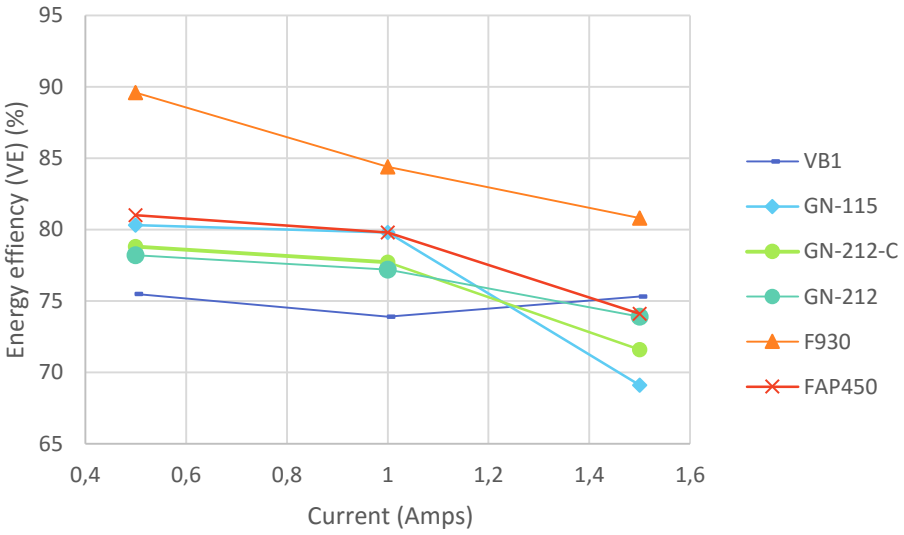


*Figure 27. EE versus current (A)*

From the behavior of the charge-discharge evaluation of the VB1 membrane, it is clear that the CE increases at higher currents and that the VE declines at higher currents. As can be seen in Figure 28, a maximum EE is obtained somewhere around 39-40 $mAcm^{-2}$.

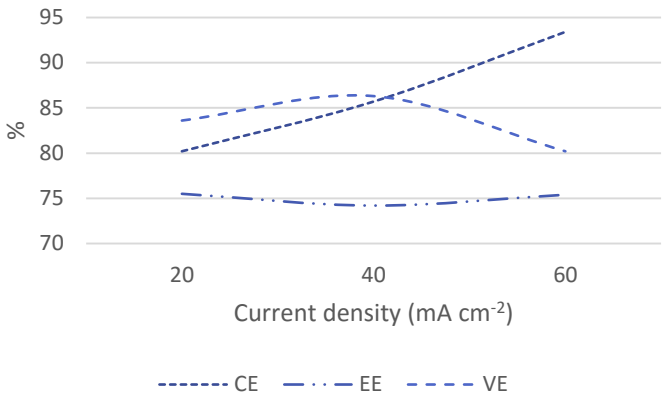


*Figure 28. Experimental results of CE, VE and EE versus current density (mA cm-2) for the VB-1 30µm membrane indicating trends for CE, EE and VE versus current (I).*

In Figure 29 it is clear that higher currents give higher CE which is explained by shorter cycle time and less time for the vanadium ions to permeate through the membrane. As expected due to the constant volume of electrolyte, the total cycle time for the charge-discharge cycle was decreased with higher current densities. The shorter cycle times provides a narrower timespan for vanadium ions to permeate through the membrane and participate in self-discharge reactions, which decreases the amount of vanadium ions making it through the membrane during one cycle which increases the CE.

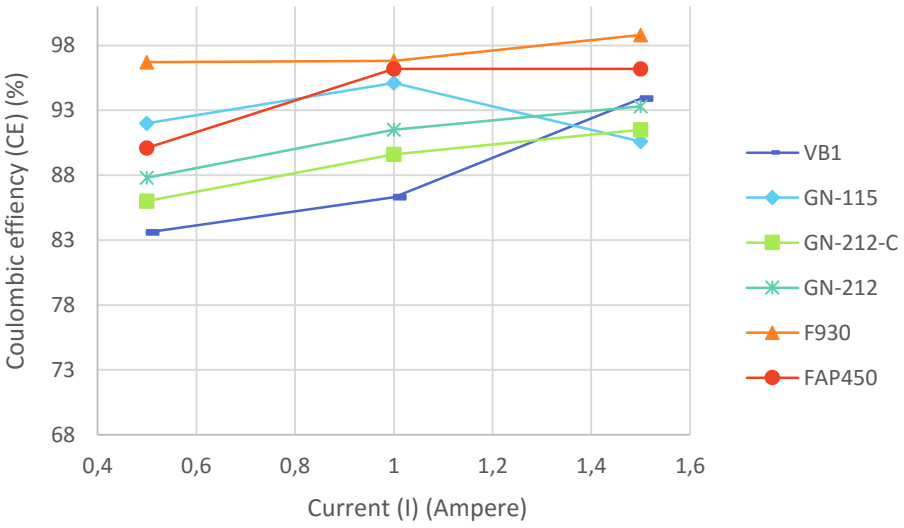


*Figure 29. Coulombic efficiency (CE) versus current (A)*

The VE decreases at higher currents, as seen in Figure 30, due to the increased voltage losses in the cell at higher currents. At higher currents, the charge voltage increased while the discharge voltage decreased as seen in Table 19. The reason behind this is the

influence of higher ohmic and polarization losses in the cell at higher current densities according to the equation 22 and equation 23 below.

$$V_{Charge} = OCV + iR + \eta_C + \eta_a \quad (22)$$

$$V_{discharge} = OCV - iR - \eta_C - \eta_a \quad (23)$$

Where OCV is the open circuit voltage, *iR* are the ohmic losses, $\eta_C$ is the concentration over potential which is a function of current and flowrate, and $\eta_a$ is the activation over potential which also increases with increasing current density.

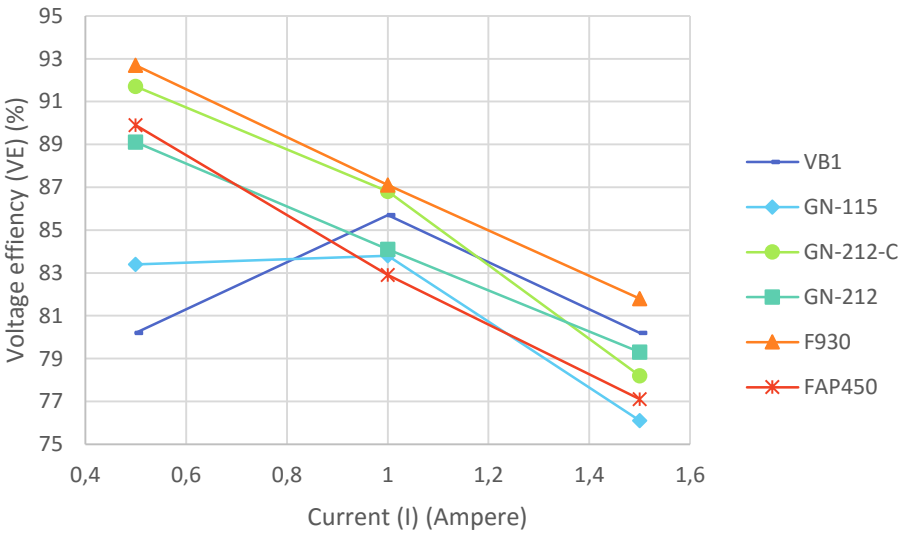


*Figure 30. Voltage efficiency (VE) versus current (A)*

During discharge, the current was not maintained at constant 1500 mA for either the VB1 or the GN-115 Membrane as seen in *Appendix A*, Figure 56 and Figure 64. Instead, the discharge current went from 1500 mA to about 1000 mA during the discharge cycle as a result of transient equipment instability that could not be controlled.

### 5.1.10 Internal cell resistance

By measuring the approximate voltage at 50% SOC from the different charge-discharge curves for all the membranes, a rough estimate of the internal resistance of the cell was obtained. These data have been compiled in Appendix D. Table 19 contains the voltage at approximately 50% SOC for the different membranes and were plotted versus current

(500 mA, 1000mA, 1500mA). The slope of the function voltage versus current was multiplied with the surface area of the membrane to obtain the overall resistance of the cell, as visualized in *Appendix D*.

However, as 50% SOC may vary throughout the experiments, only a rough estimate of the cell resistance was obtained. Furthermore, as the discharge and charge cycles also differ in time for a few membranes, it is a very rough estimate. This value was, however, used in order to spot any severe irregularities between the membranes and used to evaluate the experimental setup rather than the membrane properties itself.

*Table 19. Compiled voltages at 50% SOC for all membranes for cell polarization plots.*

| | 500 mA | | 1000 mA | | 1500 mA | |
|---|---|---|---|---|---|---|
| | *Charge (V)* | *Discharge (V)* | *Charge(V)* | *Discharge (V)* | *Charge (V)* | *Discharge (V)* |
| VB1 | **1,42** | **1,33** | **1,47** | **1,30** | **1,52** | **1,25** |
| GN-115 | **1,46** | **1,33** | **1,51** | **1,27** | **1,54** | **1,22** |
| GN-212 | **1,46** | **1,32** | **1,48** | **1,28** | **1,54** | **1,26** |
| GN-212C | **1,45** | **1,31** | **1,48** | **1,28** | **1,55** | **1,23** |
| F930 | **1,45** | **1,34** | **1,48** | **1,30** | **1,51** | **1,25** |

The values that were obtained from these experiments are compiled in Table 20 and it is clear that all internal resistances are about the same size for all the different membranes. The lower values for the charging cell resistances for F930 and GN-212 are attributed to errors in the estimated 50% SOC points in the charging curves at different charging currents. A more accurate method to obtain cell polarization plots would involve charging the cell up to 50% SOC and then carrying out a series of charging steps for 30 seconds at a particular current, followed by discharging at the same current for 30 seconds. The charging and discharging voltage values are plotted as a function of current density and the cell resistivity is obtained from the slope of this line. This procedure allows the SOC to be accurately controlled during the measurements, but due to time limitations, such experiments could not be carried out. Further measurements of cell resistance using this procedure are therefore recommended.

*Table 20. Internal resistance in Ωcm-2 measured at approximate 50% SOC for some membranes*

| | INTERNAL RESISTANCE ($\Omega CM^{-2}$) |
|---|---|

| MEMBRANE | **Charge** | **Discharge** |
|---|---|---|
| **VB1** | 2,5 | 2 |
| **F930** | 1,5 | 2,25 |
| **GN-115** | 2 | 2,75 |
| **GN-212C** | 2,5 | 2 |
| **GN-212** | 1 | 1,38 |

## 5.2 Summary of permeability rates of vanadium ions across the membranes

The results in this section were obtained by collecting samples at different time intervals from the blank solution of the diffusion test cell and using Fick's law of diffusion to determine the diffusion coefficients as explained in section 4.2.3 and 4.3. Samples from the blank (1 ml) were periodically drawn from the blank at different time intervals depending on the color of the blank. Usually, the cell was left over night and kept running for approximately 25 hours for each vanadium ion and the temperature was kept between 25-28°C using the previously described water cooling system. The samples were sent for ICP analysis to determine the vanadium concentration of each sample. The raw data from ICP analysis are compiled in tables for the different membranes in *Appendix B*. Some of the samples were diluted prior being sent to ICP analysis and some samples were further diluted by the chemical analysis team.

The molecular diffusion for a one-dimensional system through a membrane is explained by Fick's first law of diffusion which was described in detail in section 4.2.3. This equation was used to determine the diffusion coefficients using the compiled raw data from ICP analysis. Units in this section are given in $cm^2min^{-1}$ and have thus been multiplied with the membrane thickness. The membrane thickness is stated for every membrane in each of the following sections.

The value of the $CB_0$ is 1 M and represents the initial concentration of the vanadium ions on the enrichment side. CA represents the vanadium concentration of the blank which changes with time.

### 5.2.1 GN-115

All measured diffusion coefficients which were obtained from the slopes of the lines in Figure 32, for the GN-115 membrane, are compiled in Table 21. For the GN-115, it was found that the diffusion rates were in the following order $V^{4+} > V^{5+} > V^{3+} > V^{2+}$. The thickness for the membrane was 125 um. The concentration was almost linear for each ion versus time as can be seen in Figure 31.

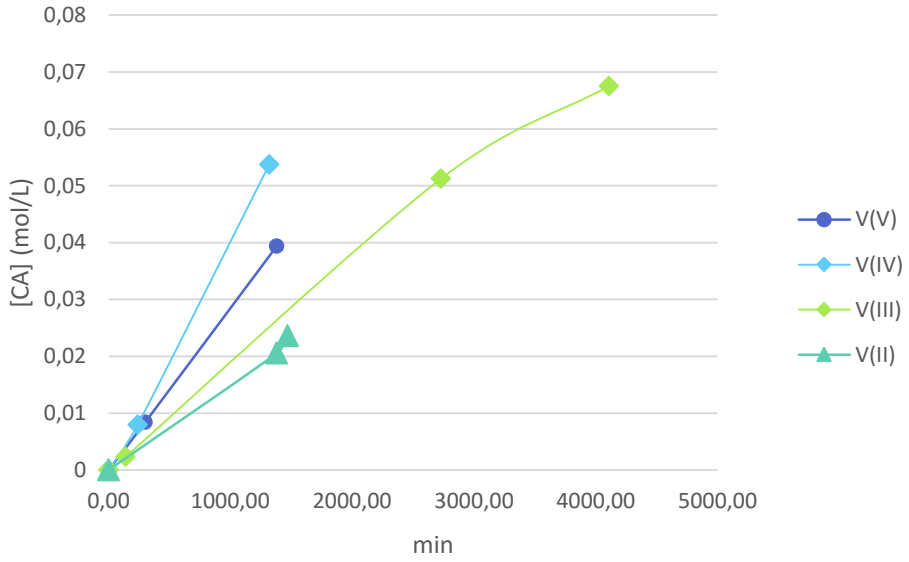


*Figure 31. Concentration versus time for all vanadium ions for the GN-115 membrane*

In order to obtain the diffusion coefficient, the procedure explained in section 4.2.3 was used. The slopes of –LN(CB0-2CA) versus time found in Figure 32, was multiplied with the volume ($cm^3$) and divided with the membrane area ($cm^2$).

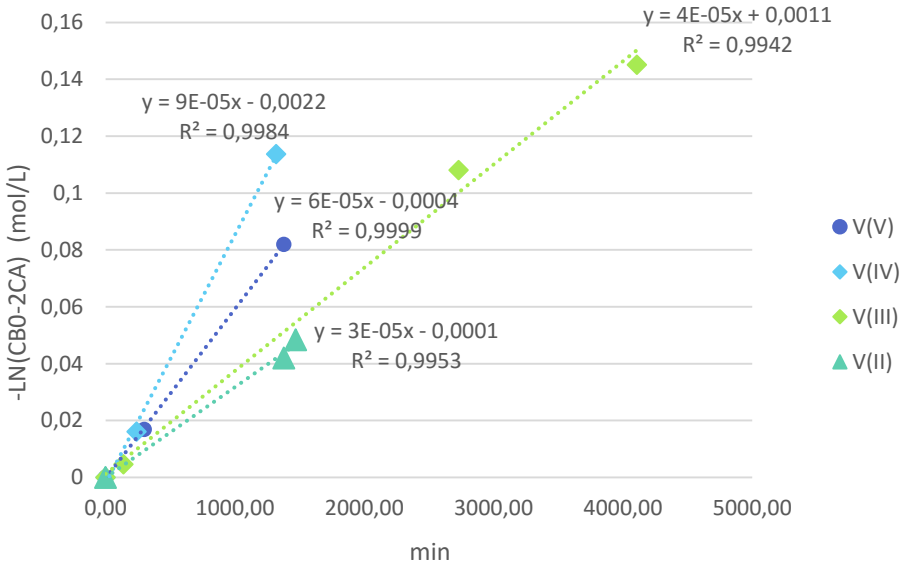


*Figure 32. –LN(CB0-2CA) versus time for the GN-115 membrane*

The calculated diffusion coefficients are compiled in Table 21. The V(II) ion diffused quickest through the membrane and V(IV) ion diffused the slowest. The difference of the V(II) and the V(IV) is about a factor of 3, otherwise they are all the same order of magnitude.

*Table 21. Permeability of vanadium ions through the GN-115 membrane*

| **Vanadium ions** | $V^{2+}$ | $V^{3+}$ | $V^{4+}$ | $V^{5+}$ |
|---|---|---|---|---|
| **Diffusion coefficient/ x $10^{-7}$ $cm^2min^{-1}$** | 7,5 | 10 | 23 | 15 |

### 5.2.2 FAP450

The thickness of the FAP450 was 60 um and was used to calculate the diffusion coefficients from the slopes in Figure 34. Table 22 consists of the diffusion coefficients of the FAP-450 membrane. It was found that the diffusion coefficients were in the order $V^{2+}$, $V^{5+} > V^{4+} > V^{3}+$. Figure 33 represents concentration of the blank versus time for all four vanadium ions for the FAP-450 membrane. The values were obtained from *Appendix B*, section FAP-450.

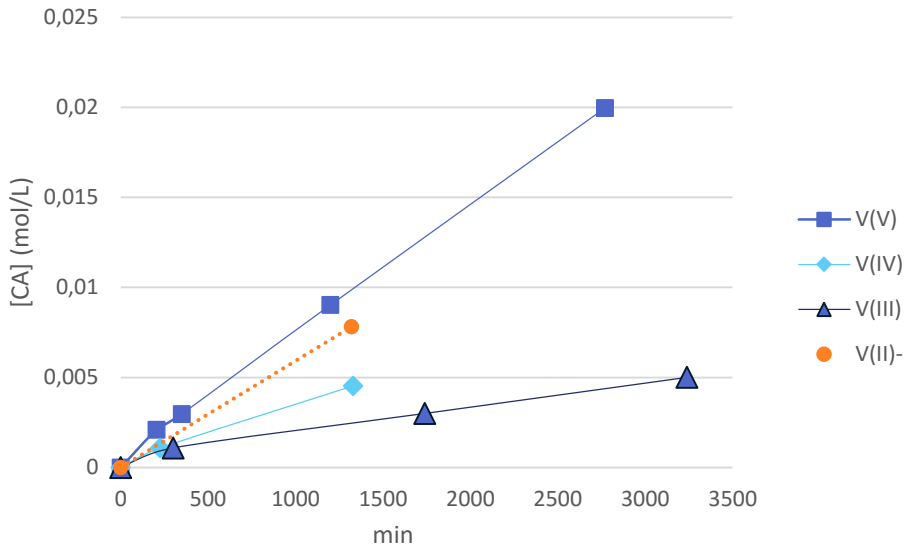


*Figure 33. Concentration versus time for the FAP450 membrane*

As was the case with the GN-115 membrane, the slope of each line in Figure 34 was used to calculate the diffusion coefficients which are compiled in Table 22. It was found that the V(II) and V(V) diffused with about the same rate while the V(III) ion diffused quicker than all the other. The internal difference between the highest and the lowest diffusion coefficient in Table 22 is about a factor of 3.

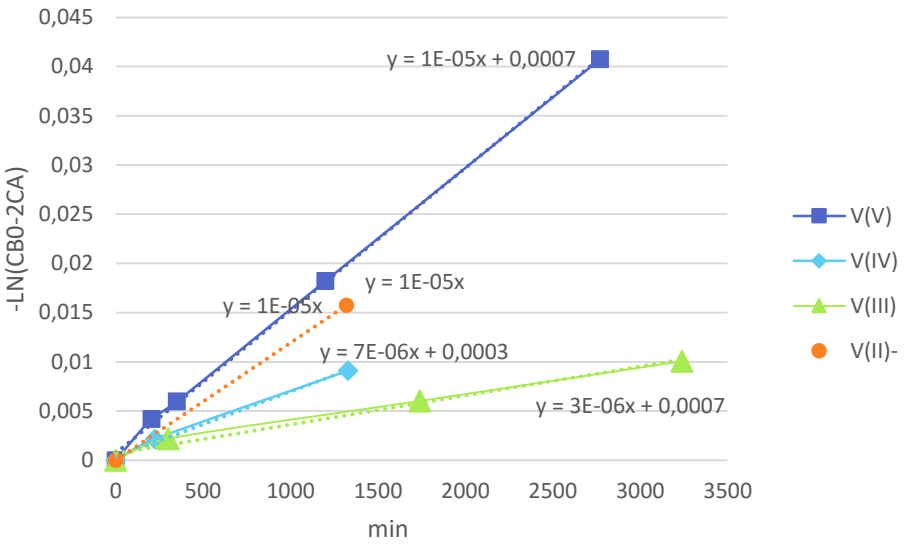


*Figure 34. –LN(CB0-2CA) versus time for the FAP450 for all vanadium ions*

*Table 22. Permeability rates for all vanadium ions through the FAP450.*

| **Vanadium ions** | $V^{2+}$ | $V^{3+}$ | $V^{4+}$ | $V^{5+}$ |
|---|---|---|---|---|
| **Diffusion coefficient/ x $10^{-7}$ $cm^2min^{-1}$** | 1,2 | 0,4 | 0,7 | 1,2 |

### 5.2.3 F930

The thickness of the F930 membrane was 30 um which was used to calculate the diffusion coefficients in Table 23. It was found that the diffusion coefficients were in the order $V^{2+} > V^{5+} > V^{3+} > V^{4+}$. Low errors in regard of diffusion coefficients are obtained for all ions except for the V(V) from which the diffusion coefficient may vary as values differed from the linear approximation which are plotted in Figure 35.

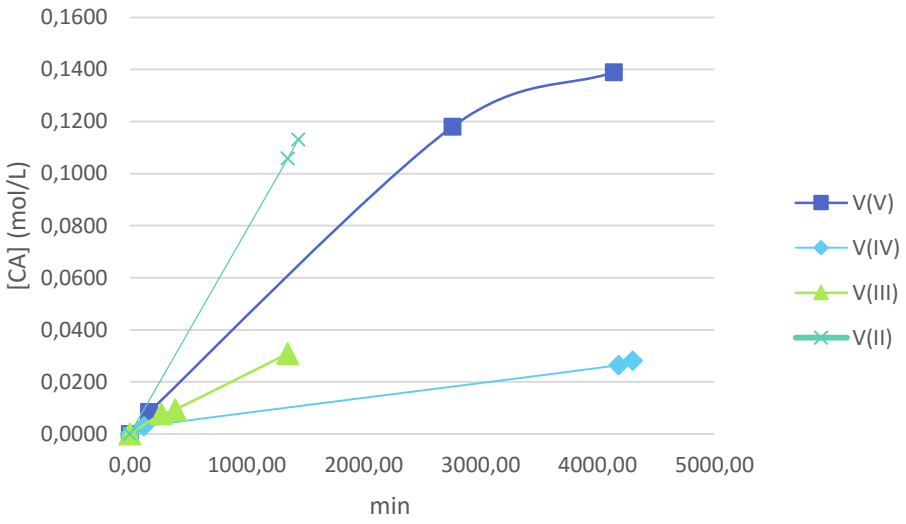


*Figure 35. Concentration versus time for all vanadium ions using the F930 membrane*

Figure 36 represents the plots from which the diffusion coefficients were determined. It was found that the internal difference between the ions were quite severe as listed in Table 23. The smallest diffusion coefficient was obtained for the V(IV) ions with a value of 0,6e-07 $cm^2min^{-1}$ and the highest was obtained for the V(II) ion at 12e-07. The difference between these two values is a factor of 20.

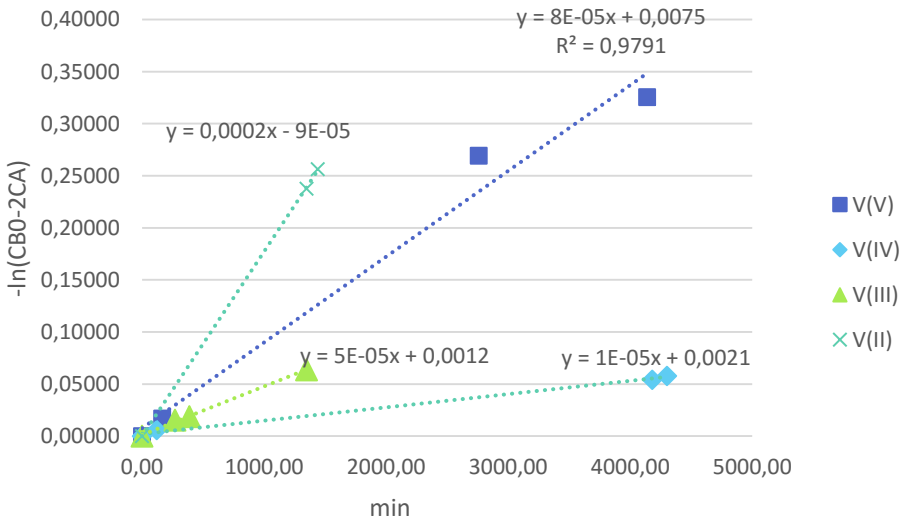


*Figure 36. –LN(CB0-2CA) versus time for the F930 membrane*

*Table 23. Permeability rates through the F930 membrane*

| **Vanadium ions** | $V^{2+}$ | $V^{3+}$ | $V^{4+}$ | $V^{5+}$ |
|---|---|---|---|---|
| **Diffusion coefficient/ x $10^{-7}$ $cm^2min^{-1}$** | 12 | 3,0 | 0,6 | 4,8 |

### 5.2.4 VB2

The thickness of the VB2 membrane was 30um. The diffusion coefficients are compiled in Table 24 and they were found to be in the following order; $V^{2+} > V^{4+} > V^{3+}$. $V^{5+}$ was not measured for this membrane. All experimental values for the VB2 have very low $R^2$ values.

The slopes of the different ions in Figure 38 was used to determine the diffusion coefficients for V(II), V(III) and V(IV).

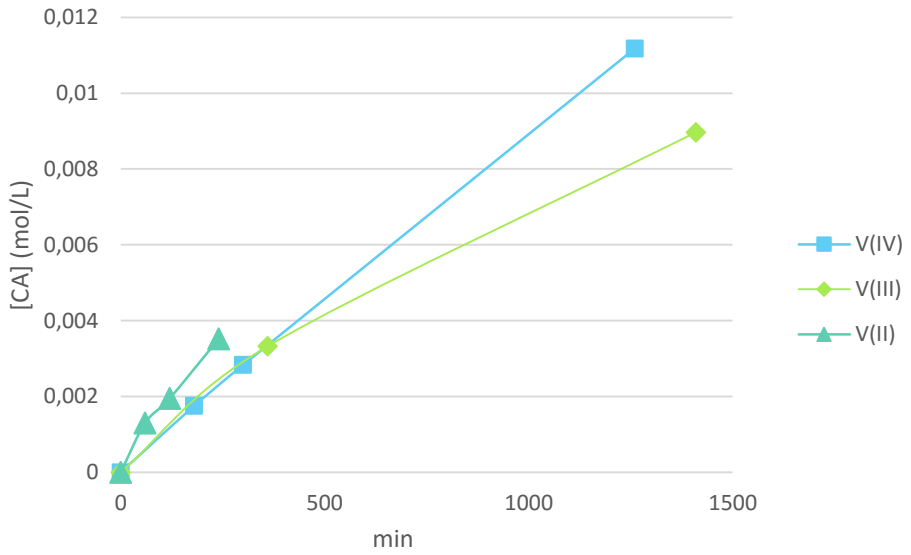


*Figure 37. Concentration versus time for the different vanadium ions using the VB2 membrane in a diffusion cell*

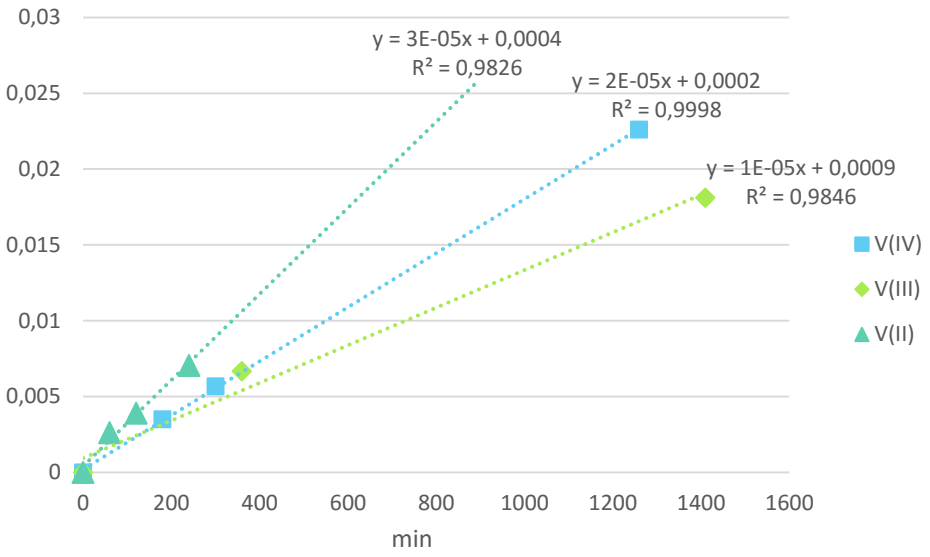


*Figure 38. Plots of –ln(CA-2CB) versus time (h) for the VB2*

The obtained diffusion coefficients for the V(II), V(III) and V(IV) respectively are compiled in Table 24. The lowest value was obtained for the V(III) and the highest for the V(II) and the internal difference was a factor of 3.

*Table 24. Permeability rates through the VB2 membrane*

| **Vanadium ions** | $V^{2+}$ | $V^{3+}$ | $V^{4+}$ | $V^{5+}$ |
|---|---|---|---|---|
| **Diffusion coefficient/ x $10^{-7}$ $cm^2min^{-1}$** | 0,12 | 0,04 | 0,08 | n.a |

### 5.2.5 Summary of permeability rates for all membranes

In this section, all permeability rates are compiled and compared with each other. It was found that the VB2 membrane had the lowest permeability rate for the $V^{2+}$ and the $V^{5+}$ ions, respectively. The VB2 and the F930 membranes had an internal difference between the ions of a factor of 3 and the F930 had the highest internal difference of a factor 20. The FAP450 had the second lowest permeability for the $V^{3+}$ and $V^{2+}$, $V^{4+}$ ions among the tested membranes. It also had the lowest value of V(V). However, due to lack of time and experimental errors, the VB2 was not tested for V(V) permeability in this study and may provide better (or worse) results. Table 25 consists of all the measured diffusion coefficients for easy comparison.

*Table 25. Compiled permeability rates for all membranes*

| **Diffusion coefficient/ x $10^{-7}$ $cm^2min^{-1}$** | **Vanadium ions** | **Membrane thickness (µm)** |
|---|---|---|

| Membranes | $V^{2+}$ | $V^{3+}$ | $V^{4+}$ | $V^{5+}$ | |
|---|---|---|---|---|---|
| VB2 | 0,12 | 0,04 | 0,08 | n.a | 60 |
| F930 | 12 | 3,0 | 0,6 | 4,8 | 30 |
| FAP450 | 1,2 | 0,4 | 0,7 | 1,2 | 60 |
| GN-115 | 7,5 | 10 | 23 | 15 | 125 |

Table 26 contains the order of diffusion coefficients between the different vanadium ions, although in most cases any differences are within experimental error.

In general however, it can be seen that VB2 membrane has the lowest vanadium ion permeability, however this membrane is also considerably thicker than the other membranes (except for GN-115. It should also be mentioned that this membrane was not evaluated in the charge-discharge cycling tests due to limited sample availability, so further testing of this membrane is recommended).

*Table 26. Order of permeability rate for the different membranes.*

| Membranes | Permeability order |
|---|---|
| VB2 | $V^{2+} > V^{4+} > V^{3+}$ |
| F930 | $V^{2+} > V^{5+} > V^{3+} > V^{4+}$ |
| FAP450 | $V^{2+}$ and $V^{5+} > V^{4+} > V^{3+}$ |
| GN-115 | $V^{4+} > V^{5+} > V^{3+} > V^{2+}$ |

## 5.3 Membrane chemical resistance in V(V) solution

The results from this section were obtained following the experimental procedure explained in section 4.6 and simply by immersing the membrane to be tested in V(V) electrolyte solution for extended times. The experimental results of this part of the study are compiled in *Appendix D*.

It was found that the GN-115 (which was the only membrane tested for its chemical stability) increased about 10% in weight and about 26% in thickness due to the influence of the electrolytes The width and the length increased about 6% as seen in the summarized result in Appendix D, Table 60. As the membrane did indeed swell due to the influence of the electrolyte, it is possible that the pore size of the membrane might have changed which could indeed influence the properties of the membrane, including the high vanadium ion permeability values reported in Section 5.2.1.

# CHAPTER 6

## 6.1 Computer simulations using electrochemical and thermal models

As explained in the membrane section, the total vanadium transfer across the membrane cannot be controlled. Therefore, it is imperative to implement active controllers based on mathematical models of the battery, which can optimize the energy efficiency as well as to determine when to remix the electrolytes in order to reestablish the capacity. Tang et al. have developed such a model [5], which was used to simulate the VRB during extended charge-discharge operation in this study. Parameters used for all simulations are compiled in Table 27. Table 28 consists of specific membrane properties and parameters which were used when simulating these specific membranes. Figure 39 represents a charge-discharge curve from simulations (left) and from a physical battery (right).

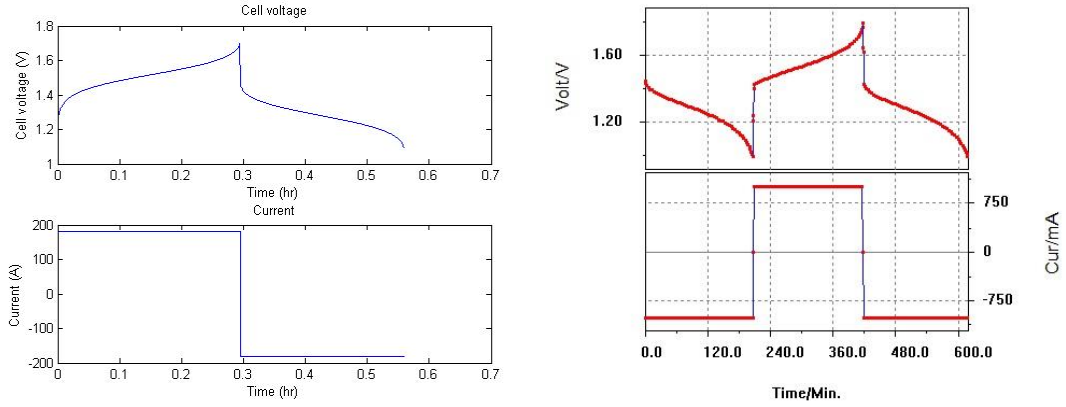


*Figure 39. Left: Charge/discharge curve for the VRB simulations. Right: Charge/discharge curve from experiment setup*

The models developed at UNSW by Ao Tang and co-workers [2, 3, 5] are based on conservation of energy and mass and were used to study the capacity loss due to vanadium cross-contamination as well as side-reactions during charge-discharge cycling. As the influence of gassing might be quite severe above SOC 90% and below 10%, this is the operating conditions for the battery throughout the simulations. The Nernst Equation, equation 24, is used in conjunction with conservation of mass to describe the dynamic cell voltage which can be used to predict the capacity after long term charge-discharge cycling.

$$E = E^{\circ} + \frac{RT}{F}\ln\left\{\left(\frac{c_{VO_2^+}\cdot c_{H^+}^2}{c_{VO^{2+}}}\right)\left(\frac{c_{V^{2+}}}{c_{V^{3+}}}\right)\right\} \quad (24)$$

Where F is the Faraday constant, R is the universal gas constant, T is the temperature in Celsius, $E^{\circ}$ is the standard electrode potential (at standard conditions) and $c_i$ is the concentration of the different vanadium ions.

*Table 27. Parameters and constants for charge-discharge simulation of the VRB battery*

| Symbol | Description | Value (unit) |
|---|---|---|
| **F** | Faraday's constant | 96485 (C/mol) |
| **$N_A$** | Avogadro's constant | $6.022 \cdot 10^{23}$ ($mol^{-1}$) |
| **h** | Planck's constant | $6.626 \cdot 10^{-34}$ (Js) |
| **T** | Temperature | 298 (K) |
| **e** | Elementary charge | $1.6022 \cdot 10^{-19}$ (C) |
| **R** | Ideal gas constant | 8.3145 ($J\ K^{-1}mol^{-1}$) |
| **S** | Membrane area | 30 ($dm^2$) |
| **$k_i$** | Diffusion coefficient for component i | Values from Table 28($dms^{-1}$) |
| **R** | Cell resistance | 2 ($\Omega cm^2$) |
| **Vs** | Volume of each half cell | 1 (L) |
| **i** | Current density | 0.060 ($Acm^2$) |
| **A** | Electrode surface area | 3000 ($cm^2$) |
| **cycle** | Number of cycles | 100 |
| **V_upp** | Upper cell voltage limit | 1.7 (V) |
| **V_low** | Lower cell voltage limit | 1.1 (V) |
| **n** | Number of cells | 40 |
| **d** | Normalized membrane thickness | 1 |

*Table 28. Specific parameters used for MATLAB simulations (replaces ki in Table 27). All units are given in dms-1 with membrane thickness included. $k_i$ represents vanadium with charge i.*

| Symbol ($dms^{-1}$) | **F930** | **FAP450** | **GN-115** |
|---|---|---|---|
| **k2** | 6,7E-07 | 3,3E-08 | 1,0E-07 |
| **k3** | 1,7E-07 | 1,0E-08 | 1,3E-07 |
| **k4** | 3,3E-08 | 2,0E-08 | 3,0E-07 |
| **k5** | 2,7E-07 | 3,3E-08 | 2,0E-07 |

The total losses in the system are attributed to ohmic and ionic over potential where the over potential can be divided into activation- and concentration over potential. The latter describing the issue of active components not reaching the surface of the electrodes fast enough and activation over potential describing the necessary potential to drive the reaction at the current rate.

## 6.2 Simulation of extended charge-discharge operation using experimentally determined permeability rates

The values from Table 27 and Table 28 were used for all simulations in this section using software developed by UNSW. In this section, the simulations do not take any air oxidation of the V(II) into account and they show what the worst case scenario would be if the electrolytes were not remixed. In real systems, this behavior goes unnoticed because the electrolytes are remixed after a certain number of cycles to make sure that the capacity is kept at close to 100% at all times.

Furthermore, 1.7 V represents about 90% SOC and will be attributed as upper voltage limit. In the same way, 1.1 V is the lower voltage limit which represents about 10% SOC.

### 6.2.1 F930

F930 gave the second highest values from the cell performance and membrane evaluation section in section 5.1. Therefore, the diffusion coefficients from this membrane was used in simulations to evaluate any capacity loss over extended cycles. The capacity drop can be seen in Figure 40 where about 90% of the initial capacity is lost after 60 cycles due to self-discharge reactions.

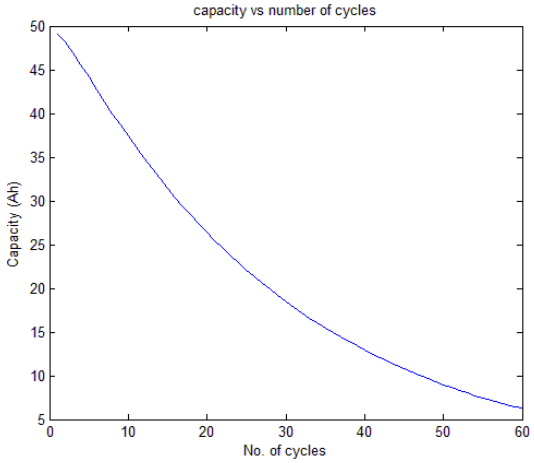


*Figure 40. Capacity vs number of cycles for the F930 membrane.*

At the beginning of the experiment, only V(V) and V(II) exist at the upper voltage limit of 1.7 V and at the lower voltage limit of 1.1 V, almost only V(III) and V(IV) is present as visualized in Figure 41. However, as self-discharge reactions (section 3.4.1) occur, the concentration starts to shift towards V(IV) instead of V(V) at the upper voltage limit and towards V(II) and V(IV) at the lower voltage limit.

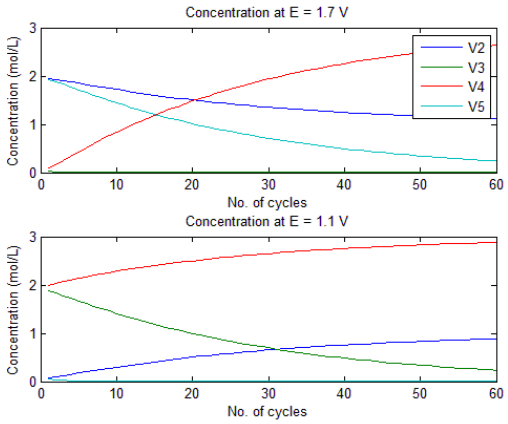


*Figure 41. Concentration profiles of all vanadium ions versus number of cycles using the F930 membrane.*

From Figure 42, it can be seen that there is a constant decrease of the concentration of the V(II) and V(V) versus time. The V(IV) continues to increase until the capacity is

almost zero. As there is almost no V(V) and V(II) present at upper voltage limit, the discharge time goes down as represented by Figure 43. In this figure, the current versus time for each charge-discharge cycle in the first few cycles are equally long. However, as the simulation continues to increase, the current versus time changes shape with shorter discharge and charge cycles. This is due to the decrease of available vanadium to charge and discharge observed in Figure 41 and Figure 42.

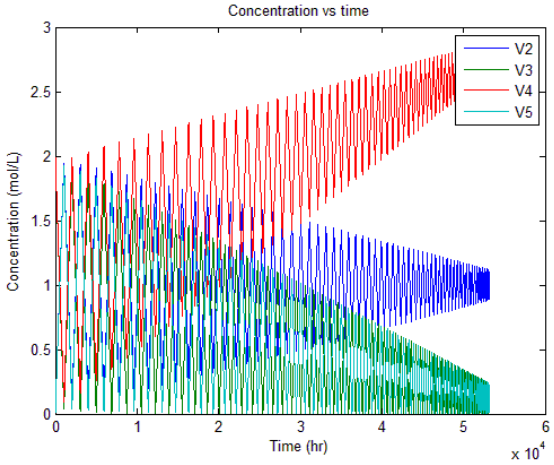


*Figure 42. Concentration versus time using the F930 membrane for 60 cycles*

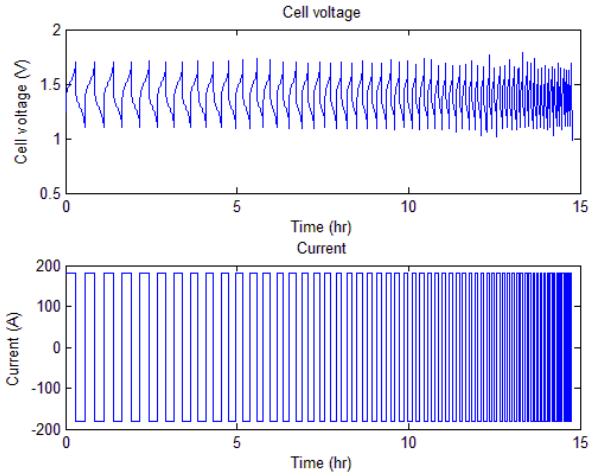


*Figure 43. Current versus time for the F930 membrane.*

### 6.2.2 FAP450

The FAP450 membrane is recommended for VRB use by Fumatech™ due to high EE, CE and VE. In this study, the F930 gave slightly higher values in section 5.2 for four charge-discharge cycles as compiled in section 5.1.10. However, the capacity loss for the FAP450 over extended use (60 cycles) in MATLAB proved a very small capacity drop as seen in Figure 44. After 60 cycles, the capacity only dropped from 50,45Ah to about 50,1Ah. This represents a capacity drop of about 0.7%.

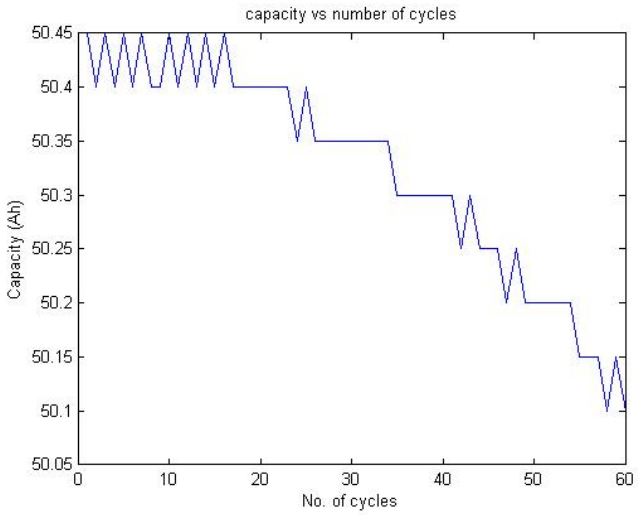


*Figure 44. Capacity versus number of cycles for the FAP450 membrane*

As there is almost no capacity drop after 60 cycles, almost only V(II) and V(V) should be present at the upper voltage limit even after 60 cycles. In the same way, only V(III) and V(IV) should be present at the lower voltage limit of 1.1 V. Figure 45, which contains the concentration gradients obtained from the simulations, show exactly this behavior.

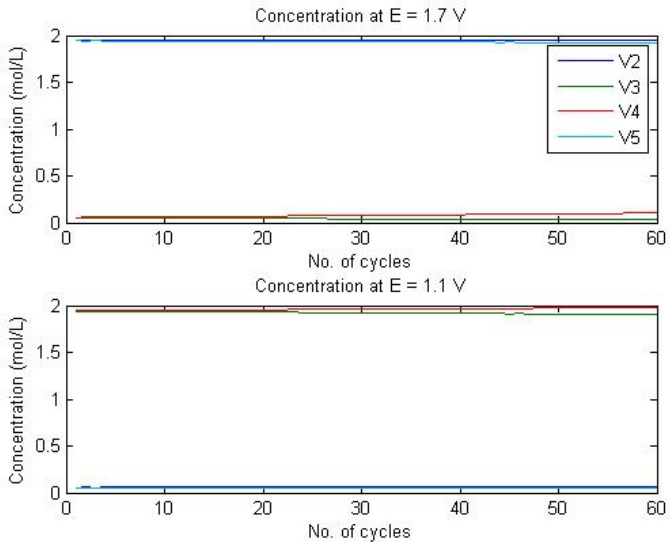


*Figure 45. Concentration gradients for the vanadium ions versus number of cycles using the FAP450 membrane.*

Furthermore, the cell voltage and the cycle time for charge and discharge respectively are uniform as seen in Figure 46. This is due to the same available concentration for charge- and discharge respectively over extended use.

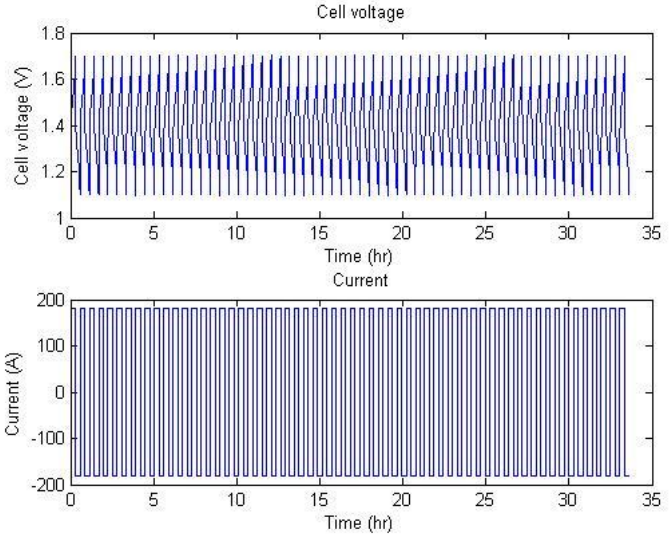


*Figure 46. Current versus time for the FAP450 membrane*

### 6.2.3 GN-115

Figure 47 shows the capacity drop over extended use of the GN-115 membrane. About 50% capacity was lost after 60 cycles due to the crossover of vanadium species through the membrane. Therefore, the GN-115 proved to be a better choice than the F930 even though the F930 outperformed the GN-115 at laboratory scale evaluation inside the VRB (section 5.1).

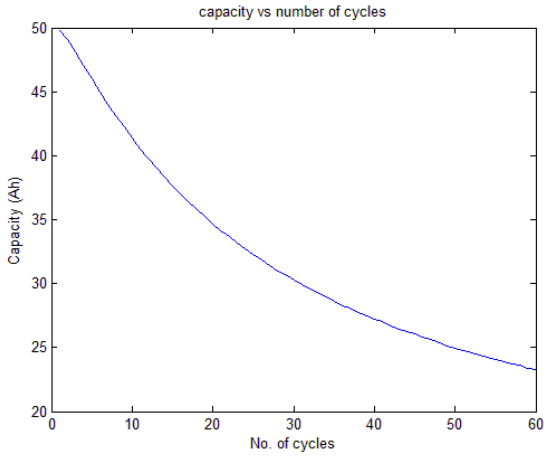


*Figure 47. Capacity versus number of cycles for the GN-115 membrane*

Instead of a buildup of V(IV) as was the case with the F930 membrane in Figure 42, the GN-115 shows a buildup of V(III) after extended use as compiled in Figure 48. This is interesting as the permeability rates for the GN-115 was higher for all ions (except the V(II) ion, Table 25) when compared to the F930 membrane. The only difference was that the GN-115 membrane had the same order of magnitude in regard of ion permeability and the F930 did not.

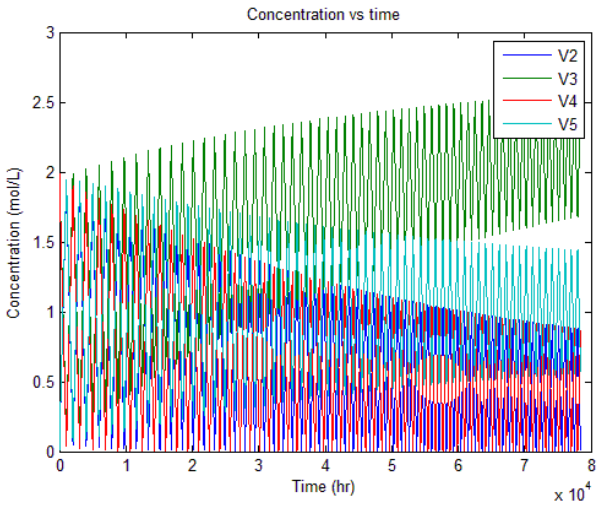


*Figure 48. Concentration of vanadium ions versus time using the GN-115 membrane*

From the concentration gradient figures in Figure 49, the same behavior as in Figure 48 is noticed. The concentration at the OCV of 1.7 V contains initially of V(II) and V(V), but after 60 cycles, the concentration of V(II) have dropped to about half the initial concentration of 2 M. The concentration of V(V) has dropped to about 1.5 M from the initial 2 M. Furthermore, the concentration of V(III) increases from 0 M initially to close to 2 M after 60 cycles.

At the lower SOC, at a OCV of 1.1 V, the V(IV) decreases from 2 M to 1 M and the concentration of V(V) is increasing from 0 M to about 0.5 M. The V(III) increases from 2M to about 2.5 M. This indicates that there is an increasing difference between the concentration of V(V) and V(II).

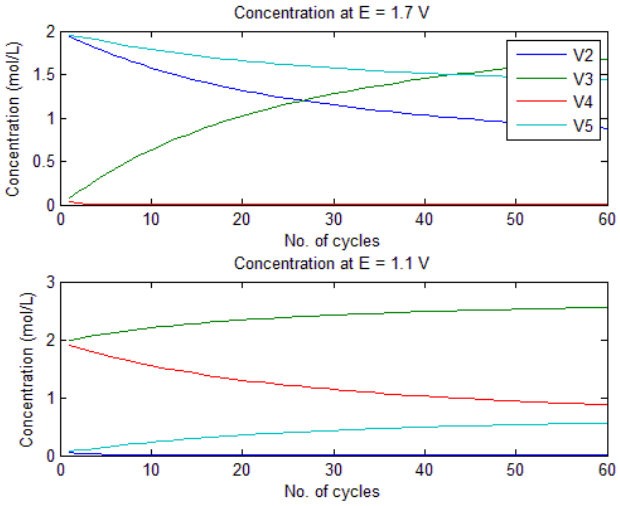


*Figure 49. Vanadium concentration at upper- and lower voltage limit respectively for the GN-115 membrane.*

## 6.3 Thermal modelling and simulations of the VRB using permeability rates from the different membranes

The self-discharge reactions explained in section 3.4.1 are exothermic and will lead to an increase in the electrolyte temperature. Especially at stand-by when the electrolytes which are still in the cell-stack starts to participate in self-discharge reactions which leads to an accumulation of heat inside the stack. In order to not get irreversible precipitation of vanadium ions in the electrolytes, it is imperative to maintain the operation temperature. Depending on the outside temperature and fluctuations during the day and they year, additional cooling or heating may have to be applied. In this section, the permeability rates determined in section 5.2 are used in thermal simulations from software developed at UNSW.

Each membrane was simulated for a period of 5 days and the temperature goes from 10°C at night to 25°C during the day.

In this section the parameters stated in Table 29 and the diffusion rates from Table 25 were used. The peaks of the blue lines in this section is from when the pumps are switched off and the battery is in standby mode. Therefore, heat is accumulated by the self-discharge reactions taking place in the cell stack and thus also an increase in electrolyte temperature. After the pumps are switched on again, the temperature of the cell stack reaches the temperature of the electrolytes which are stored in the tanks.

*Table 29. Parameters used for thermodynamic simulations of the VRB*

| **Simulation Parameters** | |
|---|---|
| Number of cell stacks | 40 |
| Vanadium concentration | 1.6 M |
| Capacity (kWh) | 40 |
| Cell charge resistivity | 2.1 $\Omega cm^{-2}$ |
| Cell discharge resistivity | 2.2 $\Omega cm^{-2}$ |
| Formal potential | 1.35 V |
| Minimum temperature | 10C |
| Maximum temperature | 25C |
| Discharge time | From 14:00 to 22:00 |
| Simulation days | 5 |
| **Current and Operation SOC** | |

| | |
|---|---|
| Charge current | 50 A |
| Discharge current | 100 A |
| Lower SOC | 20 % |
| Upper SOC | 80% |
| Flow factor for charging | 8 |
| Flow factor for discharge | 8 |
| **Tank Design** | |
| Height | 1 m |
| Wall thickness | 1 cm |

### 6.3.1 FAP450

The FAP450 membrane had low permeability rates. However, without any cooling, the stack and air temperature continue to increase from a starting temperature of 14°C day 0 to about 23°C on day 5 as seen in Figure 50. The temperature of the tank increases at the end of the warm period of the day and is kept almost constant during colder hours of the night. This means that the cooling effect of 10°C outdoor temperature keeps the electrolyte at a constant temperature while an outdoor temperature of 25°C increases the electrolyte temperature. If the electrolyte is not cooled during the night, and instead kept constant, additional cooling may be needed as heat would otherwise accumulate in the system. This indicates that additional cooling may be required in order to maintain the operating temperature of the VRB while using FAP450 membranes.

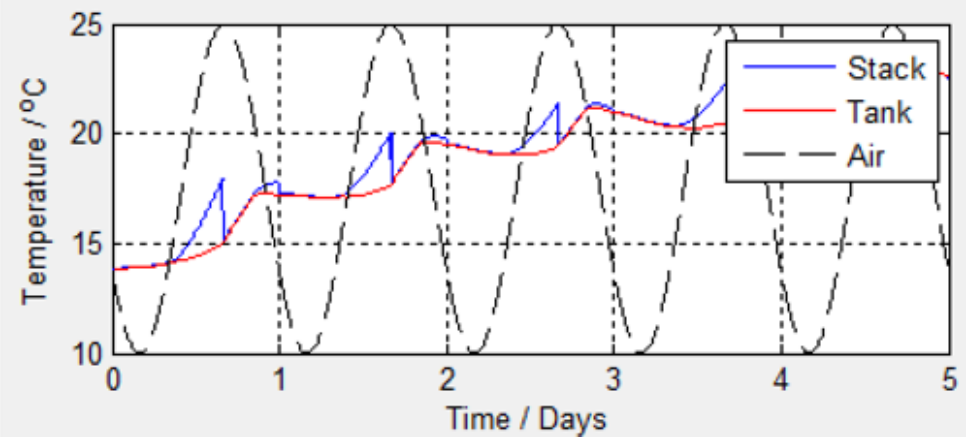


*Figure 50. Temperature of cell stack, electrolyte storage tank and surrounding air versus time for the FAP450 membrane in VRB thermodynamic simulations*

### 6.3.2 F930

As expected due to the higher diffusion coefficients of the F930, more heat is developed when using this membrane compared to the FAP450 as seen in Figure 51. The

temperature of the stack increases enormously during certain periods of the day and reaches more than 37°C after 5 days of VRB charge-discharge operation. The heat of the stack is dispersed to the tank which reaches a temperature of about 25°C after 5 days. Clearly, higher permeability rates leads to higher temperatures and it is imperative to implement active cooling systems and temperature monitoring for these systems.

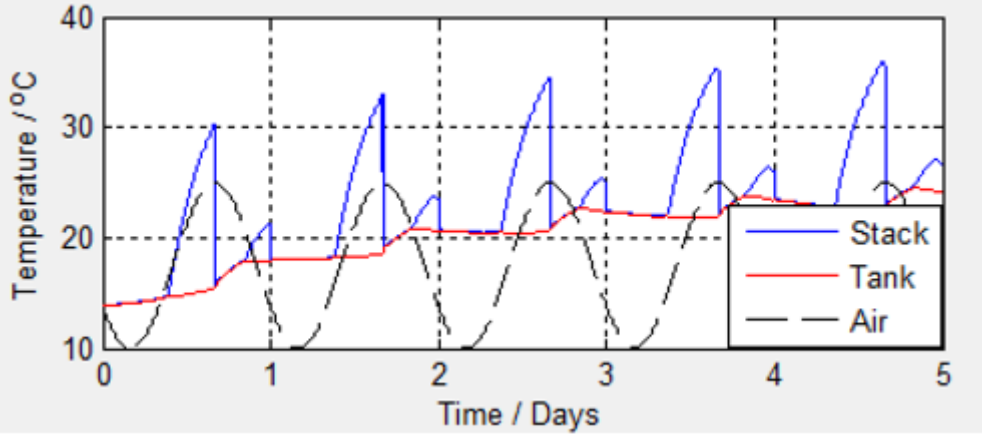


*Figure 51. Temperature of cell stack, electrolyte storage tank and surrounding air versus time for the F930 membrane in VRB thermodynamic simulations*

### 6.3.3 GN-115

Figure 52 contains the thermodynamic simulation graph using the permeability rates determined in section 5.2.1. As expected, due to the larger diffusion coefficients of the GN-115 compared to FAP-450, the peaks of the stack temperature is much higher for the GN-115. The temperature increases to about 40 degrees and increasing after 5 days of use. This means that external cooling should be applied to the cell stack at standby – or the pumps have to run without being turned off.

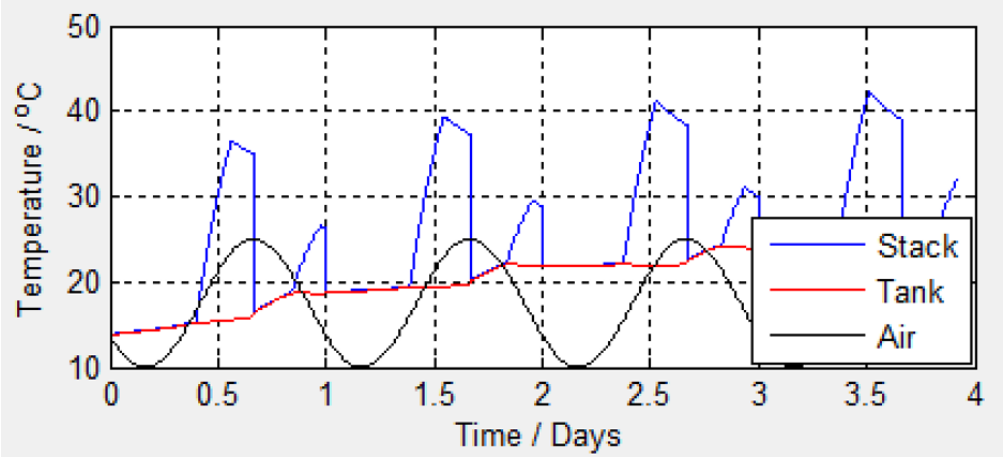


*Figure 52. Thermodynamic simulation of the GN-115 membrane for 4-5 days of use.*

The electrolyte tanks reaches about 25°C after 4 days of use. Also, there is a risk that it may increase a bit more as it has not yet levelled off completely. The cell stack temperature is in the risk zone with temperatures reaching as high as 40-45°C.

### 6.3.4 Nafion

Based on thermodynamic simulations of the widespread Nafion 115 membrane, it can be seen that the cell stack temperature reaches about 40-45°C when the pumps are switched off. Figure 53 consists of the stack temperature, tank temperature and air temperature of the Nafion-115 thermodynamic simulation. This is noticed by the blue peaks at 0.5 days, 1,5 days and so on. However, the tank temperature is almost leveling off at around 26°C which is still in the safe operating temperature of the VRB (10-50°C).

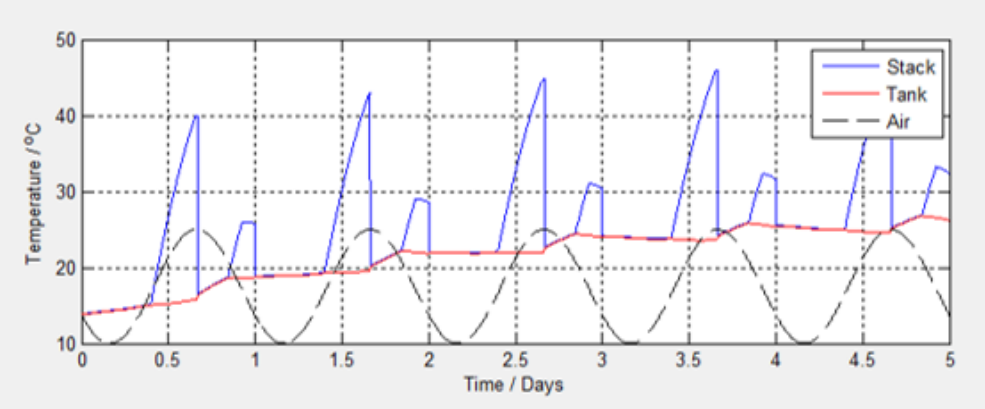


*Figure 53. Temperature of cell stack, electrolyte storage tank and surrounding air versus time for the Nafion-115 membrane in VRB thermodynamic simulations*

## 6.4 Summary computer simulations

From the simulations in section 6.2, it is concluded that the FAP450 performed better than the other two membranes over extended use in the VRB battery, showing almost no capacity drop over extended charge-discharge operation. It is very interesting that the FAP450 outperformed the F930 completely even though the latter performed better during the charge-discharge cycling test in Section 5.1. These differences highlight the experimental errors associated with each of the procedures used in this study and would also exist in similar reported studies in the published literature. Despite efforts to eliminate the sources of some of these errors, including temperature control and water transfer effects due to osmotic pressure variations between the vanadium and blank solutions, dilution errors are difficult to control, as would be slight variations in

membrane properties between different samples used in each test. The simulation results presented here should therefore be considered as qualitative estimates of cell behavior with different membranes.

Even though the F930 had lower diffusion coefficients than the GN-115, the latter outperformed the F930. This could be due to the large difference between the different ions and their diffusion coefficients for the F930 where large differences of a factor of 20 is observed between the ions. For the GN-115, the diffusion coefficients differ internally with about a factor of 3 as seen in Table 25. With a large difference in diffusion coefficients between the ions, buildup of vanadium ions on one side will occur which will lead to a severe drop in capacity. If instead the vanadium diffuse with the same rate, about the same number of ions diffuse from the anode side, as from the cathode side of the battery – leading to a net stability of available vanadium ions to charge and discharge respectively.

The differences observed between the F930 and the FAP450 during charge-discharge evaluation, which were favored F930, are not seen at all during computer simulations. Instead, the FAP450 completely outperforms the F930 membrane with almost no capacity drop at all. This might be due to FAP450 having the same order of magnitude between the diffusion coefficients for all ions as previously discussed. This would explain why the F930 is also outperformed by the GN-115 even though the F930 have smaller diffusion coefficients for some ions compared to the GN-115. The only difference between the two is that the GN-115 have a factor of 3 difference in diffusion rates between the ions and the F930 have a factor 20.

During a small number of cycles, this difference might not be noticed and the F930 may perform better in the short run (as noticed in Section 5.1). However, in the long run, simulations show that any differences in diffusion coefficients will lead to severe capacity drops if the electrolytes are not remixed as there will be a buildup of vanadium ions on one side and a dilution on the other as the side with a deficit in vanadium ions determines the available capacity of the battery.

Based on the thermodynamic simulations in Section 6.3, it is concluded that higher permeability rates gives higher cell stack temperatures during standby as well as higher tank temperatures after extended days of use. It was shown that the FAP450 gave low to nonsignificant temperature increase while the GN-115 had the highest temperature

increase with F-930 close behind. However, what's interesting with these results is that the FAP-450 even seem to perform better than the often used Nafion 115 membrane.

# CHAPTER 7

## 7.1 Perspective and conclusions

Several membrane were evaluated as potential candidate for use in the VRB. Of the membranes tested, the anion exchange membrane FAP450 has previously been used in commercial VRB systems by Gildemeister, Germany. On the other hand, the F-930, VB1, VB2 and GN-212 membrane have not been previously been employed commercially. These are all perfluorinated cation exchange membranes, but their properties may vary depending on their method of fabrication that will influence the degree of cross-linking and therefore the degree of swelling of each membrane in the VRB electrolyte.

As a general trend, as expected, the CE increased at higher current densities for all membranes according to Figure 29. This is due to the decreased cycle time which provides shorter time for the diffusion of different vanadium ions through the membrane. Therefore, the CE increases.

The VE drops of at higher current densities as a result to increased internal resistances at higher currents. Therefore, there is no general trend for the EE as it is the product of CE and VE. Moreover, thinner membranes provide higher EE at higher current densities due to easy movement of ions through the membrane. Thicker membranes gives higher resistances and cannot cope with high current densities because of the inhibited movement of ions. When comparing the GN-212 and the GN-212C (of which the only difference is a graphite in the latter) because of the graphite inside the membrane, higher voltage efficiencies are obtained.

Any corrosion of the copper current collector would decrease the CE of the battery as electrons would be consumed in these reactions. However, the risk of corrosion (and also gassing) was mitigated by utilizing a low upper voltage limit of 1.65 V and a graphite paper as additional protection for the copper current collector. Therefore, any decrease in CE was attributed to permeability of vanadium ions through the membrane. However, as it is hard to prevent any oxygen ingress, some CE could be attributed to oxygen impurities during the experiments.

The VB-1 (30μm) proved quite low CE which was expected because it is thin compared to the minimum thickness of 100μm which is usually used in VRB system [37]. The

CE is suffering as a result of too high vanadium permeability rates through the membrane. However, this thin membrane will allow higher ion conductivities and thus allowing higher voltage efficiencies at higher current densities. At low current densities (500 mA) it takes longer for the battery to reach 1.0 V and therefore the permeability of vanadium ions further affect the energy efficiency of the battery as more ions have time to move through the membrane and participate in self-discharge reactions. From these membrane experiments, it is concluded that a thinner membrane seems to have beneficial applications when the battery is used at high current densities but not at low current densities.

Permeability measurements showed that the VB2 had the smallest diffusion coefficients for all ions measured. However due to time restrictions, V(V) was not measured for the VB2 and could therefore not be simulated in MATLAB. The FAP-450 proved to give about 10 times lower diffusion coefficients for most of the ions compared to the F930. Also, the FAP450 had the same order of magnitude for all measured diffusion coefficients. From simulations of the VRB using the FAP-450, almost no capacity drop was noticed after 60 cycles.

From the results of Section 5.2, it seemed that the F930 would perform better than the GN-115 over extended use in the VBR. However, this was not the case as GN-115 gave 50% capacity drop after 60 cycles and the F930 had 90% capacity drop. The only difference between the two in regard of permeability rates was that the internal differences between the rate of which ions travelled through the membranes was different. The internal difference among the ions was a factor of 3 for GN-115 and a factor of 20 for the F930.

From the membrane evaluation in the laboratory scale VRB, it was noticed that the FAP450 and F930 gave about the same CE (around 96-98%). However, when comparing the F930 with the GN-115 the latter had lower CE (about 90-95%) indicating that the diffusion coefficients for the GN-115 should be higher than for the F930 and the FAP450. This was exactly the result obtained from the permeability measurements which indicates consistency throughout the experiments.

It was concluded that FAP450 was the best membrane for use in the VRB. Furthermore, it is also concluded that studies of vanadium permeability must be performed on all ions and not only V(IV) which is the case in many papers around the world today. The

membrane must not only provide low permeability rates but also show low differences between the available ions in the VRB. Otherwise, there will be a buildup on one side and a deficit on the other which will lead to capacity drops.

Thermal modelling and simulations showed that the best membrane for thermal management of the VRB is also the FAP450 which was expected due to the low permeability rates measured in section 5.2. After 6 days of use, the electrolyte tanks were increasing in temperature to about 25°C. For the F930 on the other hand, the cell stack increased in temperature very quickly and reached as much as 37°C in the cell stack with and increasing electrolyte tank temperature to over 30°C. Compared to Nafion 115 however, both membrane showed superior thermal properties and this is associated with the very high degree of swelling reported for Nafion.

As the copper current collector was differently polished, was corroded differently between the experiments due to leaking or other parameters and as the 50% SOC was an approximate value between the experiments - the internal resistance should not be used for membrane evaluation. Instead, it can be used to compare different experimental setups and to spot any short-circuiting. Short-circuiting would give a low internal resistance and for the GN-212 the internal resistance was about 1Ωcm2 which was about half to 1/3 in comparison with the other membranes. However, as the coulombic efficiency was high (around 87-93%) any short circuiting could be neglected and instead the low resistance could be attributed to low membrane resistivity, good polishing of the copper current collector and low resistivity of the electrode surface.

## 7.2 Influence of experimental setup and membrane preparation

As the temperature can affect the membrane swelling ratio and pore size, it could also influence permeability rates. All permeability experiments in this study was conducted using a water bath to cool the electrolytes from any increase in temperature from the overheating pumps after extended use.

Furthermore, even though the upper voltage limit of 1.8 V indicates a certain SOC it may be only affected by one of the electrolytes. For example, even though the V(3) was not fully converted to V(2), but the V(V) was completely converted, the voltage limit could be reached. This source of error was controlled by balancing the electrolytes until V(2) and V(5) was reached which was observed by the color of the electrolytes. However, the color change was not significant and different starting SOC may affect

the possibility to maintain a static discharge current. For instance, the GN-212C and the GN-212 membrane acted differently at 1500 mA discharge and this could be due to different starting SOC.

## 7.3 Comparison with other literature reports

The highest CE was recorded at 98,8% using the F930 membrane at 1500mA (60mAcm$^{-2}$), the highest VE was 92,7 for the F930 at 500m A and the highest EE was 89,7% at 500mA (20mAcm$^{-2}$). These values correspond well to a recent study by Xuanli et Al. in [36]. In this study, Xuanli et al. got a maximum CE of about 90% (at 60 mAcm$^{-2}$) and EE of about 75% using the same experimental procedure as in this study. Table 30 contains a comparison of determined diffusion coefficients from this work and diffusion coefficients from previous studies. The obtained values are about the same order of magnitude even though some experiments were conducted differently.

*Table 30. Comparison of measured diffusion coefficients and coefficients from previous work*

| **Diffusion coefficient/ x $10^{-7}$ $cm^2min^{-1}$** | **Vanadium ion** | | | |
|---|---|---|---|---|
| **Membranes** | $V^{2+}$ | $V^{3+}$ | $V^{4+}$ | $V^{5+}$ |
| VB2 | 0,12 | 0,04 | 0,08 | n.a |
| F930 | 12 | 3,0 | 0,6 | 4,8 |
| FAP450 | 1,2 | 0,4 | 0,7 | 1,2 |
| GN-115 | 7,5 | 10 | 23 | 15 |
| SPPEK* [34] | | 3,15 | 2,76 | 0,72 |
| Nafion 115 [35] | 52,8 | 19,2 | 40,8 | 35,4 |
| Nafion 115 [50] | 31,8 | 11,4 | 24,6 | 21 |
| Nafion 115 [51] | 6 | 1,14 | 2,58 | 1,44 |
| SPPEK* [34] | | 3,15 | 2,76 | 0,72 |
| SPPEK* [34] | | 3,15 | 2,76 | 0,72 |
| Nafion 117 [36] | | 35,4 | 30 | 7,02 |

The measured diffusion coefficients all had very high coefficients of determination ($R^2$) which is a statistical measure of how well the regression line approximates the data points in the series. These $R^2$ values are all found in *Appendix B*, Table 53 (VB2),

Table 55 (FAP450), Table 57 (F930) and Table 59 (GN-115). This indicates that the experimental results are quite consistent.

## 7.5 Ideas and future work

This project was conducted as a master thesis and therefore, it was under a certain time constraint of 20 weeks á 40 hours. Therefore, only a few new, commercially available membranes were tested and evaluated. The same procedure applied to membranes in this work should be conducted for more membranes for all the different vanadium ions present in the VRB in order to be able to simulate the use of the battery in actual VRB systems.

In this study, the diffusion coefficients temperature dependence was not evaluated. Instead, the temperature of the electrolytes was held constant at 30°C throughout the experiments by using a cooling coil immersed in a water bath. However, the battery may face electrolyte temperatures around 60°C during stand-by which may heavily change the diffusion coefficients due to membrane swelling or membrane degradation. It is important to understand the behavior of the membranes and the electrolytes at higher temperatures which could be interesting in future work.

Furthermore, as mentioned in the introduction, preferred water transfer through the membrane could be a big problem and membranes should therefore be monitored in this regard. In this study, the water transfer was minimized by balancing the osmotic pressure between the blank and the electrolyte. However, some water will inevitably be transferred through the membrane and membranes should always be tested for water permeability as well as vanadium permeability and chemical stability.

BIBLIOGRAPHY

# 8. Bibliography

[1] M. Skyllas-Kazacos, G. Kazacos, G. Poon och H. Verseema, ”Recent advances with UNSW vanadium-based redox flow batteries,” *Int. J. Energy Res.* , vol. 34, pp. 182-189, 2010.

[2] A. Thang, J. Bao och M. Skyllas-Kazacos, ”J. Power Sources,” 2010.

[3] A. Thang, J. Bao och M. Skyllas-Kazacos, ”Thermal modelling of battery configuration and self-discharge reactions in vanadium redox flow battery,” 2012.

[4] L. Qingtao, H. Zhang, J. Chen, P. Qian och Y. Zhai, ”Modification of Nafion membrane using interfacial polymerization for vanadium redox flow battery applications,” *J. Membr. Sci,* vol. 311, nr 1-2, pp. 98-103, 2008.

[5] A. Tang, ,. J. Bao och M. Skyllas-Kazacos, ”Dynamic modelling of the effects of ion diffusion and side reactions on the capacity loss for vanadium redox flow battery,” *J. of Power Sources,* vol. 196, pp. 10737-10747, 2011.

[6] A. A. Shah, M. J. Watt-Smith och F. C. Walsh, ”A dynamic performance model for redox-flow batteries involving soluble species,” *Electrochemia Acta,* nr 53, pp. 8087-8100, 2008.

[7] H. Al-Fetlawi, A. A. Shah och F. C. Walsh, ”Non-isothermal modelling of the all-vanadium redox flow battery,” *Electrochhimica Acta,* nr 55, pp. 78-89, 2009.

[8] M. A. Muneer, ”Energy supply, its demand and security issues for developed and emerging economies,” *Renewable and Sustainable Energy Reviews,* vol. 11, pp. 1388-1413, 2007.

[9] ”The World Bank,” 15 06 2016. [Online]. Available: http://data.worldbank.org/indicator/EG.USE.PCAP.KG.OE.

[10] ”U.S. Energy Information Administration,” 16 02 2016. [Online]. Available: http://www.eia.gov/dnav/pet/pet_pri_gnd_dcus_nus_w.htm.

[11] ”Oil and gas running out much faster than expected, says study,” *The periodical,* 2nd October 2003.

[12] ”BP Stastistical Review of World Energy June 2015,” JUNE 2015. [Online]. Available: bp.com/statisticalreview.

[13] ”Energy Storage Association,” [Online]. Available: http://energystorage.org/energy-storage/technologies/vanadium-redox-vrb-flow-batteries. [Använd 28 10 2015].

[14] ”Blanc, C. and Rufer, A., 2010. Understanding the vanadium redox flow batteries. INTECH Open Access Publisher”.

[15] ”Smart Grid Dashboard,” EirGrid, 2016. [Online]. Available: http://smartgriddashboard.eirgrid.com/. [Använd 23 03 2016].

[16] C. Blanc, Modeling of a Vanadium Redox Flow Battery Electricity Storage System, Dissertation, 2009.

[17] S. Leavery och S. Hild, ”Mitigating Power Fluctuations from Renewable Energy Sources,” 2012.

[18] ”"Directive 2009/28/ec of the European parliament and of the council of 23april 2009 on the promotion of the use of energy from renewable sources and amending and subsequently repealing directives 2001/77/ec and 2003/30/ec" http://eur-lex.europa.eu”.

[19] E. W. E. A. tech. rep., ”Powering the energy debate - annual report 2010,” 2010.

[20] G. Kear, A. A. Shah och F. C. Walsh, ”Development of the all-vanadium redox flow battery for energy storage: a review of technological, financial and policy aspects,” *Int. J. Energy Research,* 2011.

[21] C. Dongyang, M. A. Hickner, E. Agar och E. Caglan Kumbur, ”Optimized Anion Exchange Membranes for Vanadium Redox Flow Batteries,” *ACS Appl. Mater. Interfaces,* vol. 5, pp. 7559-7566, 2013.

[22] R. M. Darling, A. Z. Weber, M. C. Tucker och M. L. Perry, ”The influence of Electric Field on Crossover in Redox-Flow Batteries,” i *Journal of The Electrochemical Society,* vol. 163, 2015, pp. A5014-A5022.

[23] D. Chen, S. Wang, M. Xiao och Y. Meng, ”Preparation and properties of sulfonated poly(fluorenyl ether ketone) membrane for vanadium redox flow battery application,” *J. of Power Sources,* vol. 195, pp. 2089-2095, 2010.

[24] L. U. T. L. Li, ”American Institute of Chemical Engineers,” [Online]. Available: http://www3.aiche.org/proceedings/Abstract.aspx?PaperID=288194.

[25] C. Menictas och M. Skyllas-Kazacos, ”Performance of vanadium-oxygen redox fuel cell,” *J Appl Electrochem,* nr 41, pp. 1223-1232, 2011.

[26] H. Priffi, A. Parasuraman, S. Winardi, T. M. Lim och M. Skyllas-Kazacos, ”Membranes for Redox Flow Battery Applications,” *Membranes,* vol. 2, pp. 275-306, 2012.

[27] A. Parasuraman, T. M. Lim, C. Menictas och M. Skyllas-Kazacos, ”Review of material research and development for vanadium redox flow battery applications,” *Electrochimica Acta,* nr 101, pp. 27-40, 2013.

[28] T. Sukkar och M. Skyllas-Kazacos, ”Water transfer behaviour across cation exchange membranes in the vanadium redox battery,” *J. Membr. Sci,* vol. 222, pp. 235-247, 2003.

[29] J. Li, Y. Zhang, S. Zhang och X. Huang, ”Sulfonated polyimide/s-MoS2 composite membrane with selectivity and good stability for vanadium redox flow battery,” *J. Membr. Sci. ,* nr 490, pp. 179-189, 2015.

[30] M. Skyllas-Kazacos och T. Sukkar, ”Modification of membranes using polyelectrolytes to improve water transfer properties in the vanadium redox battery,” *J. Membr. Sci. ,* nr 222, pp. 249-264, 2003.

[31] B. Schwenzer, J. Zhang, S. Kim, L. Li, J. Liu och Z. Yang, ”Membrane Development for Vanadium Redox Flow Batteries,” *ChemSusChem,* vol. 4, pp. 1388-1406, 2011.

[32] M. Skyllas-Kazacos, F. Grossmith, P. Llewellyn och A. Fane , ”Evaluation of membranes for all-vanadium redox cell,” i *Stationary Energy Storage: Load Levelling and Remote Applications | Battery and energy technology divisions,* Vol 88-11.

[33] T. Mohammadi och M. Skyllas-Kazacos, ”Modification of anion-exchange membranes for vanadium redox battery applications,” *J. Power Sources,* vol. 63, pp. 179-186, 1996.

[34] N. Wang, J. Yu, Z. Zhou, D. Fang, S. Liu och Y. Liu, ”SPPEK/TPA composite membrane as a separator of vanadium redox flow battery,” *J. of Membrane Sci. ,* vol. 437, pp. 114-121, 2013.

[35] C. Sun, J. Chen, H. Zhang, X. Han och Q. Luo, ”Investigations on transfer of water and vanadium ions across Nafion membrane in an operating vanadium redox flow battery,” *J. of Power Sources,* vol. 195, pp. 890-897, 2010.

[36] L. Xuanli, L. Zhengzhong, X. Jingyu, W. Zenghua, Z. Wentao, C. Liquan och Q. Xinping, ”Influences of Permeation of Vanadium Ions through PVDF-g-PSSA Membranes on Performances of Vanadium Redox Flow Batteries,” *J. Phys. Chem. B* , vol. 109, pp. 20310-20314, 2005.

[37] L. Xianfeng , Z. Huamin, M. Zhensheng, Z. Hongzhang och I. Vankelecom, ”Ion exchange membranes for vanadium redox flow battery (VRB) applications,” *Energy Environ. Sci,* vol. 4, pp. 1147-1160, 2011.

[38] ”Vanadium Redox Flow Batteries: An In-Depth Analysis,” EPRI, Palto Alto, CA, 2007.

[39] J. Sun, D. Shi, H. Zhong, X. Li och H. Zhang, ”Investigations on the self-discharge process in vanadium flow battery,” *J. Power Sources,* vol. 294, pp. 562-568, 2015.

[40] T. Sukkar och M. Skyllas-Kazacos, ”Modification of membranes using polyelectrolytes to improve water transfer properties in the vanadium redox battery,” *J. Membr. Sci. ,* vol. 222, pp. 249-264, 2003.

[41] X. Li, H. Zhang, Z. Mai, H. Zhang och I. Vankelecom, ”Ion exchange membranes for vanadium redox flow battery (VRB) applications,” *Energy Environ. Sci. ,* vol. 4, p. 1147, 2011.

[42] T. Sukkar och M. Skyllas-Kazacos, ”Membrane stability studies for vanadium redox cell applications,” *J. Applied Electrochemistry ,* nr 34, pp. 137-145, 2004.

[43] L. Li, S. Kim, W. Wang, M. Vijayakumar, Z. Nie, B. Chen, J. Zhang, G. Xia, J. Hu, G. Graff, J. Liu och Z. Yang, ”A Stable Vanadium Redox-Flow Battery with High Energy density for large-scale energy storage,” *Adv. Energy. Mater,* nr 1, pp. 394-400, 2011.

[44] K. SooWhan, M. Vijayakumar, W. Wang och J. Zang, ”Chloride supporting electrolytes for all-vanadium redox flow batteries,” *Physical Chemistry Chemical Physics ,* vol. 13, pp. 18186-93, Sep 2011.

[45] V. Yu och D. Chen, ”Estimating the Concentration Imbalance of a Vanadium Redox Flow Battery With Crossover Using a Constrained Extended Kalman Filter,” i *ASME 2013 Dynamic Systems and Control Conference,* Palto Alto, 2013.

[46] M. Skyllas-Kazacos, C. Menictas och M. Kazacos, ”Thermal stability of concentrated V(V) electrolytes in the vanadium redox cell,” *J. of Applied Electrochemical Society* , nr 143, p. L86, 1996.

[47] N. Kausar, R. Howe och M. Skyllas-Kazacos, ”Raman spectroscopy studies of concentrated vanadium redox battery positive electrolytes,” *J. App. Electrochemistry,* nr 31, pp. 1327-1332, 2001.

[48] M. Skyllas-Kazacos, C. Peng och M. Cheng, ”Evaluation of precipitation inhibitors for supersaturated vanadyl electrolytes for the vanadium redox battery,” *Electrochemical and Solid-State Letters 2,* nr 3, pp. 121-122, 199.

[49] M. Skyllas-Kazacos och M. Kazacos, ”Stabilized electrolyte solutions, methods of preparation thereof and redox cells and batteries containing stabilized in electrolyte solutions”. US Patent 6,143,443, 7 November 2000.

[50] C. Sun, J. Chen, H. Zhang, X. Han och Q. Luo, ”Investigations on transfer of water and vanadium ions across Nafion membrane in an operating vanadium redox flow battery,” *J. Power Scources,* vol. 195, nr 3, pp. 890-897, 2010.

[51] J. Sun, D. Shi, H. Zhong, X. Li och H. Zhang, ”Investigations on the self-discharge process in vanadium flow battery,” *J. of Power Sources,* nr 294, pp. 562-568, 2015.

[52] B. Hibbert, Introduction to electrochemistry, NSW: THE MACMILLIAN PRESS LTD, 1993.

[53] C. Menictas, D. R. Hong, Z. H. Yan, J. Wilson, M. Kazacos och M. Skyllas-Kazacos, ”Status of the Vanadium Redox Battery Development Program,” i *Electrical Engineering Congress,* Sydney, Australia, 1994.

# Appendix A Membrane Evaluation at charge-discharge cycling

VB-1 30 µm

VB-1 experimental data at 1000 mA (40 mA $cm^{-2}$)

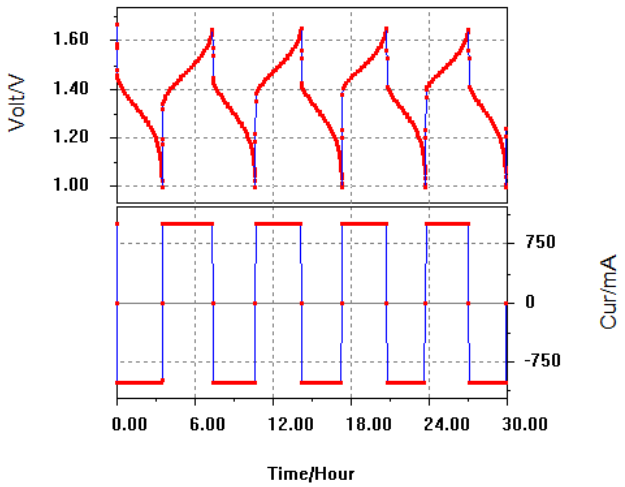


*Figure 54. Experimental charge-discharge curve for membrane evaluation of the VB1 30 at 1000 mA (40 mA cm-2) with a total cycle time of 30 hours.*

*Table 31. Compiled experimental results for the VB1 30 at 1000 mA (40 mA cm-2) with an average EE of 74,0%.*

| I = 1000 mA [40 mA $cm^{-2}$] | | | | | | | |
|---|---|---|---|---|---|---|---|
| Cycle | **CC Discharge (mJ)** | **CC Charge (mJ)** | **Total chg capa (mAH)** | **Total dischg capa (mAH)** | **EE (%)** | **CE (%)** | **VE (%)** |
| **1** | 4164 | 5671 | 3838 | 3230 | 73,4 | 84,2 | 87,2 |
| **2** | 3933 | 5280 | 3526 | 3073 | 74,4 | 87,2 | 85,2 |
| **3** | 3786 | 5098 | 3388 | 2952 | 74,2 | 87,1 | 85,2 |
| **4** | 3639 | 4915 | 3272 | 2837 | 74,0 | 86,7 | 85,3 |
| | | | | **Average** | 74,0 | 86,3 | 85,7 |

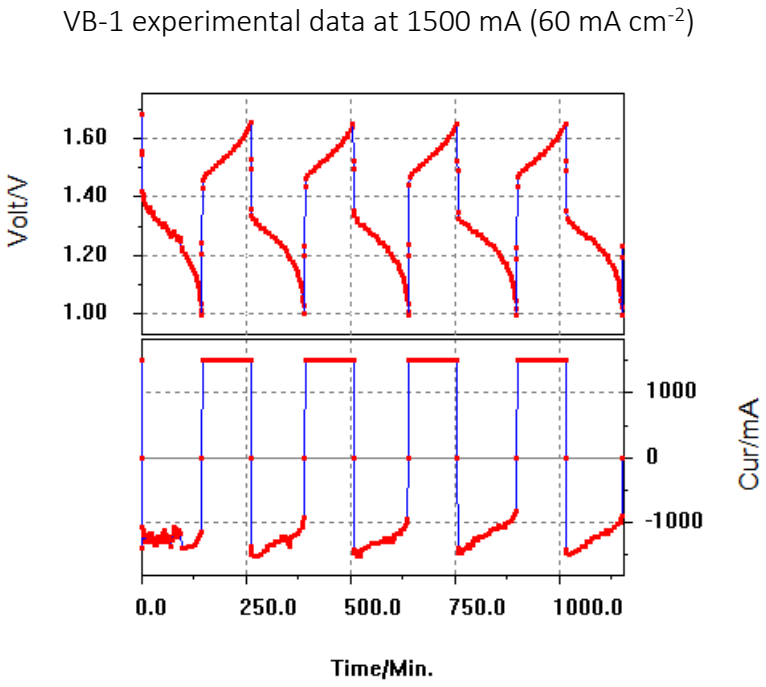


*Figure 55. Experimental charge-discharge curve for membrane evaluation of the VB1 30 at 1500 mA (60 mA cm-2) with a total cycle time of about 21 hours.*

*Table 32. Compiled experimental results for the VB1 30 at 1500 mA (60 mA cm-2) with an average EE of 75,5%.*

| I = 1500 mA [60 mA $cm^{-2}$] | | | | | | | |
|---|---|---|---|---|---|---|---|
| Cycle | **CC Discharge (mJ)** | **CC Charge (mJ)** | **Total chg capa (mAH)** | **Total dischg capa (mAH)** | **EE (%)** | **CE (%)** | **VE (%)** |
| **1** | 3371 | 4460 | 2893 | 2721 | 75,6 | 94,1 | 80,3 |
| **2** | 3366 | 4476 | 2899 | 2719 | 75,2 | 93,8 | 80,2 |
| **3** | 3361 | 4446 | 2872 | 2704 | 75,6 | 94,1 | 80,3 |
| **4** | 3372 | 4497 | 2905 | 2723 | 75,0 | 93,7 | 80,0 |
| | | | | **Average** | 75,4 | 93,9 | 80,2 |

During discharge, the current went from 1500 mA to about 1000 mA which was due to the insufficient flowrate to provide the reactions with reactants in the cell stack. However, it is certain that higher CE are obtained at higher current densities. This is due to the shorter

amount of time necessary for charge-discharge which gives the permeability of vanadium ions less time to move through the membrane providing higher CE.

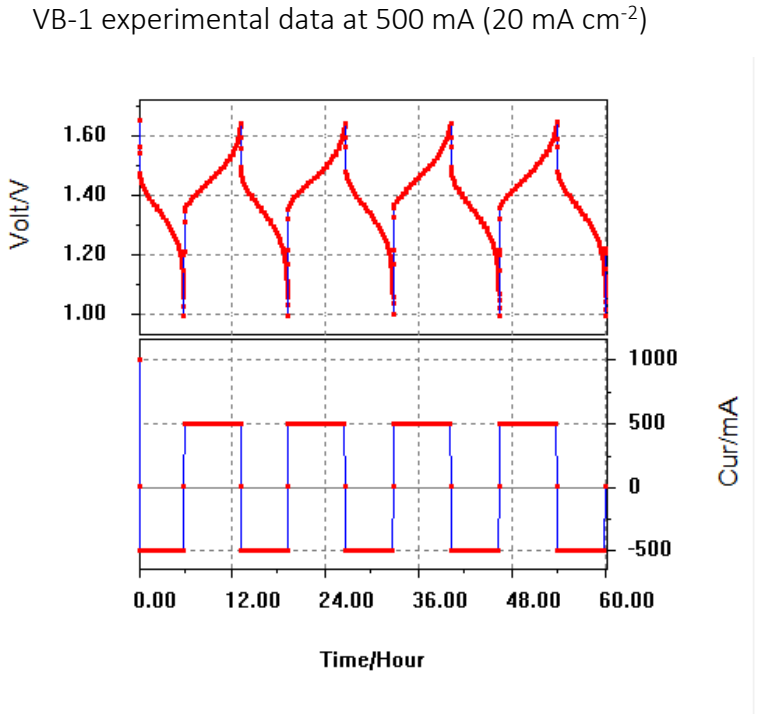


*Figure 56. Experimental charge-discharge curve for membrane evaluation of the VB1 30 at 500 mA (20 mA cm-2) with a total cycle time of 60 hours.*

*Table 33. Compiled experimental results for the VB1 30 at 500 mA (20 mA cm-2) with an average EE of 75,6%.*

| I = 500 mA [20 mA $cm^{-2}$] | | | | | | | |
|---|---|---|---|---|---|---|---|
| Cycle | **CC Discharge (mJ)** | **CC Charge (mJ)** | **Total chg capa (mAH)** | **Total dischg capa (mAH)** | **EE (%)** | **CE (%)** | **VE (%)** |
| **1** | 4015 | 5296 | 3612 | 3015 | 75,8 | 83,5 | 90,8 |
| **2** | 4088 | 5406 | 3669 | 3065 | 75,6 | 83,6 | 90,4 |
| **3** | 4121 | 5449 | 3685 | 3087 | 75,6 | 83,8 | 90,4 |
| **4** | 4141 | 5503 | 3722 | 3103 | 75,2 | 83,4 | 90,2 |
| | | | | **Average** | 75,6 | 83,6 | 90,5 |

Compilation of VB-1 experimental data at 1350 mA (54 mA $cm^{-2}$) without pipe

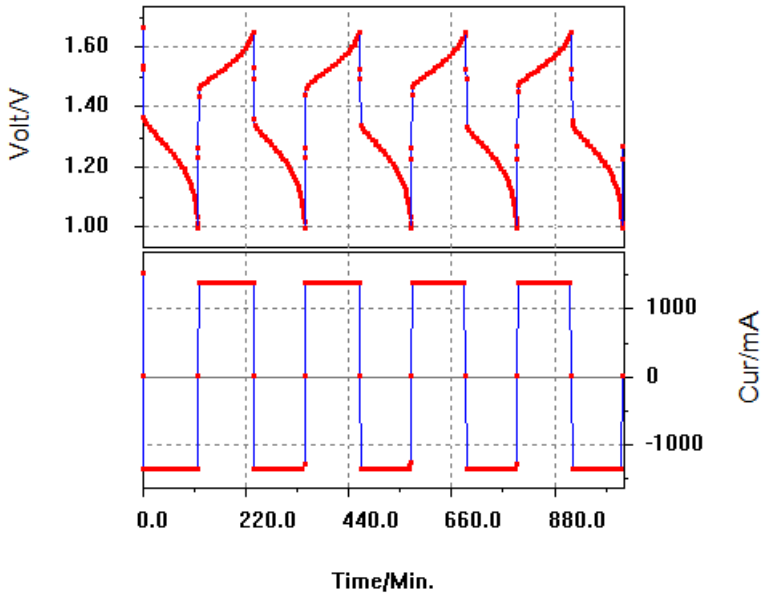


*Figure 57. Experimental charge-discharge curve for membrane evaluation of the VB1 30 at 1350 mA (54 mA cm-2) with a total cycle time of about 17 hours.*

*Table 34. Compiled experimental results for the VB1 30 at 1350 mA (54 mA cm-2)*

| I = 1350 mA [54 mA $cm^{-2}$] | | | | | | | |
|---|---|---|---|---|---|---|---|
| Cycle | **CC Discharge (mJ)** | **CC Charge (mJ)** | **Total chg capa (mAH)** | **Total dischg capa (mAH)** | **EE (%)** | **CE (%)** | **VE (%)** |
| **1** | 2994 | 4025 | 2615 | 2430 | 74,4 | 93,0 | 80,0 |
| **2** | 2968 | 4005 | 2596 | 2414 | 74,1 | 93,0 | 79,7 |
| **3** | 2944 | 3980 | 2576 | 2399 | 74,0 | 93,1 | 79,5 |
| **4** | 2976 | 3998 | 2583 | 2401 | 74,4 | 93,0 | 80,0 |
| | | | | **Average** | 74,2 | 93,0 | 79,8 |

1350 mA (VB-1) with inserted pipe to decrease oxidation of V(II) to V(III)

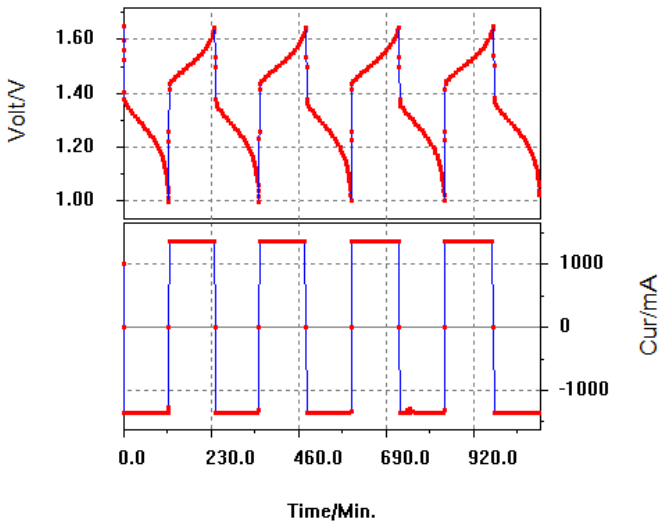


*Table 35. Compiled experimental results for the VB1 30 at 1350 mA (54 mA cm-2) with inserted pipe to decrease risk of oxidation of V(II). An average EE of 79,9%.*

| I = 1350 mA [54 mA $cm^{-2}$] | | | | | | | |
|---|---|---|---|---|---|---|---|
| Cycle | **CC Discharge (mJ)** | **CC Charge (mJ)** | **Total chg capa (mAH)** | **Total dischg capa (mAH)** | **EE (%)** | **CE (%)** | **VE (%)** |
| **1** | 3288 | 4107 | 2700 | 2542 | 80,1 | 94,1 | 85,1 |
| **2** | 3175 | 4177 | 2743 | 2591 | 76,0 | 94,5 | 80,4 |
| **3** | 3235 | 4241 | 2780 | 2629 | 76,3 | 94,6 | 80,7 |
| **4** | 3281 | 4357 | 2855 | 2680 | 75,3 | 93,8 | 80,3 |
| | | | | **Average** | 79,9 | 94,3 | 81,6 |

## FAP450 Fumatech®

Separation membranes fumasep ® Anion-exchange membrane for redox flow batteries. Anion exchange membrane reinforced with PEEK/PTFE. Thickness 130-160um. Selectivity >91%. Stable in pH as low as 1.

FAP450 experimental data at 1000 mA (40 mA $cm^{-2}$)

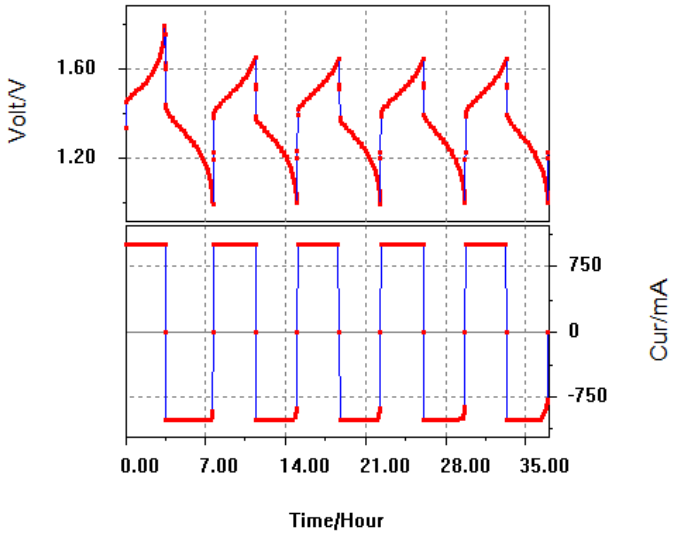


*Figure 58. Charge-discharge graph using FAP-450 membrane at 1000 mA (40mAcm-2)*

*Table 36. Compiled experimental results of the FAP450 membrane at 50mAcm-2*

| I = 1000 mA [40 mA $cm^{-2}$] | | | | | | | |
|---|---|---|---|---|---|---|---|
| Cycle | **CC Discharge (mJ)** | **CC Charge (mJ)** | **Total chg capa (mAH)** | **Total dischg capa (mAH)** | **EE (%)** | **CE (%)** | **VE (%)** |
| **1** | 4482 | 5625 | 3712 | 3572 | 79,7 | 96,2 | 82,8 |
| **2** | 4434 | 5567 | 3654 | 3531 | 79,6 | 96,6 | 82,4 |
| **3** | 4521 | 5652 | 3735 | 3581 | 80,0 | 95,9 | 83,4 |
| **4** | 4400 | 5509 | 3634 | 3497 | 79,9 | 96,2 | 83,1 |
| | | | | **Average** | 79,8 | 96,2 | 82,9 |

FAP450 experimental data at 1500 mA (60 mA $cm^{-2}$)

*Table 37. FAP450 experimental results at 60mAcm-2*

| I = 1500 mA [60 mA $cm^{-2}$] | | | | | | | |
|---|---|---|---|---|---|---|---|
| Cycle | **CC Discharge (mJ)** | **CC Charge (mJ)** | **Total chg capa (mAH)** | **Total dischg capa (mAH)** | **EE (%)** | **CE (%)** | **VE (%)** |
| **1** | 3693 | 4961 | 3189 | 3050 | 74,4 | 95,6 | 77,8 |
| **2** | 3593 | 4812 | 3091 | 2974 | 74,7 | 96,2 | 77,6 |
| **3** | 3376 | 4581 | 2927 | 2812 | 73,7 | 96,1 | 76,7 |
| **4** | 3207 | 4337 | 2762 | 2674 | 73,9 | 96,8 | 76,3 |
| | | | | **Average** | 74,1 | 96,2 | 77,1 |

FAP450 experimental data at 500 mA (20 mA $cm^{-2}$)

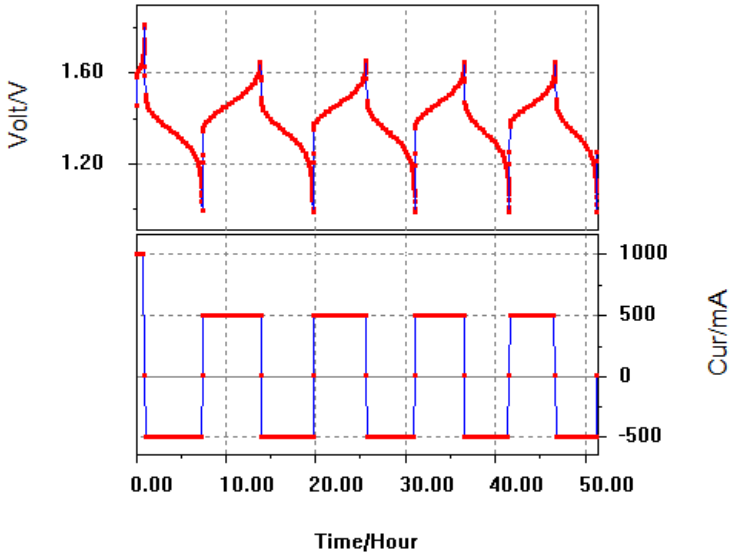


*Figure 59. Charge-discharge of the FAP450 at 500mA (20mAcm-2)*

*Table 38. Experimental data of FAP450 at 20mAcm-2*

| I = 500 mA [20 mA $cm^{-2}$] | | | | | | | |
|---|---|---|---|---|---|---|---|
| Cycle | **CC Discharge (mJ)** | **CC Charge (mJ)** | **Total chg capa (mAH)** | **Total dischg capa (mAH)** | **EE (%)** | **CE (%)** | **VE (%)** |
| **1** | 3844 | 4758 | 3228 | 2893 | 80,8 | 89,6 | 90,2 |
| **2** | 3543 | 4365 | 2965 | 2675 | 81,2 | 90,2 | 90,0 |
| **3** | 3285 | 4039 | 2736 | 2485 | 81,3 | 90,8 | 89,5 |

| | | | | | | | |
|---|---|---|---|---|---|---|---|
| **4** | 3028 | 3751 | 2551 | 2288 | 80,7 | 89,7 | 90,0 |
| | | | | **Average** | 81,0 | 90,1 | 89,9 |

## F930 Fumatech®

These are proton conductive membranes. Per-fluorinated sulfonic acid/PTFE copolymer with high chemical stability and high ionic conductance for fuel cell applications or electrolysis. Thickness: 0,025-0,035mm. perfluorosulfonic acid membranes for PEMFC.

### F930 experimental data at 1000 mA (40 mA $cm^{-2}$)

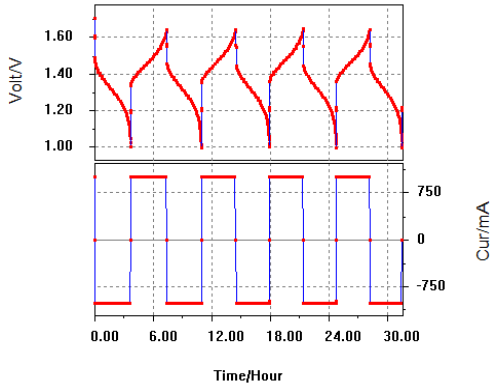


*Figure 60. Charge-discharge grapgh from 40mAcm-2 F930 membrane*

*Table 39. Compiled experimental results for the F930 membrane at 40mAcm-2*

| I = 1000 mA [40 mA $cm^{-2}$] | | | | | | | |
|---|---|---|---|---|---|---|---|
| Cycle | **CC Discharge (mJ)** | **CC Charge (mJ)** | **Total chg capa (mAH)** | **Total dischg capa (mAH)** | **EE (%)** | **CE (%)** | **VE (%)** |
| **1** | 4522 | 5381 | 3647 | 3492 | 84,0 | 95,8 | 87,7 |
| **2** | 4394 | 5198 | 3503 | 3401 | 84,5 | 97,1 | 87,0 |
| **3** | 4300 | 5094 | 3418 | 3301 | 84,4 | 97,4 | 86,7 |
| **4** | 4233 | 5006 | 3375 | 3274 | 84,6 | 97,0 | 87,2 |
| | | | | **Average** | 84,4 | 96,8 | 87,1 |

F930 experimental data at 1500 mA (60 mA $cm^{-2}$)

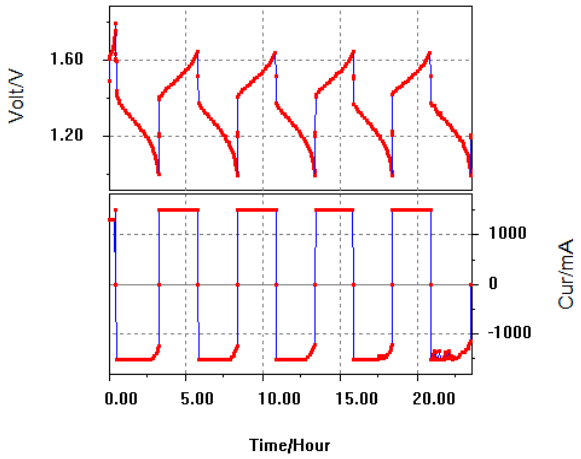


*Figure 61. Charge-discharge graph of the F930 membrane at 60mAcm-2*

*Table 40. Charge- and discharge capacity, energy input and output during charge and discharge at 60mAcm-2 for the F930 membrane.*

| I = 1500 mA [60 mA $cm^{-2}$] | | | | | | | |
|---|---|---|---|---|---|---|---|
| Cycle | **CC Discharge (mJ)** | **CC Charge (mJ)** | **Total chg capa (mAH)** | **Total dischg capa (mAH)** | **EE (%)** | **CE (%)** | **VE (%)** |
| **1** | 4624 | 5730 | 3778 | 3718 | 80,7 | 98,4 | 82,0 |
| **2** | 4562 | 5655 | 3719 | 3673 | 80,7 | 98,8 | 81,7 |
| **3** | 4504 | 5613 | 3687 | 3631 | 80,2 | 98,5 | 81,4 |
| **4** | 4563 | 5604 | 3677 | 3656 | 81,4 | 99,4 | 81,9 |
| | | | | **Average** | 80,8 | 98,8 | 81,8 |

F930 experimental data at 500 mA (20 mA $cm^{-2}$)

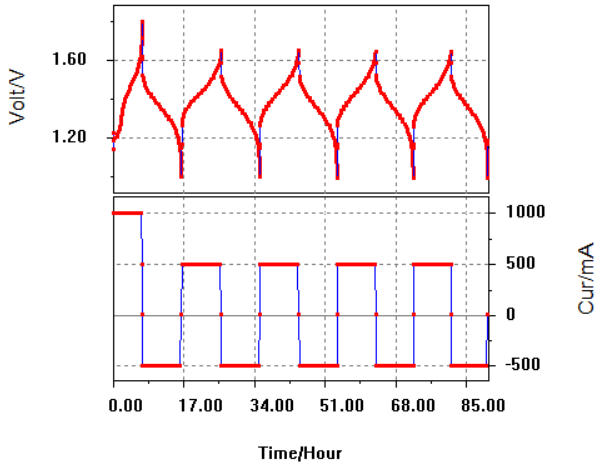


*Figure 62. Charge-discharge graph of the F930 at 20mAcm-2*

*Table 41. Charge- and discharge capacity, energy input and output during charge and discharge at 20mAcm-2 for the F930 membrane.*

| I = 500 mA [20 mA $cm^{-2}$] | | | | | | | |
|---|---|---|---|---|---|---|---|
| Cycle | **CC Discharge (mJ)** | **CC Charge (mJ)** | **Total chg capa (mAH)** | **Total dischg capa (mAH)** | **EE (%)** | **CE (%)** | **VE (%)** |
| **1** | 6154 | 6906 | 4773 | 4593 | 89,1 | 96,2 | 92,6 |
| **2** | 6096 | 6800 | 4694 | 4547 | 89,6 | 96,9 | 92,5 |
| **3** | 6016 | 6697 | 4629 | 4484 | 89,8 | 96,9 | 92,7 |
| **4** | 5902 | 6568 | 4541 | 4397 | 89,9 | 96,8 | 92,9 |
| | | | | **Average** | 89,6 | 96,7 | 92,7 |

## General Energy GN-115

Made especially for vanadium batteries with low swelling ratio and high water content. Perfluorinated ion exchange membrane.

GN-115 experimental data at 1000 mA (40 mA $cm^{-2}$)

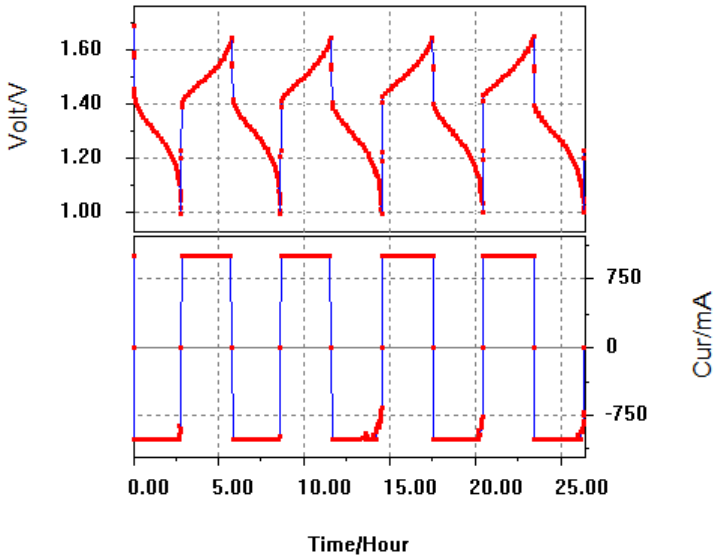


*Figure 63. Charge-discharge cycling of membrane 115. Discharge was not sustained at a current discharge voltage. Instead, it varied from 1000 mA to 750mA at cycle no.2,3 and 4.*

*Table 42. Charge- and discharge capacity, energy input and output during charge and discharge at 40mAcm-2 for the GN-115 membrane with an average EE of 79,8%.*

| I = 1000 mA [40 mA $cm^{-2}$] | | | | | | | |
|---|---|---|---|---|---|---|---|
| Cycle | **CC Discharge (mJ)** | **CC Charge (mJ)** | **Total chg capa (mAH)** | **Total dischg capa (mAH)** | **EE (%)** | **CE (%)** | **VE (%)** |
| **1** | 3560 | 4445 | 2949 | 2788 | 80,1 | 94,5 | 84,7 |
| **2** | 3573 | 4469 | 2951 | 2821 | 79,9 | 95,6 | 83,6 |
| **3** | 3583 | 4531 | 2981 | 2835 | 80,1 | 95,1 | 84,2 |
| **4** | 3579 | 4535 | 2976 | 2839 | 78,9 | 95,4 | 82,7 |
| | | | | **Average** | 79,8 | 95,2 | 83,8 |

GN-115 experimental data at 1500 mA (60 mA $cm^{-2}$)

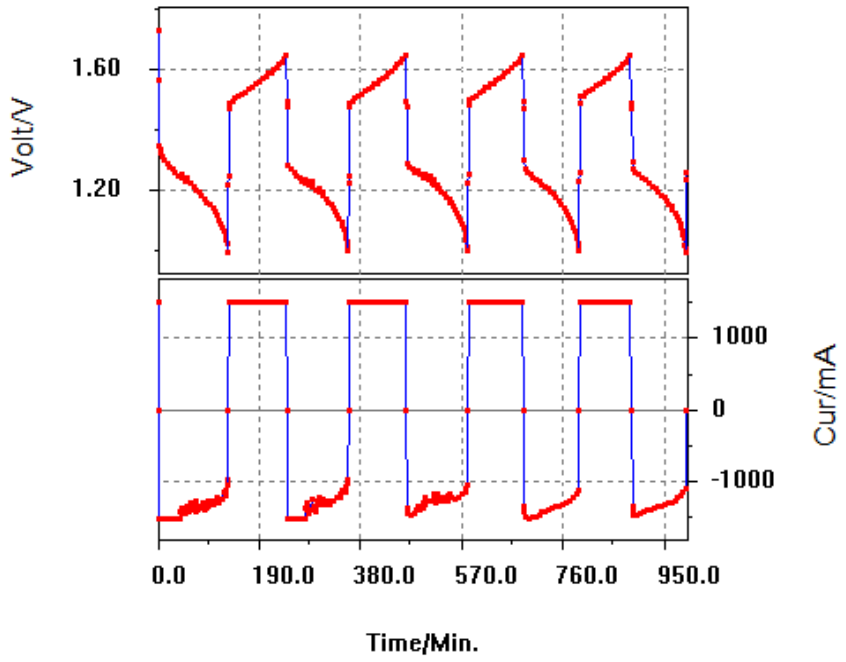


*Figure 64 Charge-discharge cycling of membrane GN-115 at 1500 mA (60mA cm-2). Varying discharge current ranging from a starting current of 1500 mA to a final current of 1000 mA.*

*Table 43. Charge- and discharge capacity, energy input and output during charge and discharge at 60mAcm-2 for the GN-115 membrane with an average EE of 69,0%*

| I = 500 mA [20 mA $cm^{-2}$] | | | | | | | |
|---|---|---|---|---|---|---|---|
| Cycle | **CC Discharge (mJ)** | **CC Charge (mJ)** | **Total chg capa (mAH)** | **Total dischg capa (mAH)** | **EE (%)** | **CE (%)** | **VE (%)** |
| **1** | 2970 | 4229 | 2709 | 2488 | 70,2 | 91,8 | 76,5 |
| **2** | 2872 | 4153 | 2658 | 2393 | 69,1 | 90,0 | 76,8 |
| **3** | 2723 | 3984 | 2541 | 2294 | 68,3 | 90,3 | 75,6 |
| **4** | 2594 | 3796 | 2414 | 2185 | 68,3 | 90,5 | 75,5 |
| | | | | **Average** | 69,0 | 90,6 | 76,1 |

GN-115 experimental data at 500 mA (20 mA $cm^{-2}$)

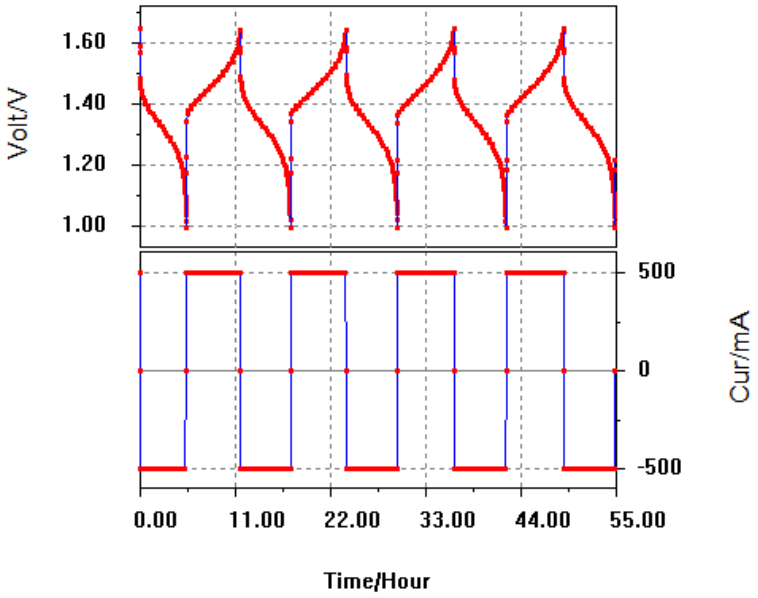


*Figure 65. Charge-discharge grapgh for the GN-115 membrane at 500mA*

*Table 44. Charge- and discharge capacity, energy input and output during charge and discharge at 20 mAcm$^{-2}$ for the GN-115 membrane with an average EE of 80,4%*

| I = 500 mA [20 mA $cm^{-2}$] | | | | | | | |
|---|---|---|---|---|---|---|---|
| Cycle | **CC Discharge (mJ)** | **CC Charge (mJ)** | **Total chg capa (mAH)** | **Total dischg capa (mAH)** | **EE (%)** | **CE (%)** | **VE (%)** |
| **1** | 3549 | 4543 | 3079 | 2865 | 78,1 | 93,1 | 83,9 |
| **2** | 3761 | 4679 | 3181 | 2940 | 80,4 | 92,4 | 87,0 |
| **3** | 3938 | 4775 | 3237 | 2996 | 82,5 | 92,6 | 89,1 |
| **4** | 3903 | 4855 | 3297 | 2961 | 80,4 | 89,8 | 89,5 |
| | | | | **Average** | 80,4 | 92,0 | 83,4 |

## General Energy GN-212

Perfluorosulfonic acid proton exchange membrane. Thickness 50um.

### GN-212 experimental data at 1000 mA (40 mA $cm^{-2}$)

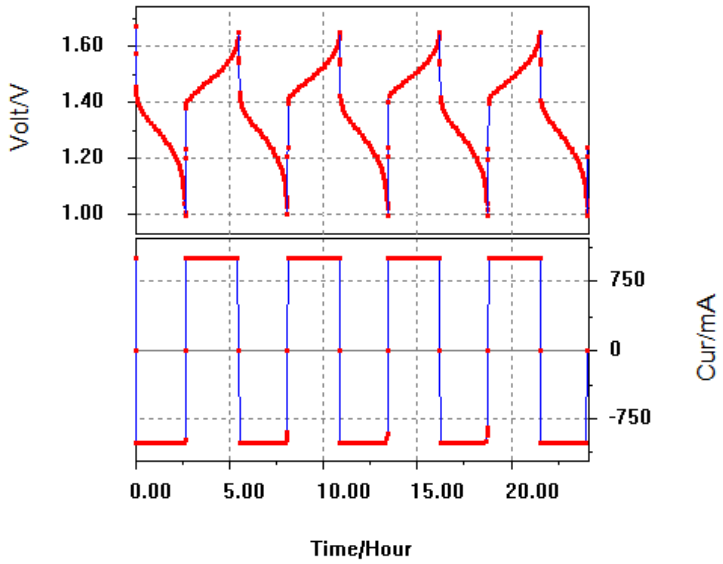


*Figure 66. Charge-discharge graph of the 40mAcm$^{-2}$ test of the GN-212 membrane*

*Table 45. Charge- and discharge capacity, energy input and output during charge and discharge at 40mAcm$^{-2}$ for the GN-212 membrane. Compiled experimental data for the GN-212 membrane at 1000 mA with an average EE of 77,2%.*

| I = 1000 mA [40 mA $cm^{-2}$] | | | | | | | |
|---|---|---|---|---|---|---|---|
| Cycle | **CC Discharge (mJ)** | **CC Charge (mJ)** | **Total chg capa (mAH)** | **Total dischg capa (mAH)** | **EE (%)** | **CE (%)** | **VE (%)** |
| **1** | 3232 | 4208 | 2819 | 2549 | 76,8 | 90,4 | 84,9 |
| **2** | 3188 | 4131 | 2752 | 2525 | 77,2 | 91,8 | 84,1 |
| **3** | 3170 | 4100 | 2721 | 2518 | 77,3 | 92,5 | 83,6 |
| **4** | 3140 | 4099 | 2731 | 2491 | 77,6 | 91,2 | 84,0 |
| | | | | **Average** | 77,2 | 91,5 | 84,2 |

GN-212 experimental data at 1500 mA (60 mA $cm^{-2}$)

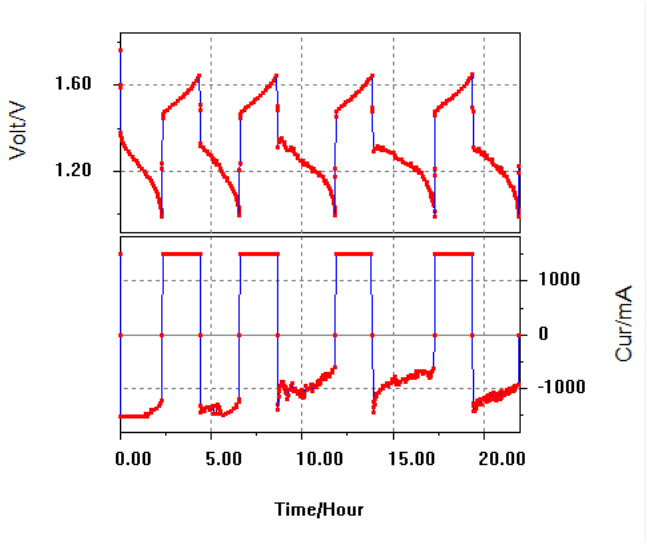


*Figure 67. Charge-discharge curve of the GN-212 membrane at 1500 mA (60 mA $cm^{-2}$). Discharge current was not maintained at 1500 mA, instead the discharge current dropped off to about 800-900 mA.*

*Table 46. Charge- and discharge capacity, energy input and output during charge and discharge at 60mA$cm^{-2}$ for the GN-212 membrane with a peak EE of 76,4%*

| I = 1500 mA [60 mA $cm^{-2}$] | | | | | | | |
|---|---|---|---|---|---|---|---|
| Cycle | **CC Discharge (mJ)** | **CC Charge (mJ)** | **Total chg capa (mAH)** | **Total dischg capa (mAH)** | **EE (%)** | **CE (%)** | **VE (%)** |
| **1** | 3505 | 4781 | 3088 | 2901 | 73,3 | 93,9 | 78,1 |
| **2** | 3607 | 4723 | 3045 | 2902 | 76,4 | 95,3 | 80,2 |
| **3** | 3494 | 4704 | 3022 | 2801 | 74,3 | 92,7 | 80,1 |
| **4** | 3439 | 4801 | 3085 | 2809 | 71,6 | 91,1 | 78,6 |
| | | | | **Average** | 73,9 | 93,2 | 79,6 |

GN-212 experimental data at 500 mA (20 mA $cm^{-2}$)

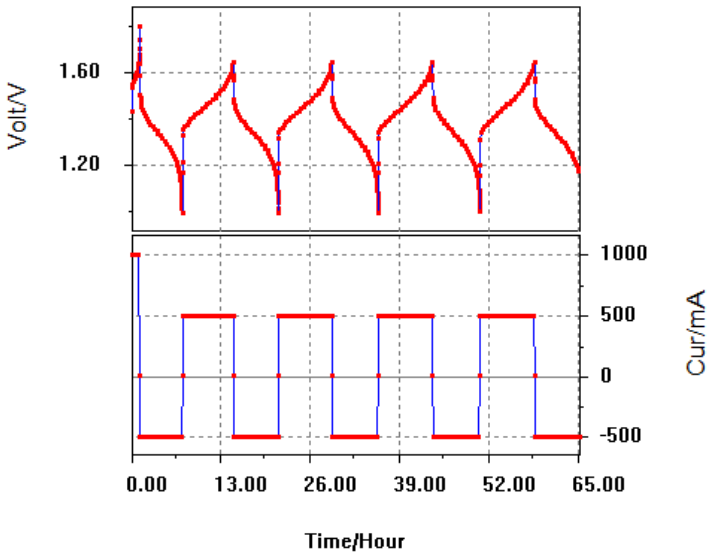


*Figure 68. Charge-discharge graph of the GN-212 membrane at 500mA (20 mAcm-2)*

*Table 47. Charge- and discharge capacity, energy input and output during charge and discharge at 20 mAcm-2 for the GN-212 membrane with an average EE of 78,2%.*

| I = 500 mA [20 mA $cm^{-2}$] | | | | | | | |
|---|---|---|---|---|---|---|---|
| Cycle | **CC Discharge (mJ)** | **CC Charge (mJ)** | **Total chg capa (mAH)** | **Total dischg capa (mAH)** | **EE (%)** | **CE (%)** | **VE (%)** |
| **1** | 4315 | 5443 | 3695 | 3271 | 77,8 | 88,5 | 87,9 |
| **2** | 4446 | 5664 | 3859 | 3370 | 78,5 | 87,3 | 89,9 |
| **3** | 4537 | 5790 | 3931 | 3442 | 78,3 | 87,6 | 89,4 |
| **4** | - | 5824 | 3957 | - | n.a | n.a | n.a |
| | | | | **Average** | 78,2 | 87,8 | 89,1 |

## General Energy GN-212C

Perfluorinated Proton-exchange membrane (PEM) including graphene with high electrochemical performance and high conductivity. Based on fluorine ion exchange resin as raw material with graphene elements to ensure high conductivity, high resistance and high water retention. Thickness is 50 um.

GN-212C experimental data at 1000 mA (40 mA $cm^{-2}$)

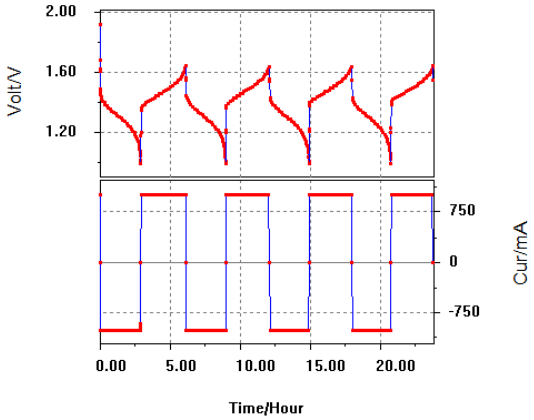


*Figure 69. Charge-discharge operation of the GN-212C membrane at 1000 mA.*

*Table 48. Charge- and discharge capacity, energy input and output during charge and discharge at 60mAcm-2 for the GN-212C membrane with a peak EE of 79,1%.*

| I = 1000 mA [40 mA $cm^{-2}$] | | | | | | | |
|---|---|---|---|---|---|---|---|
| Cycle | **CC Discharge (mJ)** | **CC Charge (mJ)** | **Total chg capa (mAH)** | **Total dischg capa (mAH)** | **EE (%)** | **CE (%)** | **VE (%)** |
| **1** | 3617 | 4695 | 3169 | 2804 | 77,0 | 88,5 | 87,0 |
| **2** | 3555 | 4611 | 3084 | 2772 | 77,1 | 89,9 | 85,8 |
| **3** | 3592 | 4542 | 3022 | 2731 | 79,1 | 90,4 | 87,5 |
| **4** | - | 4507 | - | - | - | - | - |
| | | | | **Average** | 77,7 | 89,6 | 86,8 |

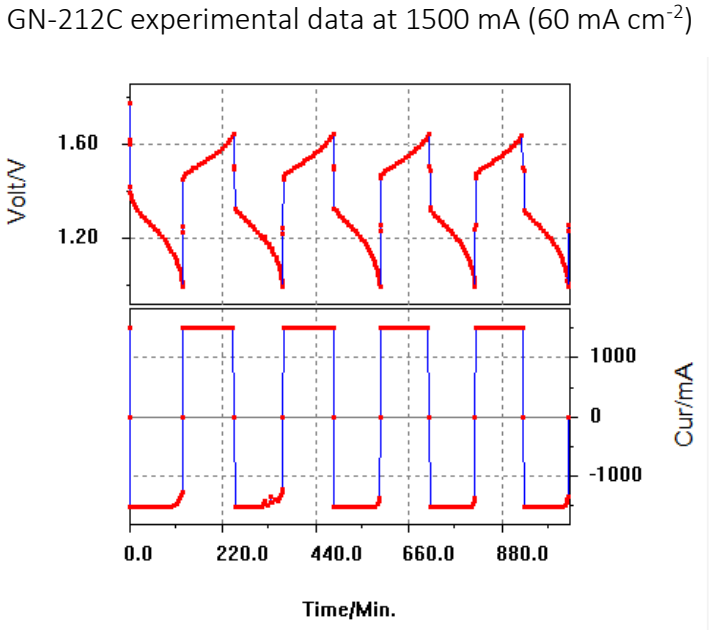


*Figure 70. Charge-discharge operation of the GN-212C membrane at 1500 mA.*

*Table 49. Charge- and discharge capacity, energy input and output during charge and discharge at 60mAcm-2 for the GN-212C membrane with a peak EE of 71,5%.*

| I = 1500 mA [60 mA cm$^{-2}$] | | | | | | | |
|---|---|---|---|---|---|---|---|
| Cycle | **CC Discharge (mJ)** | **CC Charge (mJ)** | **Total chg capa (mAH)** | **Total dischg capa (mAH)** | **EE (%)** | **CE (%)** | **VE (%)** |
| **1** | 3329 | 4630 | 2989 | 2731 | 71,9 | 91,4 | 78,7 |
| **2** | 3258 | 4562 | 2945 | 2681 | 71,4 | 91,0 | 78,5 |
| **3** | 3186 | 4449 | 2866 | 2627 | 71,6 | 91,7 | 78,1 |
| **4** | 3123 | 4360 | 2803 | 2577 | 71,3 | 91,9 | 77,6 |
| | | | | **Average** | 71,6 | 91,5 | 78,2 |

GN-212C experimental data at 500 mA (20 mA $cm^{-2}$)

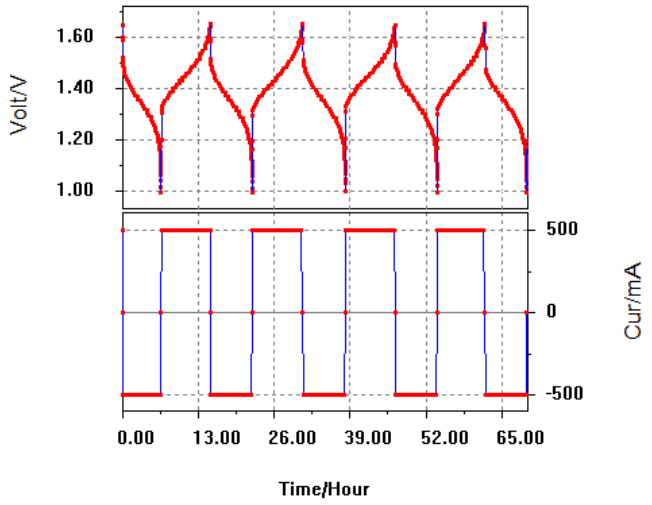


*Figure 71. Charge-discharge curve for the GN-212C at 500 mA*

*Table 50. Charge- and discharge capacity, energy input and output during charge and discharge at 20mAcm-2 for the GN-212C membrane with an average EE of 78,8% during 4 cycles.*

| I = 500 mA [20 mA $cm^{-2}$] | | | | | | | |
|---|---|---|---|---|---|---|---|
| Cycle | **CC Discharge (mJ)** | **CC Charge (mJ)** | **Total chg capa (mAH)** | **Total dischg capa (mAH)** | **EE (%)** | **CE (%)** | **VE (%)** |
| **1** | 4815 | 6093 | 4177 | 3593 | 79,0 | 86,0 | 91,9 |
| **2** | 4891 | 6243 | 4291 | 3649 | 78,3 | 85,0 | 92,1 |
| **3** | 4824 | 6153 | 4200 | 3605 | 78,4 | 85,8 | 91,4 |
| **4** | 4725 | 5936 | 4069 | 3545 | 79,6 | 87,1 | 91,4 |
| | | | | **Average** | 78,8 | 86,0 | 91,7 |

# Appendix B Raw ICP data and permeability calculations

*Table 51. Membrane thickness*

| Membrane | Thickness (μm) |
|---|---|
| **FAP450** | 60 |
| **GN115** | 125 |
| **F930** | 30 |
| **VB2** | 60 |

VB-2

*Table 52. Raw ICP data, time and dilution for each data point from which permeability rates were calculated for the VB2 membrane*

| VB2 | ID | ICP (mg/l) | time (min) | Dilution | mg/l | mol/l | ln(CB0-2CA) |
|---|---|---|---|---|---|---|---|
| **V(IV)** | E1 | 89,3 | 180 | none | | 0,001753 | 0,003512143 |
| | E2 | 144,27 | 300 | none | | 0,0028321 | 0,005680246 |
| | E5 | 569,34 | 1260 | none | | 0,0111763 | 0,022606307 |
| | | | | | | | |
| **V(III)** | H1 | 169,27 | 360 | none | | 0,0033228 | 0,006667843 |
| | H2 | 456,94 | 1410 | none | | 0,0089699 | 0,018102663 |
| | | | | | | | |
| **V(II)** | M1 | 11,066667 | 60 | 1:6 | 66,4 | 0,0013035 | 0,002610316 |
| | M2 | 16,533333 | 120 | 1:6 | 99,2 | 0,0019473 | 0,003902267 |
| | M3 | 29,858333 | 240 | 1:6 | 179,2 | 0,0035168 | 0,00705841 |

*Table 53. Linear regression coefficients and coefficient of determination from permeability experiments for the VB2 membrane.*

| **Y = k·x + m** | **K** | **M** | **$R^2$** |
|---|---|---|---|
| **V(V)** | n.a | n.a | n.a |
| **V(IV)** | 2E-05 | 0,0002 | 1,000 |
| **V(III)** | 1E-05 | 0,0009 | 0,985 |
| **V(II)** | 3E-05 | 0,0004 | 0,983 |

# APPENDIX B RAW ICP DATA AND PERMEABILITY CALCULATIONS

## FAP450

*Table 54. Raw ICP data, time and dilution for each data point from which permeability rates were calculated for the FAP450 membrane*

| FAP450 | ID | ICP (mg/l) | time (min) | Dilution | mg/l | mol/l | ln(CB0-2CA) |
|---|---|---|---|---|---|---|---|
| **V(V)** | B1 | 17,77 | 205 | 1:6 | 106,6 | 0,00209 | 0,00419 |
| | B2 | 25,27 | 350 | 1:6 | 151,6 | 0,00298 | 0,00597 |
| | B3 | 76,67 | 1200 | 1:6 | 460 | 0,00903 | 0,01823 |
| | B5 | 169,50 | 2770 | 1:6 | 1017 | 0,01996 | 0,04075 |
| | | | | | | | |
| **V(IV)** | D1 | 9,17 | 225 | 1:6 | 55 | 0,00108 | 0,00216 |
| | D2 | 38,50 | 1330 | 1:6 | 231 | 0,00453 | 0,00911 |
| | | | | | | | |
| **V(III)** | C14 | 9,25 | 300 | 1:6 | 55,5 | 0,00109 | 0,00218 |
| | C15 | 25,50 | 1740 | 1:6 | 153 | 0,00300 | 0,00603 |
| | C16 | 42,50 | 3240 | 1:6 | 255 | 0,00501 | 0,01006 |
| | | | | | | | |
| **V(II)** | A10 | 66,50 | 0 | 1:6 | 399 | 0 | 0 |
| | A11 | 164,83 | 360 | 1:6 | 989 | 0,0194144 | 0,039602793 |

*Table 55. Linear regression coefficients and coefficient of determination from permeability experiments for the FAP450 membrane.*

| **Y = k·x + m** | **K** | **M** | **$R^2$** |
|---|---|---|---|
| **V(V)** | 1E-05 | 0,0007 | 1,000 |
| **V(IV)** | 7E-05 | 0,0003 | 1,000 |
| **V(III)** | 3E-06 | 0,0007 | 0,984 |
| **V(II)** | 1E-05 | 0 | 1,000 |

# APPENDIX B RAW ICP DATA AND PERMEABILITY CALCULATIONS

## F930

*Table 56. Raw ICP data, time and dilution for each data point from which permeability rates were calculated for the F930 membrane*

| F930 | ID | ICP (mg/l) | time (min) | Dilution | mg/l | mol/l | ln(CB0-2CA) |
|---|---|---|---|---|---|---|---|
| **V(V)** | L1 | 429 | 165 | none | | 0,0084 | 0,01699 |
| | L2 | 6014 | 2760 | none | | 0,1181 | 0,26932 |
| | L3 | 7080 | 4140 | none | | 0,1390 | 0,32567 |
| | | | | | | | |
| **V(IV)** | P1 | 25 | 120 | 1:6 | 148,8 | 0,0029 | 0,00587 |
| | P2 | 224 | 4182 | 1:6 | 1345,2 | 0,0264 | 0,05425 |
| | P3 | 1434 | 4302 | none | | 0,0281 | 0,05795 |
| | | | | | | | |
| **V(III)** | F1 | 392 | 270 | none | | 0,0077 | 0,01549 |
| | F2 | 478 | 390 | none | | 0,0094 | 0,01896 |
| | F3 | 1573 | 1350 | none | | 0,0309 | 0,06375 |
| | | | | | | | |
| **V(II)** | K1 | 1797 | 1350 | 1:3 | 5390 | 0,1058 | 0,23777 |
| | K2 | 5762 | 1440 | none | | 0,1131 | 0,25647 |

*Table 57. Linear regression coefficients and coefficient of determination from permeability experiments for the F930 membrane.*

| **Y = k·x + m** | **K** | **M** | **$R^2$** |
|---|---|---|---|
| **V(V)** | 8E-05 | 0,0075 | 0,979 |
| **V(IV)** | 1E-05 | 0,0021 | 0,996 |
| **V(III)** | 5E-05 | 0,0012 | 0,842 |
| **V(II)** | 2E-04 | 9E-05 | 1,000 |

# APPENDIX B RAW ICP DATA AND PERMEABILITY CALCULATIONS

## GN-115

*Table 58. Raw ICP data, time and dilution for each data point from which permeability rates were calculated for the GN-115 membrane*

| GN-115 | ID | ICP (mg/l) | time (min) | Dilution | mg/l | mol/l | ln(CB0-2CA) |
|---|---|---|---|---|---|---|---|
| **V(V)** | A1 | 71,1785 | 300 | 1:6 | 427,1 | 0,008384 | 0,016909 |
| | A2 | 334,1185 | 1380 | 1:6 | 2005 | 0,039353 | 0,081977 |
| | | | | | | | |
| **V(IV)** | G1 | 67,797 | 240 | 1:6 | 406,8 | 0,007985 | 0,016099 |
| | G2 | 456,34 | 1320 | 1:6 | 2738 | 0,053749 | 0,113726 |
| | | | | | | | |
| **V(III)** | Y1 | 118,37 | 140 | none | | 0,002324 | 0,004658 |
| | Y2 | 2610 | 2730 | none | | 0,051235 | 0,108109 |
| | Y3 | 3439,74 | 4110 | none | | 0,067523 | 0,145080 |
| | | | | | | | |
| **V(II)** | Z1 | 348,94 | 1380 | 0,0438 | 1047 | 0,020549 | 0,041967 |
| | Z2 | 1203,94 | 1470 | none | 1204 | 0,023634 | 0,048421 |

*Table 59. Linear regression coefficients and coefficient of determination from permeability experiments for the GN-115 membrane.*

| **Y = k·x + m** | **K** | **M** | **$R^2$** |
|---|---|---|---|
| **V(V)** | 6E-05 | 0,0003 | 1,000 |
| **V(IV)** | 9E-05 | -0,002 | 0,998 |
| **V(III)** | 4E-05 | 0,0011 | 0,994 |
| **V(II)** | 3E-05 | -0,0001 | 0,995 |

# Appendix C Membrane Stability in V(V) solution

## GN-115 ® General Energy © in 1M V(V)

The GN-115 membrane was tested for its chemical resistance were immersed in 1-2M V(V), 2,5M H2SO4 solution and kept for several weeks. Furthermore, these membranes were initially weighed, measured and tested in charge-discharge operation inside a VRB battery. After soaking in V(V) solution, these membranes were reweighed, measured for any swelling and expansion.

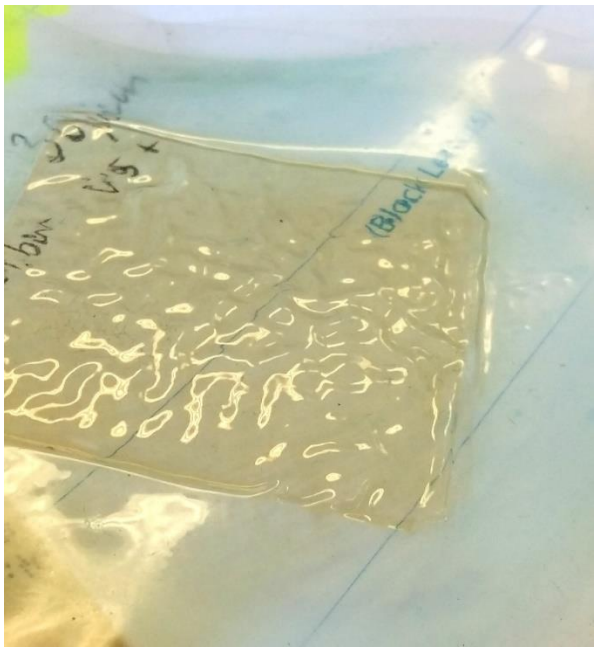

*Figure 72. Membrane GN-115 ® after 12 charge-discharge cycles in a VRB.*

The reason for the membrane to physically change use is usually because one part of the membrane is hydrophilic while the backbone is hydrophobic. Therefore, the membrane interacts with the electrolyte differently and not homogeneously which changes the shape and the form of the membrane.

The initial values of the GN-115 prior testing and after testing is compiled in Table 60. An increase of about 10% of the initial weight was noticed as well as a quite severe thickness change. However, the length and the width did not change much which indicates that the hydrophobic backbone keeps the membrane from changing in those directions and instead it increases in thickness.

# APPENDIX C MEMBRANE STABILITY IN V(5) SOLUTION

*Table 60. Swelling and water uptake of the GN-115 membrane in V(V) electrolyte after 7 weeks*

| GN-115 | **Mass (g)** | **Length (mm)** | **Width (mm)** | **Thickness (μm)** |
|---|---|---|---|---|
| Initial | 1694 | 76 | 81 | 125 |
| After 7 weeks | 1863 | 81 | 86 | 158 |
| Change (%) | *110* | *107* | *106* | *126* |

# Appendix D Estimate of cell resistance

This appendix contains a rough estimate of the internal resistance calculations of the cells with the different membranes. However, as 50% SOC is hard to measure during charge-discharge evaluation, this value should just be used as a comparison for major differences and not be attributed to specific membrane properties. Table D1 contains the approximate voltage at 50% SOC for all the different cycles.

*Table 61. Compiled the charge- and discharge voltage results from charge-discharge cycling using the VB-1 30 µm membrane.*

| | | 500 mA | | 1000 mA | | 1350 mA | | 1500 mA | |
|---|---|---|---|---|---|---|---|---|---|
| | *Units (V)* | *Chg* | *Dischg* | *Chg* | *Dischg* | *Chg* | *Dischg* | *Chg* | *Dischg* |
| VB1 – 30 µm | 1 | 1,31 | 1,50 | 1,35 | 1,43 | 1,44 | 1,37 | 1,43 | 1,36 |
| | 2 | 1,33 | 1,48 | 1,38 | 1,41 | 1,44 | 1,36 | 1,43 | 1,36 |
| | 3 | 1,33 | 1,50 | 1,37 | 1,41 | 1,44 | 1,34 | 1,44 | 1,35 |
| | 4 | 1,32 | 1,48 | 1,37 | 1,41 | 1,44 | 1,34 | 1,44 | 1,35 |
| | **Avg.** | **1,32** | **1,49** | **1,37** | **1,41** | **1,44** | **1,35** | **1,43** | **1,35** |
| At 50% SOC | | | | | | | | | |
| VB1 – 30 µm | **Avg.** | **1,42** | **1,33** | **1,47** | **1,30** | **n.a** | **n.a** | **1,52** | **1,25** |

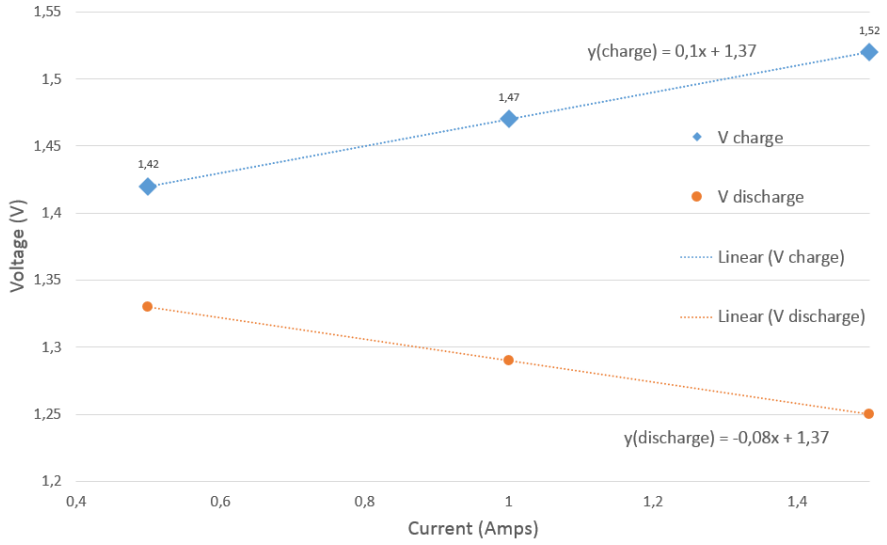


*Figure 73. Graph over voltage versus current for charge- and discharge respectively. The slope of the linear equation gives the resistance in ohms according to ohms law R = V/I*

The internal resistance was calculated by using the slope of the lines in Figure 73Figure 73 and multiplying with the membrane area as compiled in equation D1 and equation D2 below.

$$R_{Charge}^{VB-1\ 30\mu m} = \frac{dV_{charge}}{dI_{charge}} \cdot A_{membrane} = 0.1\ \Omega \cdot 25cm^2 = 2{,}5\ \Omega cm^2 \qquad (D1)$$

$$R_{Discharge}^{VB-1\ 30\mu m} = \frac{dV_{Discharge}}{dI_{Discharge}} \cdot A_{membrane} = 0.08\ \Omega \cdot 25cm^2 = 2{,}0\ \Omega cm^2 \qquad (D2)$$

**GN-115**

Using the same approach has for the VB1, Table 62 and equation D3 and D4 were used to determine the internal resistance of the cell using the GN-115 membrane.

Table 62. Charge-discharge voltage at 50% SOC for the GN-115 membrane

| | **500mA** | **1000mA** | **1500mA** |
|---|---|---|---|
| **Charge** | 1,46 | 1,51 | 1,54 |
| **Discharge** | 1,33 | 1,27 | 1,22 |

$$R_{Charge}^{Membr.115} = \frac{dV_{charge}}{dI_{charge}} \cdot A_{membrane} = 0.1\ 1\Omega \cdot 25cm^2 = 2{,}0\ \Omega cm^2 \qquad (D3)$$

$$R_{Discharge}^{Membr.115} = \frac{dV_{Discharge}}{dI_{Discharge}} \cdot A_{membrane} = 0.12\ \Omega \cdot 25cm^2 = 2{,}75\ \Omega cm^2 \qquad (D4)$$

# APPENDIX D ESTIMATE OF CELL RESISTANCE

## GN-212

*Table 63. Charge-discharge voltage at 50% SOC for the GN-212 membrane*

| | 500mA | 1000mA | 1500mA |
|---|---|---|---|
| **Charge** | 1,46 | 1,48 | 1,54 |
| **Discharge** | 1,32 | 1,28 | 1,26 |

$$R_{Charge}^{Membr.115} = \frac{dV_{charge}}{dI_{charge}} \cdot A_{membrane} = 0.04\ 1\Omega \cdot 25cm^2 = 1{,}0\ \Omega cm^2 \qquad (D5)$$

$$R_{Discharge}^{Membr.115} = \frac{dV_{Discharge}}{dI_{Discharge}} \cdot A_{membrane} = 0.055\Omega \cdot 25cm^2 = 1{,}38\ \Omega cm^2 \qquad (D6)$$

## GN-212C

*Table 64 Charge-discharge voltage at 50% SOC for the GN-212C membrane*

| | 500mA | 1000mA | 1500mA |
|---|---|---|---|
| **Charge** | 1,45 | 1,48 | 1,55 |
| **Discharge** | 1,31 | 1,28 | 1,23 |

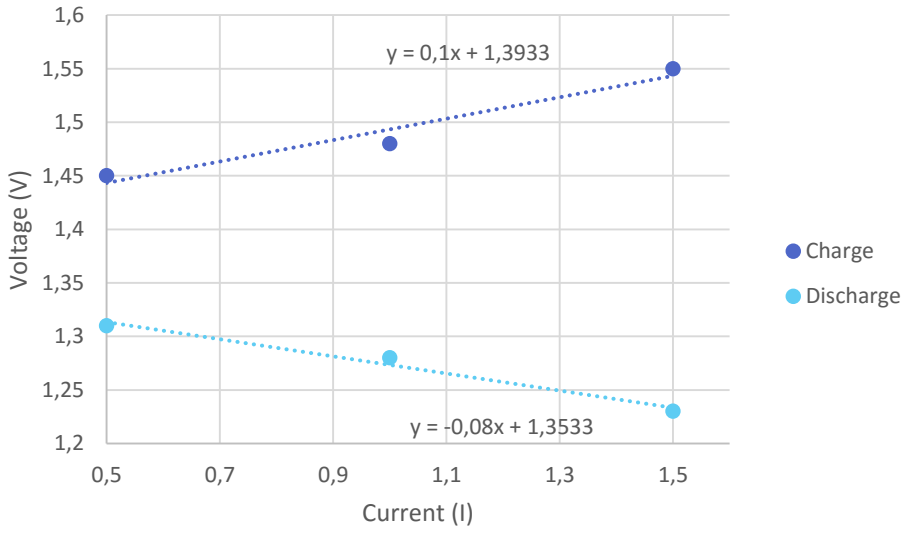


*Figure 74. Voltage versus current at 50% SOC for the GN-212C membrane*

$$R_{Charge}^{Membr.212C} = \frac{dV_{charge}}{dI_{charge}} \cdot A_{membrane} = 0{,}1\Omega \cdot 25cm^2 = 2{,}5\ \Omega cm^2 \qquad (D7)$$

$$R_{Discharge}^{Membr.212C} = \frac{dV_{Discharge}}{dI_{Discharge}} \cdot A_{membrane} = 0{,}08\Omega \cdot 25cm^2 = 2\,\Omega cm^2 \qquad (D8)$$